

Psychedelic control of neuroimmune interactions governing fear

<https://doi.org/10.1038/s41586-025-08880-9>

Received: 6 May 2024

Accepted: 11 March 2025

Published online: 23 April 2025

 Check for updates

Elizabeth N. Chung^{1,2,8}, Jinsu Lee^{1,2,8}, Carolina M. Polonio^{1,2}, Joshua Choi^{1,2}, Camilo Faust Akl^{1,2}, Michael Kilian^{1,2}, Wiebke M. Weiβ^{1,2}, Georgia Gunner³, Mingyu Ye⁴, Tae Hyun Heo^{1,2}, Sienna S. Drake^{1,2}, Liu Yang^{1,2}, Catarina R. G. L. d'Eca^{1,2}, Joon-Hyuk Lee^{1,2}, Liwen Deng³, Daniel Farrenkopf^{1,2}, Anton M. Schüle^{1,2}, Hong-Gyun Lee^{1,2}, Oreoluwa Afolabi^{1,2}, Sharmin Ghaznavi^{5,6}, Stelios M. Smirnakis⁴, Isaac M. Chiu³, Vijay K. Kuchroo^{1,2,7}, Francisco J. Quintana^{1,2,7} & Michael A. Wheeler^{1,2,8}

Neuroimmune interactions—signals transmitted between immune and brain cells—regulate many aspects of tissue physiology¹, including responses to psychological stress^{2–5}, which can predispose individuals to develop neuropsychiatric diseases^{6–9}. Still, the interactions between haematopoietic and brain-resident cells that influence complex behaviours are poorly understood. Here, we use a combination of genomic and behavioural screens to show that astrocytes in the amygdala limit stress-induced fear behaviour through epidermal growth factor receptor (EGFR). Mechanistically, EGFR expression in amygdala astrocytes inhibits a stress-induced, pro-inflammatory signal-transduction cascade that facilitates neuron–glial crosstalk and stress-induced fear behaviour through the orphan nuclear receptor NR2F2 in amygdala neurons. In turn, decreased EGFR signalling and fear behaviour are associated with the recruitment of meningeal monocytes during chronic stress. This set of neuroimmune interactions is therapeutically targetable through the administration of psychedelic compounds, which reversed the accumulation of monocytes in the brain meninges along with fear behaviour. Together with validation in clinical samples, these data suggest that psychedelics can be used to target neuroimmune interactions relevant to neuropsychiatric disorders and potentially other inflammatory diseases.

Neuroimmune communication facilitates tissue adaptations to environmental changes¹. Indeed, the immune system engages in bidirectional communication with the brain during psychological stress^{2–5}. Signals from immune cells to the brain can influence the development of neuropsychiatric diseases such as major depressive disorder (MDD)^{6–9}. Thus, although immunotherapies that target peripheral signals induced by psychological stress may be a viable therapeutic area in neuropsychiatric disorders such as MDD^{3,4,6–10}, many relationships between behavioural changes and immunoregulatory mechanisms in the brain remain to be defined.

To investigate links between brain–immune communication in neuropsychiatric disorders, we can draw parallels to other brain diseases in which tissue-resident glial cells in the brain, such as astrocytes, have emerged as key players in the immunoregulation of the central nervous system (CNS)¹¹. Astrocytes also have direct roles in the regulation of psychological stress responses^{12–15} and influence affective behaviours related to neuropsychiatric disorders including compulsion^{16,17}, fear^{14,18,19} and helplessness^{12,20}. Therefore, defining the immunoregulatory mechanisms of astrocytes in chronic stress may provide a link

between inflammation and affective behaviour and potentially offer new therapeutic avenues for treating MDD.

Subsets of amygdala astrocytes limit fear

To define neuroimmune interactions dysregulated over time in response to chronic psychological stress (Fig. 1a), we exposed mice to periods of chronic restraint stress followed by behavioural testing using contextual fear conditioning and the elevated plus maze (EPM) task (Extended Data Fig. 1a). Stress-induced changes in task acquisition across groups were not different (Extended Data Fig. 1b). However, mice that underwent 18 days of restraint stress showed increased fear behaviour relative to control mice (Fig. 1b and Extended Data Fig. 1c,d). Moreover, after 18 days of chronic stress, plasma levels of corticosterone and the cytokines IL-1 β , IL-12, TNF and the chemokine MIP2 were increased (Fig. 1c and Extended Data Fig. 1e,f). These results implicate potential links among chronic stress, peripheral inflammatory responses, fear behaviour and neuroimmune interactions.

¹The Gene Lay Institute of Immunology and Inflammation, Brigham and Women's Hospital, Massachusetts General Hospital, Harvard Medical School, Boston, MA, USA. ²Ann Romney Center for Neurologic Diseases, Brigham and Women's Hospital, Boston, MA, USA. ³Department of Immunology, Blavatnik Institute, Harvard Medical School, Boston, MA, USA. ⁴Department of Neurology, Brigham and Women's Hospital and Jamaica Plain Veterans Administration Hospital, Harvard Medical School, Boston, MA, USA. ⁵Department of Psychiatry, Massachusetts General Hospital, Harvard Medical School, Boston, MA, USA. ⁶Center for the Neuroscience of Psychedelics, Massachusetts General Hospital, Boston, MA, USA. ⁷Broad Institute of MIT and Harvard, Cambridge, MA, USA. ⁸These authors contributed equally: Elizabeth N. Chung, Jinsu Lee. [✉]e-mail: mwheeler@bwh.harvard.edu

Article

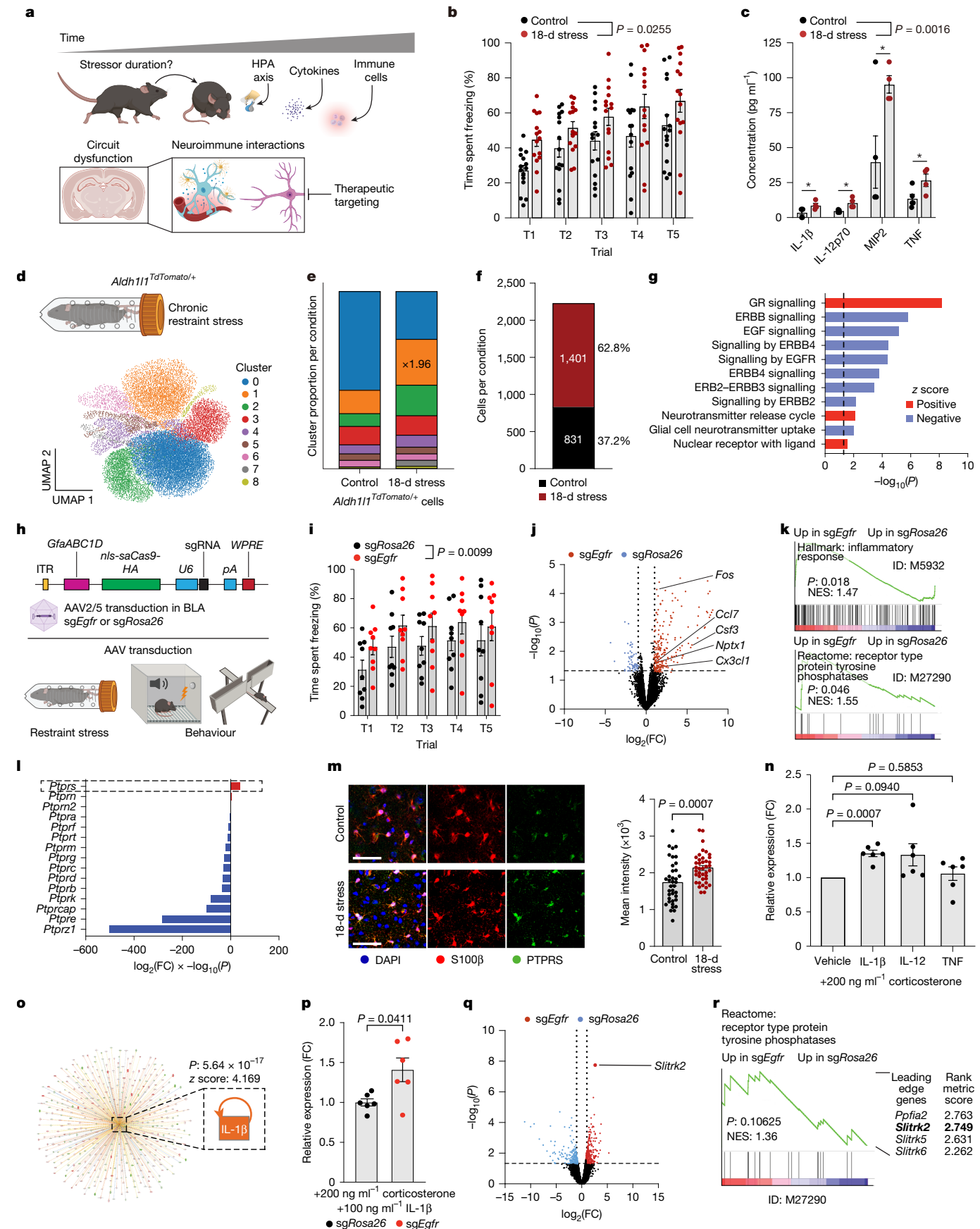


Fig. 1 | See next page for caption.

Fig. 1 | Amygdala astrocyte EGFR signalling limits stress-induced fear behaviour. **a**, Schematic of our study examining neuroimmune interactions in chronic stress. **b**, Fear behaviour of mice exposed to control handling or 18 days of restraint stress (18-d stress). $n = 15$ mice per group. Two-way repeated measures analysis of variance (ANOVA). **c**, ELISA of plasma cytokines in mice after 18 days of restraint stress ($n = 4$) and in control mice ($n = 5$). Two-way ANOVA with multiple *t*-test. **d**, Top, schematic of experiment. Bottom, uniform manifold approximation and projection (UMAP) plot of clusters detected by scRNA-seq. $n = 11,700$ cells. **e,f**, Proportion of cluster per condition (**e**) and number of cells in cluster 1 (**f**) from control mice ($n = 3$) and 18-day stressed mice ($n = 3$). **g**, Pathway analysis of cluster 1 cells. $n = 2,232$ cells. **h,i**, Schematic of the experiment (**h**) and fear behaviour (**i**) of mice transduced with sgEgfr or sgRosa26 and exposed to 7 days of restraint stress (7-d stress). $n = 9$ per group. Two-way repeated-measures ANOVA. **j,k**, Volcano (**j**) and gene set enrichment analysis (GSEA) (**k**) plots analysing bulk RNA-seq amygdala astrocyte data from mice transduced with sgEgfr ($n = 3$) or sgRosa26 ($n = 4$). GSEA identifiers (IDs) are indicated. **l**, Bar plot of all detected PTPR family members in cluster 1 cells.

m, Images (left) and quantification (right) of PTPRS levels in BLA astrocytes from 18-day stressed mice ($n = 40$ images) and from control mice ($n = 38$ images). $n = 5$ mice per group. Unpaired *t*-test. Scale bars, 50 μ m. **n**, qPCR of *Ptprs* in primary astrocytes treated for 24 h with corticosterone and 100 ng ml⁻¹ IL-1 β , 100 ng ml⁻¹ IL-12 or 50 ng ml⁻¹ TNF. $n = 6$ per group, vehicle-treated group normalized to 1. One-sample *t*-test. **o**, Qiagen Ingenuity Pathway Analysis (IPA) prediction using RNA-seq data that indicate that IL-1 β is an upstream regulator. Fisher's exact test of sgEgfr versus sgRosa26. **p**, qPCR of *Ptprs* in AAV-targeted primary astrocytes treated with the indicated compounds for 24 h. $n = 6$ per group. Mann-Whitney test. **q**, Volcano plot of bulk RNA-seq data analysing amygdala neurons from mice analysed in **j**. **r**, GSEA plot from data in **q** showing leading edge genes. *Slitrk2* is highlighted in bold. $n = 3$ mice per group. FC, fold change; HPA, hypothalamic–pituitary–adrenal; ITR, inverted terminal repeat; NES, normalized enrichment score; saCas9, *S. aureus* Cas9; sgRNA, single guide RNA. Data shown as the mean \pm s.e.m. Schematics in **a,d** and **h** were created using BioRender (<https://biorender.com>).

Multiple astrocyte populations that influence local inflammatory signals in the nervous system have been described^{11,21–25}. Moreover, astrocytes have emerged as direct targets of increased corticosterone signalling in the context of chronic stress^{12,14}. However, the processes by which astrocytes integrate inflammatory cues to shape behaviour in response to chronic stress remain largely unknown. To begin to address this question, we subjected *Aldh1l1*^{tdTomato/+} mice, which inducibly express a tdTomato reporter in *Aldh1l1*⁺ cells, to 18 days of restraint stress then performed single-cell RNA sequencing (scRNA-seq) of tdTomato⁺ cells (Supplementary Data 1). We captured 11,700 reporter cells from *Aldh1l1*^{tdTomato/+} mice, and these cells could be subdivided across 9 clusters that were associated with control mice or chronically stressed mice (Fig. 1d, Extended Data Fig. 1g–j and Supplementary Table 1).

Multiple clusters were modulated by chronic stress, some of which were overrepresented in stress conditions (clusters 1–5, 7 and 8), whereas others were overrepresented in control conditions (clusters 0 and 6) (Fig. 1e). We focused our attention on cluster 1 because it was the most numerous population of cells expanded in response to 18 days of restraint stress (Fig. 1g). Pathway analyses suggested that cluster 1 cells are transcriptionally regulated by signalling from glucocorticoid receptors (Fig. 1h and Extended Data Fig. 1k). These receptors are key transcriptional targets of stress-induced corticosterone and control behavioural phenotypes when activated by psychological stress in astrocytes^{12,14}. We next performed a pseudotime analysis using RNA velocity, and the results suggested that cluster 1 is associated with late-stage pseudotime and potentially linked with chronic stress responses (Extended Data Fig. 1l–o).

In addition to glucocorticoid receptor activation, pathway analyses of cluster 1 cells pointed to a significant downregulation of signalling by the epidermal growth factor receptor (EGFR) family²¹ (Fig. 1g). Consistent with these data, an analysis of differentially expressed genes in cluster 1 cells revealed that *Egfr* was significantly downregulated (Extended Data Fig. 1p). Of note, cluster 2, which was maximally expanded in response to chronic stress but less numerous than cluster 1, was also marked by significantly reduced *Egfr* expression together with downregulation of pathways that are protective during chronic stress. Cluster 0 cells that were associated with control mice were marked by increased IL-10 signals and decreased inflammatory pathways (Extended Data Fig. 1q and Supplementary Table 2). Together, these data suggest that low *Egfr* expression levels might be linked with stress-induced behavioural changes.

Because multiple brain areas have important roles in stress-induced fear behaviour²⁶, we examined astrocyte *Egfr* expression across the brain from a previously published mouse brain atlas²⁷ to identify regions potentially influenced by astrocyte EGFR signalling. Among all brain areas re-examined, the amygdala had the lowest astrocyte *Egfr* expression levels (Extended Data Fig. 2a), which we independently validated

by immunostaining (Extended Data Fig. 2b). These data suggest that in response to 18 days of restraint stress, the amygdala may be more susceptible to behavioural changes that are controlled by *Egfr*-dependent mechanisms in astrocytes. The amygdala is a limbic area composed of multiple subnuclei and appraises environmental threats²⁸, but is sensitive to immune-cell-derived cues released during psychological-stress exposure^{5,29}, which can enhance fear behaviour³⁰.

We previously linked *Egfr*⁺ astrocytes to anti-inflammatory signalling in autoimmunity^{21,31}. Therefore, we speculated that *Egfr*⁺ astrocytes act as negative regulators of local inflammatory responses triggered by chronic stress that can activate amygdala circuits. We tested this hypothesis after 7 days of restraint stress, a time point at which there were otherwise no significant changes in fear behaviour or plasma cytokine levels (Extended Data Figs. 1b,c and 2c–e). To study whether *Egfr*⁺ amygdala astrocytes limit fear behaviour, we used an astrocyte-specific adeno-associated virus (AAV)-based CRISPR–Cas9 system to knockdown (KD) *Egfr* or, as a control, target the inert *Rosa26* locus (Fig. 1h and Extended Data Fig. 2f). Mice with genetic inactivation of *Egfr* in amygdala astrocytes showed increased fear behaviour after 7 days of restraint stress. This finding indicates that *Egfr*⁺ astrocytes reduce stress-induced behavioural changes (Fig. 1i and Extended Data Fig. 2g).

An analysis of *Egfr* KD amygdala astrocytes by bulk RNA-seq revealed increased activation of inflammatory pathways, a finding consistent with the known anti-inflammatory properties of EGFR in astrocytes^{21,31}. Activation of *Nptx1* and *Fos* were also increased, which are related to the stabilization of fear-memory formation by amygdala astrocytes³² (Fig. 1j,k, Extended Data Fig. 2h,i and Supplementary Table 3). Loss-of-function of EGFR in astrocytes resulted in increased transcriptional signals associated with receptor protein tyrosine phosphatases (Fig. 1k), which are induced by NF- κ B signalling³³ and engage in heterotypic cell–cell interactions³⁴.

We next investigated our scRNA-seq dataset of tdTomato⁺ cells isolated from *Aldh1l1*^{tdTomato/+} mice exposed to 18 days of restraint stress and from control mice (Fig. 1f). The analysis identified *Ptprs* as the most significantly upregulated of all receptor protein tyrosine phosphatase family members in cluster 1 cells linked with chronic stress (Fig. 1l). Notably, *Ptprs* and other family members were also differentially represented across clusters (Extended Data Fig. 2j). First, we detected increased PTPRS expression in astrocytes located in the basolateral amygdala (BLA), the main input subnucleus of the amygdala, from mice after 18 days of restraint stress²⁸ (Fig. 1m). To define cytokines that might influence the expression of receptor protein tyrosine phosphatases in astrocytes during chronic stress, we quantified *Ptprs* expression in primary astrocytes treated with corticosterone and with IL-1 β , IL-12 or TNF, cytokines that were upregulated in the plasma of mice after 18 days of stress (Fig. 1c). The combination of corticosterone and IL-1 β increased

Article

Ptprs expression (Fig. 1n), similar to the detection of increased IL-1 β activity in *Egfr* KD amygdala astrocytes isolated from mice that underwent 7 days of restraint stress (Fig. 1o). However, we note that multiple factors can potentially modulate astrocyte *Ptprs* expression *in vivo*. Likewise, *Egfr* KD in primary astrocytes enhanced *Ptprs* expression in response to treatment with both IL-1 β and corticosterone (Fig. 1p). These data suggest that EGFR loss-of-function in the presence of IL-1 β and corticosterone leads to increased *Ptprs* expression in astrocytes.

In addition to other receptors, PTPRS binds SLTRK2, a single-pass transmembrane receptor expressed on neurons that influences the stability of neuron contacts³⁵. Bulk RNA-seq analyses of amygdala neurons from mice in which *Egfr* was knocked down in astrocytes showed upregulation of *Slitrk2* (Fig. 1q, Extended Data Fig. 3a–d and Supplementary Table 4) and increased transcriptional responses linked to receptor protein tyrosine phosphatase activity (Fig. 1r). We therefore propose that in the amygdala, astrocyte crosstalk with neurons influences stress-induced fear behaviour.

NR2F2⁺ amygdala neurons drive fear

To define potential mechanisms controlled by astrocyte–neuron communication, we analysed transcription factors expressed in amygdala neurons isolated from mice in which *Egfr* was knocked down in astrocytes and from control mice. These analyses revealed five upregulated transcription factors that were also predicted to act as transcriptional regulators (Fig. 2a). We focused on the three most significantly expressed in neurons: NR2F2, ETS1 and C/EBP γ (Fig. 2b). We tested whether astrocyte–neuron PTPRS–SLTRK2 signalling affects expression of the transcriptional regulators predicted by our RNA-seq analyses. To that end, primary astrocytes and neurons were co-cultured using AAV-based KD of astrocyte *Ptprs* and neuron *Slitrk2*; non-targeted KD was used as a control (Fig. 2c). KD of both astrocyte *Ptprs* and neuron *Slitrk2*, but not each separately (Extended Data Fig. 3e), decreased *Nr2f2* expression in neurons (Fig. 2c). These data suggest that this neuronal transcriptional program is regulated by astrocyte–neuron crosstalk and is potentially relevant during chronic stress.

To test whether these transcriptional programs control fear behaviour, we bilaterally targeted the amygdala to KD *Nr2f2*, *Cebpg* or *Ets1* and subjected mice to 7 days of restraint stress (Fig. 2d). This time point was chosen because we had detected transcriptional signatures of these factors after 1 week of stress (Fig. 2a,b). Consistent with our *in vitro* and genomic studies (Fig. 2a–c), inactivation of *Nr2f2* but not *Ets1* or *Cebpg* decreased stress-induced fear behaviour (Fig. 2e and Extended Data Fig. 3f,g). Bulk RNA-seq and ATAC-seq analyses showed that the activation of pathways linked to chronic stress, fear behaviour and synaptic domains in *Nr2f2* KD mice were downregulated (Fig. 2f–j, Extended Data Fig. 3h,i and Supplementary Tables 5 and 6). Consistent with this finding, immunostaining studies showed reduced numbers of VGLUT2⁺HOMER1⁺ puncta in the BLA of *Nr2f2* KD mice (Fig. 2k) together with decreased excitatory neuron coverage in the BLA (Extended Data Fig. 3j). Overall, these data suggest that in the context of chronic stress and fear, amygdala astrocytes influence NR2F2 transcriptional programs in neurons.

Regulation of amygdala responses

We next sought to identify the molecular cues that modulate astrocyte–neuron interactions in amygdala subnuclei during chronic stress. Our cellular data showed that chronic stress and fear conditioning synergize to modulate astrocyte and neuron function (Extended Data Fig. 4a–f and Supplementary Table 7). Therefore, we performed spatial transcriptomics, using Stereo-seq, on mice that underwent 18 days of restraint stress followed by fear conditioning (Extended Data Fig. 5a–f). We assigned cell types using an atlas of the mouse nervous system²⁷ recently applied to the amygdala³⁶, and spatially defined

the amygdala on the basis of anatomical and cell-type markers in conjunction with immunohistochemistry (Extended Data Fig. 6a,b). This analysis detected *Slc17a7*⁺ and *Slc17a6*⁺ excitatory neurons, inhibitory neurons, astrocytes, oligodendrocytes and microglia that were evenly distributed across samples (Fig. 3a,b, Extended Data Fig. 6c–j and Supplementary Tables 8–13).

Because NR2F2 influenced fear behaviour and excitatory BLA neuron features (Fig. 2e,k and Extended Data Fig. 3j), we subclustered *Slc17a7*⁺ and *Slc17a6*⁺ excitatory amygdala neurons. This analysis identified that cluster 2 excitatory neurons are associated with a late-stage pseudo-time trajectory after 18 days of restraint stress and fear conditioning (Fig. 3c,d and Supplementary Table 13). Anatomically, most neurons linked with the stress-associated subset of cluster 2 excitatory neurons were confined to either the BLA²⁸ or the nucleus of the lateral olfactory tract. The latter brain region is an amygdala subnucleus interconnected with the BLA that amplifies olfactory cue-driven fear behaviour³⁷ such as those present in our contextual fear-conditioning paradigm (Fig. 3e–g). Consistent with our genetic inactivation and genomic studies, cluster 2 excitatory neurons were localized near astrocytes that expressed undetectable levels of *Egfr* (Fig. 3h) and expressed significantly higher levels of *Nr2f2* than other excitatory neuron clusters (Fig. 3i).

An analysis of cluster 2 excitatory neurons revealed activation of pathways predicted to be driven by several of the same cytokines and chemokines that we detected in the plasma of mice subjected to 18 days of stress, including IL-1 β and IL-12 (Figs. 1c and 3j). However, we did not directly detect peripheral immune cells in the amygdala in our spatial transcriptomic studies (Fig. 3b), perhaps owing to transcriptional dropout of these and other less abundant cell types and the analysis of single sections per animal. We also did not detect markers of peripheral monocytes, such as *Ccr2*, in the cells we classified as microglia (Extended Data Fig. 6k,l). This result is consistent with those of chronic stress studies that focused on the nucleus accumbens, where peripheral myeloid cells are observed to remain in the vasculature^{6,38}. Finally, we used the amygdala spatial transcriptomic data to directly quantify the expression of cytokines related to each activated pathway we detected. The analysis revealed negligible to undetectable expression of *Il1a*, *Il1b*, *Il1a*, *Il1b* and *Il6* (Extended Data Fig. 6m). Based on the prediction of excitatory amygdala neuron transcriptional responses related to IL-1 β and IL-12, coupled with our plasma cytokine studies (Fig. 1c) and recent reports of neural circuit regulation by peripheral immunity during chronic stress^{2,5,6,38}, we speculate that the neuron–glial interactions we detected in the amygdala are tuned by peripheral immune cells.

Psychedelics tune neuroimmune interactions

Multiple populations of peripheral immune cells influence behaviour during chronic stress^{2,5,6,39}. Beyond the brain vasculature, immune cells in the brain meninges also control complex behaviours^{40–42}. Hence, we first evaluated by fluorescence-activated cell sorting (FACS) the abundance of immune-cell subsets in the meninges, the deep cervical lymph nodes (dCLNs) and the spleen from chronically stressed mice and from control mice (Supplementary Data 2–4). We observed an increase in several meningeal immune-cell populations from mice that underwent restraint stress for 18 days. By contrast, we did not observe significant recruitment to the dCLNs or the spleen and did not detect increases after 7 days of stress (Extended Data Fig. 7a–c).

We focused on inflammatory monocytes because of previous reports detailing the heterogeneity of monocyte recruitment to the brain and other organs in the context of chronic stress^{2,6,38,43}. Meningeal monocyte recruitment was increased after 18 days of restraint stress, whereas splenic monocytes were decreased (Fig. 4a). Thus, we examined whether monocyte trafficking from the spleen to the meninges could account for these changes. Using mice that ubiquitously express the photoconvertible fluorescent protein Kaede (*Cag*^{Kaede} mice), we measured the trafficking of splenic immune cells

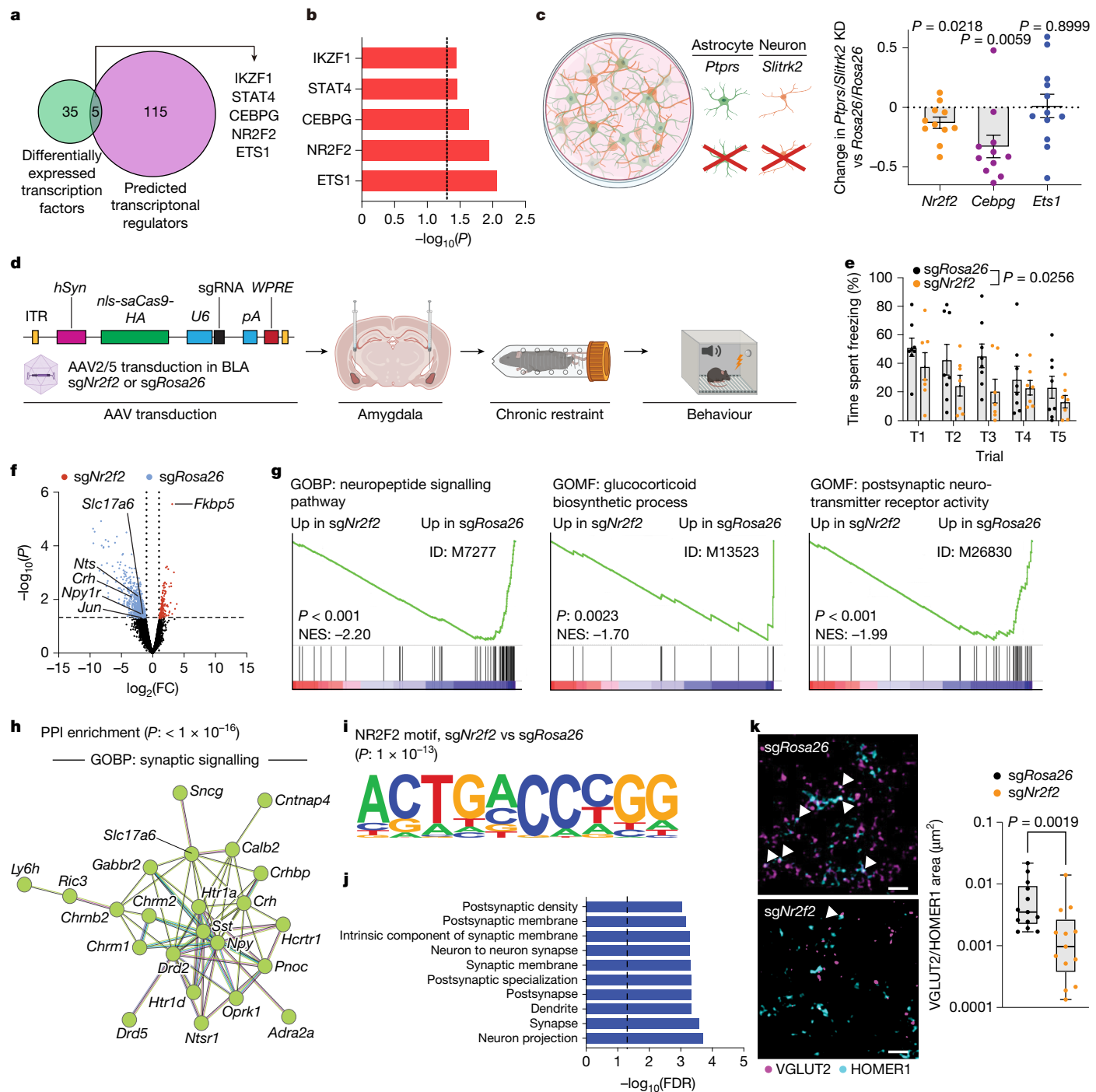


Fig. 2 | Amygdala neuron *Nr2f2* expression promotes fear behaviour. **a**, Venn diagram illustrating the overlap between transcription factors upregulated in bulk RNA-seq data of amygdala neurons isolated from mice transduced with AAVs targeting astrocyte *Egrfr* relative to *Rosa26* control after 7 days of restraint stress and fear conditioning, and showing predicted transcriptional regulators. $n=3$ mice per group. **b**, Ranking by P value of differentially expressed regulators shown in **a**. **c**, Left, schematic of the cell-type-specific KD strategy used in astrocyte–neuron co-cultures. Right, qPCR expression data of primary neurons 7 days after KD (*Nr2f2*, $n=11$; *Cebpg*, $n=11$; *Ets1*, $n=12$). One sample t -test performed relative to *Rosa26*-targeting control for each gene. **d**, Experimental schematic for neuron targeting and behavioural analysis. **e**, Fear behaviour of mice transduced with *sgNrf2* ($n=7$) or *sgRosa26* ($n=8$) and exposed to 7 days of restraint stress. Two-way repeated-measures ANOVA. **f–h**, Volcano plot (**f**).

GSEA plots (**g**) and StringDB-generated protein–protein interaction (PPI) network (**h**) obtained from bulk RNA-seq analysis of amygdala neurons from mice targeted using *sgNrf2* ($n=3$) or *sgRosa26* ($n=4$) that underwent 7 days of restraint stress and fear conditioning. **i,j**, ATAC-seq analysis showing the NR2F2 motif sequence (**i**) and downregulated cellular compartments following *Nr2f2* KD in amygdala neurons (**j**) from mice that underwent 7 days of restraint stress and fear conditioning. $n=4$ mice per group. **k**, Images (left) and quantification (right) of excitatory synapses (white arrowheads in the images) in the BLA of *Nr2f2*-targeted ($n=3$) or *Rosa26*-targeted ($n=3$) mice by immunostaining. $n=13$ images per group. Mann–Whitney test. Scale bars, 10 μm . FDR, false discovery rate; GOBP, gene ontology biological process; GOMF, gene ontology molecular function. Data shown as the mean \pm s.e.m. Schematics in **c** and **d** were created using BioRender (<https://biorender.com>).

Article

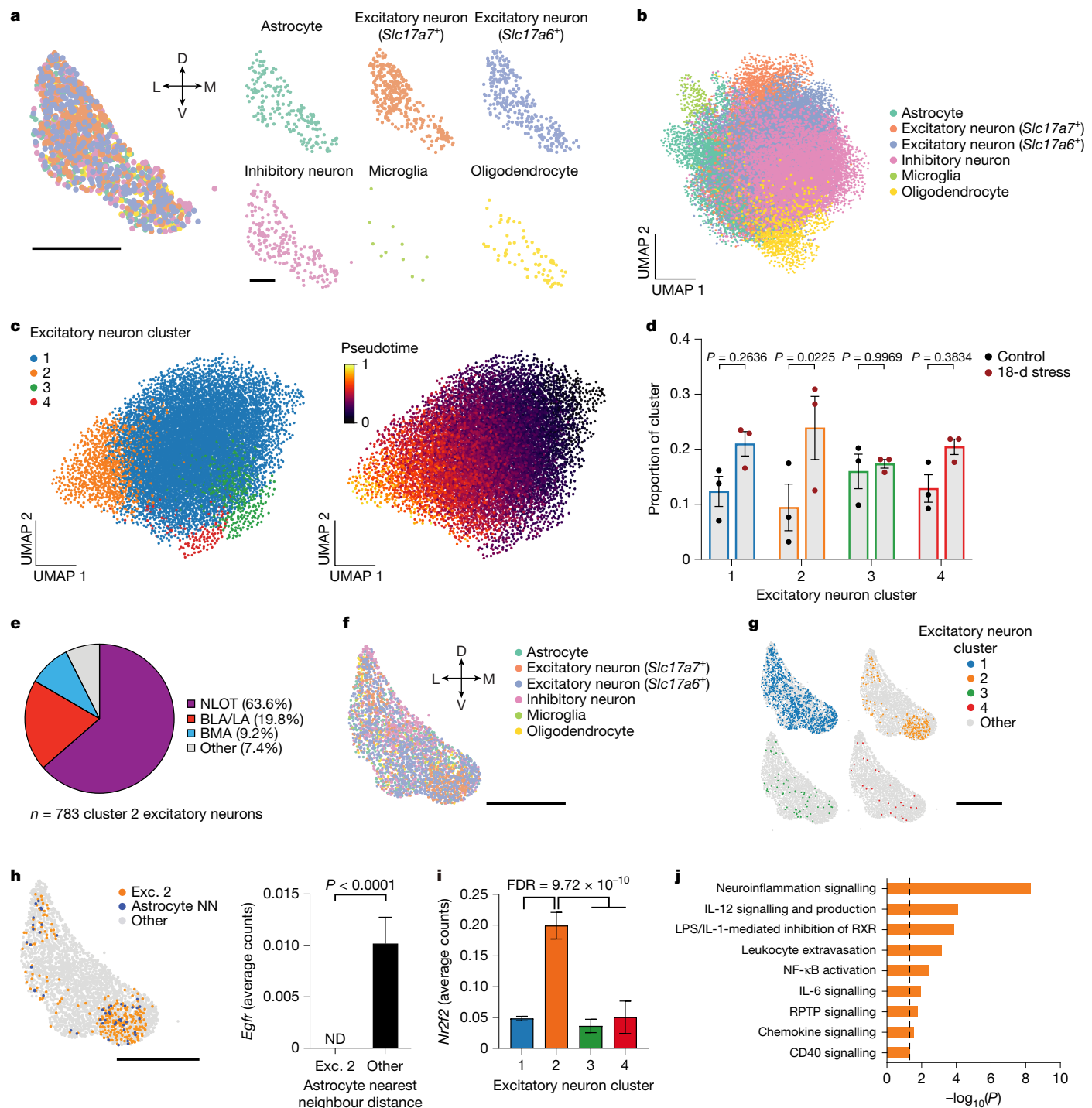


Fig. 3 | Regulation of amygdala subnuclei during chronic stress. **a**, Cell types detected in the amygdala of a representative control mouse by Stereo-seq projected into space. n = 1,121 cells. **b**, Transcriptional clustering of all replicates. n = 3 control mice, n = 3 18-day restraint stress mice. All mice underwent fear conditioning. n = 16,496 cells. **c**, Subclustered excitatory neuron clusters (left) and pseudotime labels (right). n = 7,553 cells. **d**, Cluster proportion by condition. n = 3 mice per group. Two-way ANOVA with Sidak's multiple comparisons test. **e**, Pie chart associating an amygdala subnucleus with each cluster 2 excitatory neuron detected in the amygdala. **f,g**, Visual projection of cell types (**f**) and excitatory neuron subclusters (**g**) detected in the amygdala

of a representative 18-day stressed mouse by Stereo-seq. n = 2,698 cells. **h**, Nearest neighbour analysis of *Egfr* expression in astrocytes from stressed mice, analysing the top 10% astrocytes nearest to cluster 2 excitatory neurons (Exc. 2) versus all other astrocytes. Unpaired Welch's t-test. **i**, Quantification of *Nrf2* averaged counts across excitatory neuron clusters. **j**, Inflammatory pathways upregulated in cluster 2 excitatory neurons. Data shown as the mean ± s.e.m. Scale bars, 250 μm (**a**, right), 500 μm (**a**, left) or 1 mm (**f–h**). BMA, basomedial amygdala; D, dorsal; L, lateral; LA, lateral amygdala; M, medial; ND, not detected; NLOT, nucleus of the lateral olfactory tract; NN, nearest neighbour; RPTP, receptor-type protein tyrosine phosphatase; V, ventral.

to the meninges, bone marrow and dCLNs 36 h after photoconversion and after 18 days of restraint stress (Extended Data Fig. 7d and Supplementary Data 5). In *Cag^{Kaede}* mice, more splenic immune cells

were recruited to the meninges than to other tissues. However, the proportion of splenic-derived meningeal immune cells decreased after chronic stress, which suggested that meningeal immune cells

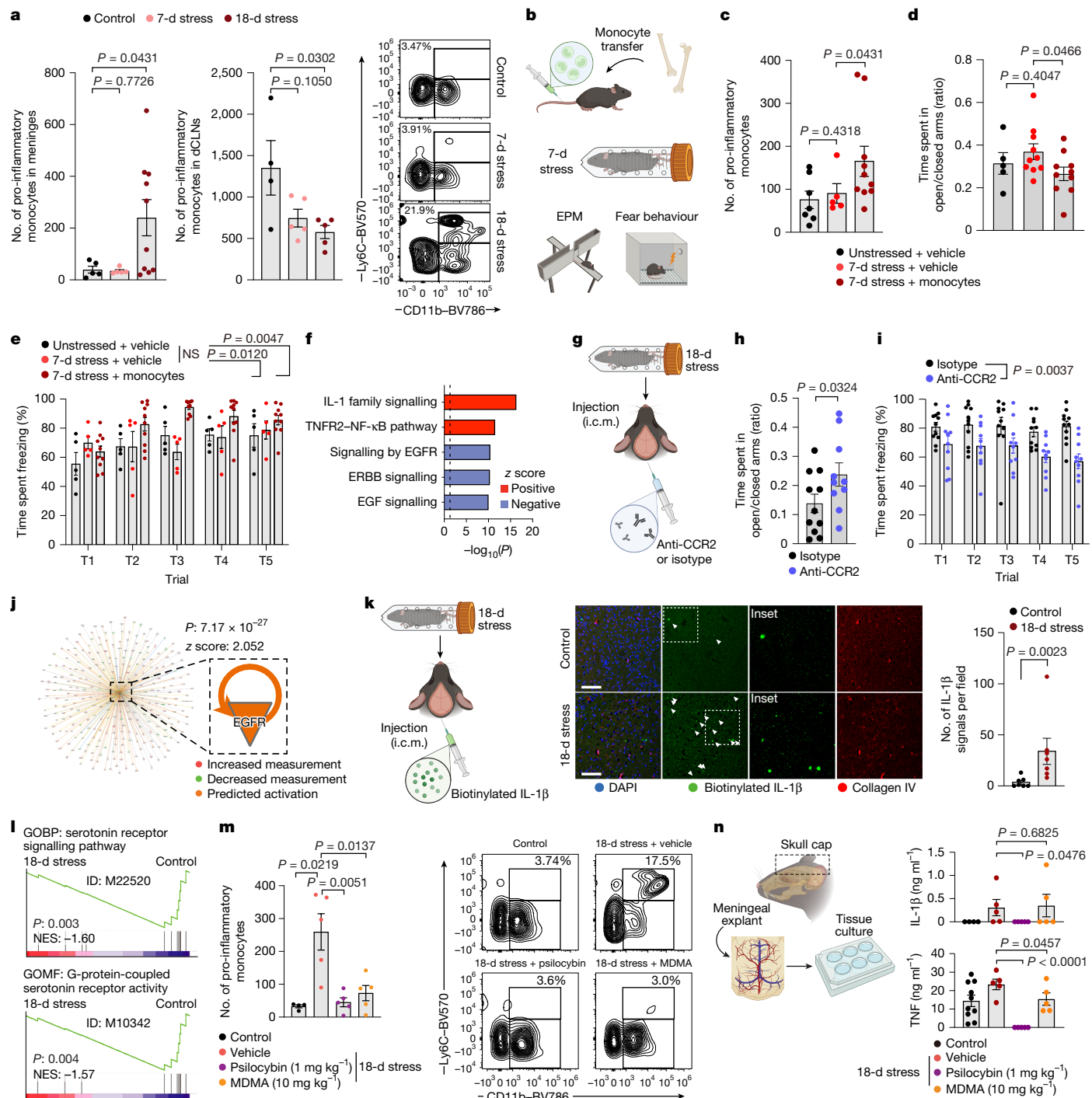


Fig. 4 | Stress-induced neuroimmune interactions are modulated by psychedelics. **a**, Left, quantification by FACS of pro-inflammatory monocytes in the meninges and dCLNs 24 h after mice were exposed to 7 or 18 days of restraint or control conditions. Right, FACS plots of meningeal monocytes. $n = 10$ for meninges from 18-day stressed mice; $n = 4$ for dCLNs from 18-d stressed mice, otherwise $n = 5$ per group. Unpaired t -test on log-transformed data. **b**, Schematic of monocyte adoptive transfer in C57Bl/6 mice. **c**, FACS analysis of meningeal monocytes 24 h after stress (unstressed mice (vehicle, $n = 7$); 7-day stressed mice (vehicle, $n = 5$); monocyte, $n = 10$). Mann–Whitney test. **d,e**, Behaviour of host mice with adoptively transferred monocytes. $n = 5$ unstressed mice; $n = 10$ otherwise. **d**, EPM data. Unpaired t -test. **e**, Fear behaviour. $n = 5$ –10 mice per group. Two-way repeated-measures ANOVA. **f**, Pathway analysis of amygdala astrocyte bulk RNA-seq data from **b**–**e**. **g**, Schematic of anti-CCR2 antibody by i.c.m. injection. **h,i**, Analysis of EPM (**h**) and fear behaviour (**i**) in anti-CCR2 antibody-treated or isotype-treated mice. $n = 10$ mice per group. Unpaired t -test for EPM. Two-way repeated-measures

ANOVA for fear behaviour. Experiments were repeated twice. **j**, EGFR transcriptional network comparing anti-CCR2 antibody-injected mice versus isotype-injected controls. Fisher's exact test. **k**, Schematic (left), imaging and quantification (middle and right, respectively) of biotinylated IL-1 β delivered by i.c.m. injection in the BLA of 18-day stressed mice or control mice. $n = 7$ images per group from $n = 4$ mice per group. Mann–Whitney test. Scale bars, 100 μ m. **l**, GSEA plots of bulk RNA-seq of meningeal monocytes from mice exposed to 18-days of restraint stress or from unstressed control mice. $n = 3$ mice per group. **m**, FACS analysis (left) and plots (right) of meningeal inflammatory monocytes 24 h after the indicated treatment. $n = 5$ per group. One-way ANOVA, Dunnett post-test. **n**, Schematic (left) and ELISA (right) of meningeal explants from mice after the indicated treatment. $n = 5$ mice per group, $n = 10$ for TNF control, $n = 4$ for IL-1 β control. One-way ANOVA, Fisher's least significant difference (LSD) test. Data shown as the mean \pm s.e.m. Schematics in **b,g,k** and **n** were created using BioRender (<https://biorender.com>).

Article

may also traffic from other tissues (Extended Data Fig. 7d). Moreover, the relative proportion of splenic monocytes trafficking to the meninges after 18 days of restraint stress was significantly lower than that of other tissues such as the bone marrow (Extended Data Fig. 7e). This finding indicates that there may be additional destinations for monocyte trafficking during chronic stress.

To examine the links between inflammatory monocytes and stress-induced fear behaviour, we used multiple orthogonal gain-of-function and loss-of-function approaches. First, we performed daily adoptive transfer of pro-inflammatory monocytes into C57BL/6 hosts undergoing 7 days of restraint stress (Fig. 4b). The results confirmed that such monocytes accumulated in the meninges (Fig. 4c). Monocyte adoptive transfer led to exacerbated fear behaviour and decreased EGFR-related transcriptional responses in amygdala astrocytes of recipient mice (Fig. 4d–f). We validated these findings in a second set of experiments using immunodeficient NSG mice undergoing 7 days of restraint stress (Extended Data Fig. 7f,g). Third, we acutely ablated meningeal monocytes using intra-cisterna magna (i.c.m.) injection of an anti-CCR2 monoclonal antibody in mice after 18 days of restraint stress (Fig. 4g and Extended Data Fig. 7h). Mice administered an anti-CCR2 antibody by i.c.m. injection showed decreased fear behaviour relative to control mice and increased EGFR pathway activity in amygdala astrocytes (Fig. 4h–j). As a fourth independent validation experiment, we inducibly expressed diphtheria toxin receptor (DTR) in monocytes (*Ccr2*^{DTR/+} mice) to chronically deplete inflammatory monocytes. Consistent with our other analyses, *Ccr2*^{DTR/+} mice exhibited decreased fear behaviour alongside depletion of meningeal and splenic monocytes. Notably, treatment with diphtheria toxin did not affect the abundance of other immune-cell subsets or amygdala microglia (Extended Data Fig. 7i–l). Systemic monocyte depletion also limited astrocyte pro-inflammatory transcriptional responses linked with IL-1, IL-6 and TNF, and increased astrocyte EGFR pathway activity (Extended Data Fig. 7m).

To determine whether meningeal factors can infiltrate the amygdala, we injected Evans blue dye by i.c.m. injection and detected dye throughout the surface of the brain (Extended Data Fig. 7n,o). Because IL-1 β was predicted to modulate some of the astrocyte responses we detected (Figs. 1c,n–p, 3j and 4f and Extended Data Fig. 7m), we analysed meningeal cytokine penetrance into the amygdala by administering biotinylated IL-1 β by i.c.m. injection (Fig. 4k and Extended Data Fig. 7p). There were significantly more IL-1 β ⁺ puncta in the BLA of 18-day stressed mice relative to control mice (Fig. 4k), a result consistent with reports of blood–brain barrier leakiness following chronic stress^{6,15,38}. In line with our results from genomic and functional studies predicting that IL-1 β regulates EGFR⁺ astrocytes, we also detected increased IL-1R expression in BLA astrocytes in 18-day stressed mice relative to control mice (Extended Data Fig. 7q). These data suggest that inflammatory monocytes mobilized in response to chronic stress modulate fear behaviour and amygdala transcriptional responses, results that are in line with previous studies^{6,44}.

To generate hypotheses regarding the regulation of meningeally recruited monocytes, we performed bulk RNA-seq. The results showed that the relative activity of serotonin signalling in meningeal monocytes was potentially reduced after 18 days of restraint stress relative to control mice (Fig. 4l and Extended Data Fig. 8a). Serotonin signalling affects multiple tissues and is modulated by the neurotransmitter serotonin and by psychedelic drugs such as psilocybin⁴⁵ and 3,4-methylenedioxymethamphetamine (MDMA)⁴⁶. Psilocybin or MDMA administration modulates affective behaviours governed by limbic areas in animals, in patients with MDD and in patients with posttraumatic stress disorder^{47–51}. As independent validation, we detected the expression of several receptors that regulate the effects of psychedelics in immune-cell subsets from the mouse ImmGen atlas (Extended Data Fig. 8b). To functionally test whether myeloid-cell subsets respond to psilocybin or MDMA, we treated primary CD11b⁺ splenic

cells with 200 ng ml⁻¹ corticosterone and 10 μ M psilocybin or 10 μ M MDMA racemate. Treatments led to downregulation of the chemokine receptors *Cxcr3* and *Cxcr4*, which was reversed by treatment with a 5-HT₂ receptor antagonist (Extended Data Fig. 8c,d). Treatment with 10 μ M psilocybin or 10 μ M MDMA racemate also decreased *Il1b* expression in lipopolysaccharides (LPS)-treated primary CD11b⁺ splenic cell cultures (Extended Data Fig. 8e), which suggested that psilocybin and MDMA can modulate some immune-cell responses.

To test whether psilocybin and MDMA affect monocyte recruitment or responses *in vivo*, we treated mice that underwent 18 days of restraint stress with vehicle, 1 mg kg⁻¹ psilocybin or 10 mg kg⁻¹ MDMA racemate. These doses roughly correspond to those used in humans^{48,49} and have been used extensively in mice^{47,50,51}. Meningeal monocyte recruitment, meningeal cytokine production and fear behaviour were all decreased in mice treated with psilocybin or MDMA relative to control mice (Fig. 4m,n, Extended Data Fig. 8f–j and Supplementary Tables 14 and 15).

In addition to inflammatory monocytes, psilocybin and MDMA treatment regulated the abundance of multiple immune-cell classes in the meninges of mice after 18 days of restraint stress (Extended Data Fig. 9a), with more modest effects observed in the spleen and dCLNs (Extended Data Fig. 9b,c). Hence, these data suggest that psilocybin and MDMA influence meningeal immune-cell abundance through non-cell autonomous mechanisms. Psychedelics can induce vasoconstriction⁵², whereas chronic stress induces vascular dysfunction^{6,15,38,53}. We therefore examined whether psilocybin or MDMA can exert effects on the vasculature to indirectly influence immune-cell abundance. Indeed, we detected expression of type 2 serotonin receptors and *Ntrk2* in non-haematopoietic meningeal cells (Extended Data Fig. 9d). Next, we measured vascularity using a fluorescent dye that binds to the vasculature. Fluorescence signals were significantly increased in mice after 18 days of restraint stress, which were reduced after psilocybin or MDMA racemate treatment (Extended Data Fig. 9e). To determine whether vasoconstriction influences inflammatory monocyte abundance, we treated 18-day stressed mice with psilocybin or MDMA racemate together with the systemic vasodilator nifedipine. The numbers of meningeal inflammatory monocytes were increased in the presence of nifedipine relative to psilocybin or MDMA alone (Extended Data Fig. 9f). By contrast, we did not observe sustained decreases in peripheral corticosterone levels after treatment with a psychedelic, nor did we observe that psychedelic-induced immune-cell redistribution is exclusively controlled by the sympathetic nervous system (Extended Data Fig. 9g–i). Beyond the vasculature, we detected transcription of type 2 serotonin receptors and *Ntrk2* in primary astrocyte cultures (Extended Data Fig. 9j). Functionally, psilocybin or MDMA racemate treatment also reduced astrocyte *Ptprs* expression *in vitro* (Extended Data Fig. 9k). Together, these data point to potential direct and indirect mechanisms by which psychedelics influence physiological responses to chronic stress and neuroimmune interactions.

Validation in humans

To validate our findings in human cells, we treated primary human astrocytes with TNF, IL-6 or IL-1 β in the presence of cortisol. The combination of IL-1 β and cortisol increased *Ptprs* expression, similar to our data in mice (Fig. 5a). *EGFR* expression was also decreased in primary astrocytes treated with IL-1 β and cortisol (Fig. 5b). Next, we used the ImmGen human immune cell atlas to validate the expression of *Htr2a*, *Htr2b*, *Htr2c* and *Ntrk2* in human immune cell subsets in blood, including monocytes (Extended Data Fig. 10a). We then cultured primary human monocytes in the presence or absence of 100 ng ml⁻¹ LPS with or without 10 μ M MDMA racemate or 10 μ M psilocybin. Quantification of bulk RNA-seq data showed that treatment with either drug reduced *Cxcr4* expression and other transcriptional modules (Fig. 5c,d, Extended Data Fig. 10b and Supplementary Tables 16 and 17), results akin to our findings in mice (Fig. 4m,n and Extended Data Fig. 8c–e,h–j).

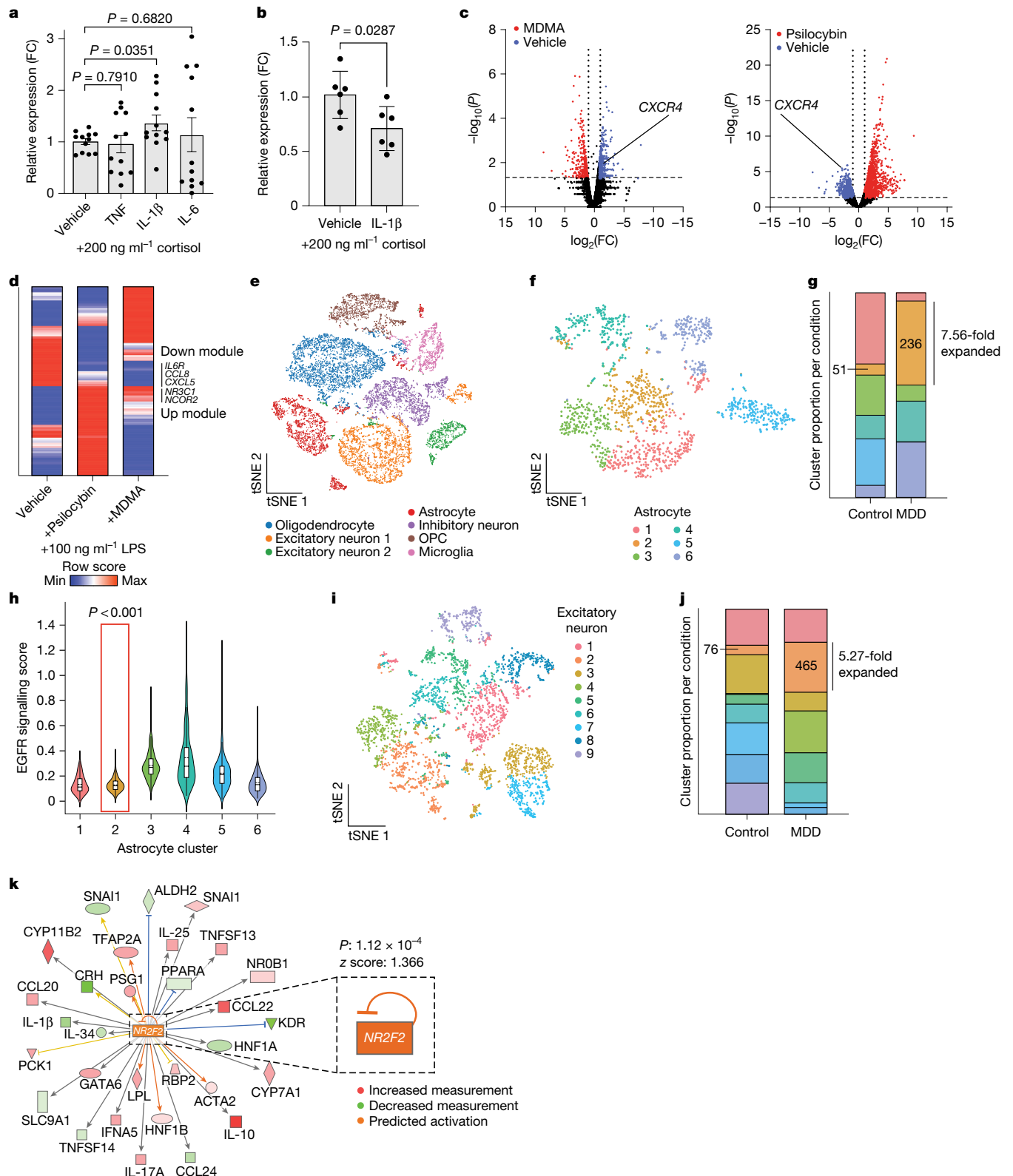


Fig. 5 | Relevance of detected neuroimmune interactions in humans.

a,b, qPCR analysis of *PTPRS* (**a**) and *EGFR* (**b**) expression in primary human astrocytes treated with the indicated compounds for 6 h. $n = 12$ (**a**) or $n = 6$ (**b**) per group. Mann–Whitney test. **c,d**, RNA-seq data from primary human monocytes treated with the indicated compounds for 6 h and shown as a volcano plot (**c**) and a hierarchically clustered heatmap (**d**) from the indicated conditions. $n = 3$ per group. **e**, snRNA-seq analyses of amygdala from healthy individuals (controls) and from patients with MDD. $n = 6$ individuals per group, $n = 13,408$ cells. **f,g**, Subclustered astrocytes (**f**) from (**e**) and bar plot showing

the proportion of each astrocyte subcluster per condition (**g**). $n = 1,511$ cells.

h, Violin plot of EGFR activation scores across all astrocyte clusters from **f**.

i,j, Subclustered excitatory neurons (**i**) and bar plot of the proportion of each cluster per condition (**j**). $n = 3,552$ cells. **k**, Prediction of an *NR2F2* gene regulatory network in cluster 2 excitatory neurons. In violin plots, the solid horizontal line indicates the median, the white box the interquartile range (25th–75th percentile), the whiskers the minimum and maximum values and the dashed line the mean. Data shown as the mean \pm s.e.m.

Article

Finally, to validate our observations in human tissues, we performed single-nucleus RNA-seq (snRNA-seq) on amygdala from 6 patients with MDD and 6 healthy individuals, matched by sex, race and age (Fig. 5e, Extended Data Fig. 10c,d and Supplementary Tables 18 and 19). We recovered 13,408 cells that we assigned to 6 different cell types, including astrocytes, microglia, excitatory neurons, inhibitory neurons, oligodendrocyte precursor cells and oligodendrocytes (Extended Data Fig. 10e,f). Next, we subclustered astrocytes to identify subsets associated with MDD, and found a population expanded in MDD marked by downregulated EGFR signalling (Fig. 5f–h and Supplementary Table 20). Examination of the pathways altered in cluster 1 and cluster 6 astrocytes showed that these two clusters were downregulated and upregulated, respectively, in MDD. In these subsets, we identified altered metabolic, neurotransmitter and extracellular matrix signalling, which have previously been implicated in MDD⁵⁴ (Extended Data Fig. 10g and Supplementary Table 21). We orthogonally validated downregulated EGFR expression in MDD by performing quantitative PCR (qPCR) of bulk patient tissue (Extended Data Fig. 10h) and by immunostaining amygdala astrocyte samples from patients with MDD (Extended Data Fig. 10i). Subclustering of excitatory neurons also revealed a group expanded in MDD that expressed NR2F2 and SLTRK2 and predicted to be controlled by increased NR2F2-driven transcriptional programs (Fig. 5i–k, Extended Data Fig. 10j and Supplementary Table 22). Together, these data suggest that the neuroimmune mechanisms we initially defined in mice may be relevant in humans and in MDD.

Discussion

This study defined mechanisms of astrocyte–neuron crosstalk in the amygdala and their potential regulation by peripheral immune cells in chronic stress and possibly MDD. Together, our results highlight the therapeutic potential of targeting immune mechanisms in neuropsychiatric disorders^{2,5,6,42}. Our data suggest that inflammatory monocytes promote stress-induced fear behaviour, with meningeal recruitment influenced by splenic reservoirs but potentially other peripheral tissues such as the skull bone marrow⁵⁵ or gut⁵⁶. These findings align with studies that have linked inflammatory monocytes to social-reward deficits⁶ and endothelial-cell dysfunction through IL-6 in chronic stress and MDD³⁸. Similar findings have been reported for other classes of immune cells, such as CD4⁺ T cells producing xanthine, which were linked to amygdala oligodendrocyte dysfunction and helplessness behaviour⁵. Moreover, meningeal type 2 innate lymphoid cells have been shown to influence inhibitory-synapse formation in the cortex⁴². Here we also detected astrocyte subsets modulated by diverse cues in chronic stress and potentially MDD. Specifically, we uncovered an interplay between astrocyte EGFR expression and NF-κB signalling, whereby these pathways may exhibit opposing influences on one another to potentially modify stress-induced fear behaviour. Additional work to elucidate the temporal and anatomical variables that influence astrocyte heterogeneity^{11,57} will provide a broader understanding of how neuroimmune interactions modulate astrocyte responses that shape complex behaviours in chronic stress¹¹. For example, EGFR ligands can be produced by brain-resident immune cells, such as amphiregulin produced by microglia²¹, thereby highlighting the need for further investigation of stress-induced neuroimmune interactions.

Our study also underscored the therapeutic potential of psychedelics beyond psychiatry, including in immunology^{52,58}. By using a phenotypic screen of shared properties among two clinically relevant psychedelics, analogous to studies of social behaviour⁵⁰, we found that both psilocybin and MDMA similarly influence immune-cell abundance in tissues. Our data suggest that brain–body communication may be an underappreciated component of psychedelic therapy. However, key unanswered questions remain. First, our study did not resolve the specific molecular mechanisms required for psychedelic-mediated

modulation of immune cells in vivo. Although we focused on certain pathways known to be activated by psychedelics, such as serotonin receptor signalling⁴⁵, defining the precise mechanisms that influence immune and vascular responses to psychedelics in vivo requires causal investigation and could be independent of, or in addition to, serotonin receptor signalling. As psilocybin and MDMA also activate serotonin signalling through complementary mechanisms^{45,46}, future work should also distinguish between these possibilities. Second, control over immune-cell behaviour and neuroimmune interactions by direct or indirect psychedelic effects remains incompletely defined. Our data suggest that psychedelic-induced vasoconstriction may regulate aspects of meningeal immune-cell abundance, with the sympathetic nervous system playing at least some part depending on the psychedelic administered. Nevertheless, the sequence of cellular events that govern immune-cell redistribution in response to psychedelics is unclear, and the definitive combination of cell types required to induce these responses remains to be defined. Last, we did not directly assess the contributions made by immune cells to psychedelic-induced plasticity, although our findings point to links between these concepts. Further research is needed to establish causal cellular and molecular mechanisms by which psychedelics influence tissue physiology more generally, which may reveal psychedelic-responsive pathways with therapeutic applications in unanticipated disorders, including in inflammatory diseases. Methods for forward genetic screening of cell–cell communication²¹, transcript-specific nucleic acid cytometry²² and genetic strategies for investigating psychedelic responsiveness^{59,60} may aid in identifying cell types controlled by psychedelics and the molecular mechanisms that regulate them.

In summary, we uncovered a psychedelic-sensitive neuroimmune signalling axis tuned by the recruitment of inflammatory monocytes to the brain meninges, which influences astrocyte–neuron responses in the amygdala and fear behaviour. Together, our findings suggest that additional work to study neuroimmune interactions and their targeting by psychedelics may lead to new therapeutic targets in both neuropsychiatric and inflammatory diseases.

Online content

Any methods, additional references, Nature Portfolio reporting summaries, source data, extended data, supplementary information, acknowledgements, peer review information; details of author contributions and competing interests; and statements of data and code availability are available at <https://doi.org/10.1038/s41586-025-08880-9>.

1. Wheeler, M. A. & Quintana, F. J. The neuroimmune connectome in health and disease. *Nature* **638**, 333–342 (2025).
2. Poller, W. C. et al. Brain motor and fear circuits regulate leukocytes during acute stress. *Nature* **607**, 578–584 (2022).
3. Chan, K. L., Poller, W. C., Swirski, F. K. & Russo, S. J. Central regulation of stress-evoked peripheral immune responses. *Nat. Rev. Neurosci.* <https://doi.org/10.1038/s41583-023-00729-2> (2023).
4. Cathomas, F. et al. Beyond the neuron: role of non-neuronal cells in stress disorders. *Neuron* **110**, 1116–1138 (2022).
5. Fan, K.-Q. et al. Stress-induced metabolic disorder in peripheral CD4⁺ T cells leads to anxiety-like behavior. *Cell* **179**, 864–879 (2019).
6. Cathomas, F. et al. Circulating myeloid-derived MMP8 in stress susceptibility and depression. *Nature* **626**, 1108–1115 (2024).
7. Pape, K., Tamouza, R., Leboyer, M. & Zipp, F. Immunoneuropsychiatry—novel perspectives on brain disorders. *Nat. Rev. Neurol.* **15**, 317–328 (2019).
8. Hodes, G. E., Kana, V., Menard, C., Merad, M. & Russo, S. J. Neuroimmune mechanisms of depression. *Nat. Neurosci.* **18**, 1386–1393 (2015).
9. Wohleb, E. S., Franklin, T., Iwata, M. & Duman, R. S. Integrating neuroimmune systems in the neurobiology of depression. *Nat. Rev. Neurosci.* **17**, 497–511 (2016).
10. Qing, H. et al. Origin and function of stress-induced IL-6 in murine models. *Cell* **182**, 372–387 (2020).
11. Lee, H.-G., Wheeler, M. A. & Quintana, F. J. Function and therapeutic value of astrocytes in neurological diseases. *Nat. Rev. Drug Discov.* **21**, 339–358 (2022).
12. Byun, Y. G. et al. Stress induces behavioral abnormalities by increasing expression of phagocytic receptor, MERTK, in astrocytes to promote synapse phagocytosis. *Immunity* **56**, 2105–2120 (2023).
13. Leng, L. et al. Menin deficiency leads to depressive-like behaviors in mice by modulating astrocyte-mediated neuroinflammation. *Neuron* **100**, 551–563 (2018).

14. Guayasamin, M. et al. Early-life stress induces persistent astrocyte dysfunction associated with fear generalisation. *eLife* <https://doi.org/10.7554/eLife.99988.2> (2024).
15. Dudek, K. A. et al. Astrocytic cannabinoid receptor 1 promotes resilience by dampening stress-induced blood-brain barrier alterations. *Nat. Neurosci.* <https://doi.org/10.1038/s41593-025-01891-9> (2025).
16. Ollivier, M. et al. Crym-positive striatal astrocytes gate perseverative behaviour. *Nature* **627**, 358–366 (2024).
17. Yu, X. et al. Reducing astrocyte calcium signaling in vivo alters striatal microcircuits and causes repetitive behavior. *Neuron* **99**, 1170–1187 (2018).
18. Suthard, R. L. et al. Basolateral amygdala astrocytes are engaged by the acquisition and expression of a contextual fear memory. *J. Neurosci.* **43**, 4997–5013 (2023).
19. Martin-Fernandez, M. et al. Synapse-specific astrocyte gating of amygdala-related behavior. *Nat. Neurosci.* **20**, 1540–1548 (2017).
20. Cui, Y. et al. Astroglial Kir4.1 in the lateral habenula drives neuronal bursts in depression. *Nature* **554**, 323–327 (2018).
21. Wheeler, M. A. et al. Droplet-based forward genetic screening of astrocyte–microglia cross-talk. *Science* **379**, 1023–1030 (2023).
22. Clark, I. C. et al. Identification of astrocyte regulators by nucleic acid cytometry. *Nature* **614**, 326–333 (2023).
23. Wheeler, M. A. et al. Environmental control of astrocyte pathogenic activities in CNS inflammation. *Cell* **176**, 581–596 (2019).
24. Wheeler, M. A. et al. MAFG-driven astrocytes promote CNS inflammation. *Nature* **578**, 593–599 (2020).
25. Sanmarco, L. M. et al. Gut-licensed IFNy⁺ NK cells drive LAMP1⁺TRAIL⁺ anti-inflammatory astrocytes. *Nature* **590**, 473–479 (2021).
26. Maddox, S. A., Hartmann, J., Ross, R. A. & Ressler, K. J. Deconstructing the gestalt: mechanisms of fear, threat, and trauma memory encoding. *Neuron* **102**, 60–74 (2019).
27. Zeisel, A. et al. Molecular architecture of the mouse nervous system. *Cell* **174**, 999–1014 (2018).
28. LeDoux, J. The amygdala. *Curr. Biol.* **17**, R868–R874 (2007).
29. Wohleb, E. S., Powell, N. D., Godbout, J. P. & Sheridan, J. F. Stress-induced recruitment of bone marrow-derived monocytes to the brain promotes anxiety-like behavior. *J. Neurosci.* **33**, 13820–13833 (2013).
30. Zheng, Z.-H. et al. Neuroinflammation induces anxiety- and depressive-like behavior by modulating neuronal plasticity in the basolateral amygdala. *Brain Behav. Immun.* **91**, 505–518 (2021).
31. Linnerbauer, M. et al. The astrocyte-produced growth factor HB-EGF limits autoimmune CNS pathology. *Nat. Immunol.* **25**, 432–447 (2024).
32. Sun, W. et al. Spatial transcriptomics reveal neuron–astrocyte synergy in long-term memory. *Nature* **627**, 374–381 (2024).
33. Luo, F. et al. Modulation of proteoglycan receptor PTPr enhances MMP-2 activity to promote recovery from multiple sclerosis. *Nat. Commun.* **9**, 4126 (2018).
34. Tonks, N. K. Protein tyrosine phosphatases: from genes, to function, to disease. *Nat. Rev. Mol. Cell Biol.* **7**, 833–846 (2006).
35. Won, S. Y., Lee, P. & Kim, H. M. Synaptic organizer: slitrks and type IIa receptor protein tyrosine phosphatases. *Curr. Opin. Struct. Biol.* **54**, 95–103 (2019).
36. Hochgerner, H. et al. Neuronal types in the mouse amygdala and their transcriptional response to fear conditioning. *Nat. Neurosci.* <https://doi.org/10.1038/s41593-023-01469-3> (2023).
37. Santiago, A. C. & Shammah-Lagnado, S. J. Efferent connections of the nucleus of the lateral olfactory tract in the rat. *J. Comp. Neurol.* **471**, 314–332 (2004).
38. Menard, C. et al. Social stress induces neurovascular pathology promoting depression. *Nat. Neurosci.* **20**, 1752–1760 (2017).
39. Clark, S. M., Soroka, J. A., Song, C., Li, X. & Tonelli, L. H. CD4⁺ T cells confer anxiolytic and antidepressant-like effects, but enhance fear memory processes in Rag2^{-/-} mice. *Stress* **19**, 303–311 (2016).
40. Rustenhoven, J. & Kipnis, J. Brain borders at the central stage of neuroimmunology. *Nature* **612**, 417–429 (2022).
41. Marin-Rodero, M. et al. The meninges host a distinct compartment of regulatory T cells that preserves brain homeostasis. *Sci. Immunol.* **10**, eadu2910 (2025).
42. Barron, J. J. et al. Group 2 innate lymphoid cells promote inhibitory synapse development and social behavior. *Science* **386**, eadi1025 (2024).
43. Dai, W. et al. A functional role of meningeal lymphatics in sex difference of stress susceptibility in mice. *Nat. Commun.* **13**, 4825 (2022).
44. McKim, D. B. et al. Sympathetic release of splenic monocytes promotes recurring anxiety following repeated social defeat. *Biol. Psychiatry* **79**, 803–813 (2015).
45. Kwan, A. C., Olson, D. E., Preller, K. H. & Roth, B. L. The neural basis of psychedelic action. *Nat. Neurosci.* **25**, 1407–1419 (2022).
46. Green, A. R., Mechan, A. O., Elliott, J. M., O’Shea, E. & Colado, M. I. The pharmacology and clinical pharmacology of 3,4-methylenedioxymethamphetamine (MDMA, “ecstasy”). *Pharmacol. Rev.* **55**, 463–508 (2003).
47. Shao, L.-X. et al. Psilocybin induces rapid and persistent growth of dendritic spines in frontal cortex in vivo. *Neuron* **109**, 2535–2544 (2021).
48. Goodwin, G. M. et al. Single-dose psilocybin for a treatment-resistant episode of major depression. *N. Engl. J. Med.* **387**, 1637–1648 (2022).
49. Mitchell, J. M. et al. MDMA-assisted therapy for moderate to severe PTSD: a randomized, placebo-controlled phase 3 trial. *Nat. Med.* <https://doi.org/10.1038/s41591-023-02565-4> (2023).
50. Nardou, R. et al. Psychedelics reopen the social reward learning critical period. *Nature* **618**, 790–798 (2023).
51. Nardou, R. et al. Oxytocin-dependent reopening of a social reward learning critical period with MDMA. *Nature* **569**, 116–120 (2019).
52. Flanagan, T. W. & Nichols, C. D. Psychedelics as anti-inflammatory agents. *Int. Rev. Psychiatry* **30**, 363–375 (2018).
53. Lehmann, M. L., Poffenberger, C. N., Elkahloun, A. G. & Herkenham, M. Analysis of cerebrovascular dysfunction caused by chronic social defeat in mice. *Brain Behav. Immun.* **88**, 735–747 (2020).
54. Daskalakis, N. P. et al. Systems biology dissection of PTSD and MDD across brain regions, cell types, and blood. *Science* **384**, eadh3707 (2024).
55. Cugurra, A. et al. Skull and vertebral bone marrow are myeloid cell reservoirs for the meninges and CNS parenchyma. *Science* **373**, eabf7844 (2021).
56. Singh, V. et al. Microbiota dysbiosis controls the neuroinflammatory response after stroke. *J. Neurosci.* **36**, 7428–7440 (2016).
57. Endo, F. et al. Molecular basis of astrocyte diversity and morphology across the CNS in health and disease. *Science* **378**, eadc9020 (2022).
58. Kyzar, E. J., Nichols, C. D., Gainetdinov, R. R., Nichols, D. E. & Kalueff, A. V. Psychedelic drugs in biomedicine. *Trends Pharmacol. Sci.* **38**, 992–1005 (2017).
59. Chiu, Y.-T. et al. A suite of engineered mice for interrogating psychedelic drug actions. Preprint at *bioRxiv* <https://doi.org/10.1101/2023.09.25.559347> (2023).
60. Muir, J. et al. Isolation of psychedelic-responsive neurons underlying anxiolytic behavioral states. *Science* **386**, 802–810 (2024).

Publisher’s note Springer Nature remains neutral with regard to jurisdictional claims in published maps and institutional affiliations.

Springer Nature or its licensor (e.g. a society or other partner) holds exclusive rights to this article under a publishing agreement with the author(s) or other rightsholder(s); author self-archiving of the accepted manuscript version of this article is solely governed by the terms of such publishing agreement and applicable law.

© The Author(s), under exclusive licence to Springer Nature Limited 2025

Article

Methods

Mice

Mice were group-housed under a standard light cycle (12-h light–dark; lights on from 7:00 to 19:00) at 20–23 °C and about 50% humidity with ad libitum access to water and food. Genotypes were confirmed by qPCR (Transnetyx). All mice were 2–3 months old at the start of tube restraint, fear conditioning and stereotaxic injection experiments. Adult male mice 8–10 weeks old and postnatal day 0 (PO)–P3 pups were used on a C57Bl/6J background (The Jackson Laboratory, 000664). Male NOD. Cg-*Prkdc*^{scid}/*Il2rg*^{tm1Wjl}/*SzJ* mice (NSG, The Jackson Laboratory, 005557) were used for adoptive-transfer studies^{61,62}. B6N.FVB-Tg(Aldh1l-cre/ERT2)1Khakh/J mice⁶³ (The Jackson Laboratory, 031008) were bred to B6.Cg-Gt(ROSA)26Sor^{tm9(CAG-tdTOMO)Hze}/J mice⁶⁴ (The Jackson Laboratory, 007909) to produce *Aldh1l*¹*TdTomato*^{+/+} reporter mice. When *Aldh1l*¹*TdTomato*^{+/+} reporter mice were used, administration of two doses of 225 mg kg⁻¹ tamoxifen (Sigma-Aldrich, T5648) diluted in corn oil (Sigma-Aldrich, C8267) was administered 2 days apart before starting experiments 1 week later. TdTomato induction was confirmed by flow cytometry. C57Bl/6-Gt(ROSA)26Sor^{tm1(HBEGF)Awai}/J female mice⁶⁵ (The Jackson Laboratory, 007900) were bred to C57Bl/6-*Ccr2*^{tm1(cre/ERT2)Peng}/J male mice⁶⁶ (The Jackson Laboratory, 035229) to generate *Ccr2*^{DTR/+} mice. When *Ccr2*^{DTR/+} mice were used, 200 mg kg⁻¹ tamoxifen (Sigma-Aldrich, T5648) diluted in corn oil (Sigma-Aldrich, C8267) was administered by oral gavage 4 days before starting experiments and every 4 days for the duration of experiments. Mice received 200 mg kg⁻¹ tamoxifen on days -4, 0 and 4, then received 100 mg kg⁻¹ tamoxifen every 4 days for the remainder of the experiments. Diphtheria toxin (5 µg kg⁻¹; Sigma-Aldrich, D0564) diluted in 1× PBS was administered by intraperitoneal injection 2 days before starting experiments and every 4 days after the start of the experiments. Depletion of cells expressing *Ccr2* was confirmed by flow cytometry. Male Tg(CAG-Kaede)15Kgwa mice were used on a C57Bl/6J background⁶⁷. All procedures were approved by the Brigham and Women's Hospital's Institutional Animal Care and Use Committee.

Restraint stress

Tubes were washed with 70% ethanol before each use. Around 30–40 air holes were drilled using a 1/16-inch drill bit into 50 ml conical tubes (Falcon) for proper ventilation. Mice were placed into tubes and placed horizontally in a tube rack for 6 h each day for up to 18 consecutive days. Stress sessions were started daily between 9:00 and 10:00. After restraint, mice were returned to their cages and the tubes were washed with soap, water and 70% ethanol.

Contextual fear conditioning

Fear conditioning was performed largely as we and others have previously done but with slight modifications^{68,69}. Mice were habituated to the testing room 30 min–1 h each day before the start of fear conditioning and testing of freezing behaviour. The testing room was isolated, dimly lit and kept consistent for each experiment. Trials were recorded for downstream analyses. For fear acquisition, mice were placed in a 22 × 22 cm mouse shuttle box (Maze Engineers) with the escape door closed and with black walls scented with 0.1% banana (Shank's Extracts, S90159) in 70% ethanol. Following a 2-min habituation period, mice were presented with a white-noise tone and chamber light–shock pairings (5 kHz, 70 dB), which consisted of 30 s of white noise and chamber light co-terminating with 1 s of a 0.7 mA foot shock. Intertrial intervals were 30 s. Mice remained in the chamber for 30 s after the fifth and final trial before being returned to their home cage. The shock chamber was washed with 0.1% banana-containing 70% ethanol between each mouse. After 1 day of fear acquisition, mice underwent testing of freezing behaviour in response to the conditioned stimulus. Mice were placed in an unfamiliar chamber with white walls scented with 0.1% lemon (Shank's Extracts, S90066) in 70% ethanol. Following 2 min of habituation, mice received the same visual and auditory cues as for the

fear-acquisition condition with the same intertrial interval but did not receive a footshock. After the fifth and final trial, mice remained in the chamber for 30 s before being returned to their home cage. Analyses of videos were performed using the Noldus EthoVision system (Noldus Information Technology, v.17.0), and for activity analysis, the activity threshold set at 11. Mice with an activity state below 0.2% were considered to be in the freezing posture, in which the mice exhibited no movement other than breathing. Periodically, automated data analysis was independently validated by manual scoring to confirm accuracy. The freezing ratio was calculated as the time spent freezing divided by the total duration of the period in which mice were exposed to the conditioned stimulus (30 s). For analyses of the effects of treatment with a psychedelic during fear behaviour, mice were first subjected to fear acquisition, then 24 h later were administered either 1 mg kg⁻¹ psilocybin or 10 mg kg⁻¹ MDMA. At 2 h after administration, mice underwent fear extinction, similar to previous studies⁷⁰.

EPM task

After 30 min of habituation in the behavioural room, mice were placed in the centre of the EPM, which consisted of two open and two closed arms. The arms measured 35 cm in length, with the maze elevated 61 cm above the ground and the closed arms surrounded by 20-cm-high walls with 1-cm-high end plates to prevent mice from falling (Maze Engineers). The room lighting was set to 100 lux to ensure no shadows on any of the arms of the maze. Behaviour was recorded over a 5-min session. After each trial, all arms and the centre area of the maze were cleaned with 70% ethanol followed by distilled water. The time spent in the open arms and closed arms were automatically analysed using Noldus EthoVision XT software (Noldus Information Technology, v.17.0). Data are shown as the ratio of the time spent in open versus closed arms.

Flow cytometry of tdTomato⁺ cells

Transgenically labelled tdTomato⁺ cells were sorted largely as previously described^{24,25,71}. In brief, mice were perfused with 1× PBS and the CNS was isolated into 10 ml enzyme digestion solution consisting of 75 µl papain suspension (Worthington, LS003126) diluted in enzyme stock solution (ESS) and equilibrated to 37 °C. ESS consisted of 10 ml 10× EBSS (Sigma-Aldrich, E7510), 2.4 ml 30% D(+)-glucose (Sigma-Aldrich, G8769), 5.2 ml 1 M NaHCO₃ (VWR, AAJ62495-AP), 200 µl 500 mM EDTA (Thermo Fisher Scientific, 15575020) and 168.2 ml ddH₂O, filter-sterilized through a 0.22 µm filter. Samples were shaken at 80 r.p.m. for 30–40 min at 37 °C. Enzymatic digestion was stopped with 1 ml of 10× hi ovomucoid inhibitor solution and 20 µl 0.4% DNase (Worthington, LS002007) diluted in 10 ml inhibitor stock solution (ISS). The 10× hi ovomucoid ISS contained 300 mg BSA (Sigma-Aldrich, A8806), 300 mg ovomucoid trypsin inhibitor (Worthington, LS003086) diluted in 10 ml 1× PBS and filter-sterilized through a 0.22 µm filter. ISS contained 50 ml 10× EBSS (Sigma-Aldrich, E7510), 6 ml 30% D(+)-glucose (Sigma-Aldrich, G8769), 13 ml 1 M NaHCO₃ (VWR, AAJ62495-AP) diluted in 170.4 ml ddH₂O and filter-sterilized through a 0.22 µm filter. Tissue samples were mechanically dissociated using a 5 ml serological pipette and filtered through a 70 µm cell strainer (Fisher Scientific, 22363548) into a fresh 50 ml conical tube. Tissue samples were centrifuged at 500g for 5 min and resuspended in 10 ml of 30% Percoll solution (9 ml Percoll (GE Healthcare Biosciences, 17-5445-01), 3 ml 10× PBS and 18 ml ddH₂O). The Percoll suspension was centrifuged at 500g for 25 min with no brake. The supernatant was discarded and the cell pellet was washed once with 1× PBS, centrifuged at 500g for 5 min and prepared for downstream applications. Cells were sorted on a FACS Aria IIu (BD Biosciences). For gating of tdTomato⁺ cells, tdTomato fluorescence was judged against a wild-type control animal using a yellow-green laser on a FACS Aria IIu.

Drop-seq

Drop-seq was performed as previously described^{24,72}. A microfluidic mask was fabricated at 125 µm in height using soft lithography.

Curing agent and PDMS prepolymer (Momentive, RTV615) were mixed 1:10 and degassed in a vacuum chamber. The PDMS mixture was poured onto the master mould, further degassed and baked at 65 °C for 4 h. The PDMS replica was punched with a 0.75-mm biopsy punch (Harris Uni-Core) and bonded to a glass slide (75 × 50 × 1.0 mm, Fisher Scientific, 12-550C) using a plasma bonder (Technics Plasma Etcher 500-II). The device was placed on a hot plate at 150 °C for 10 min, baked at 65 °C for 4 h and treated with Aquapel to render it hydrophobic. A cell suspension was prepared using flow-cytometry-sorted cells from mouse brain. Cells were counted and resuspended at 250,000 cells per ml (final concentration of 125 cells per μ l) in PBS and 16% Opti-prep (Sigma-Aldrich, D1556-250ML). The cell mixture was loaded into a 3 ml syringe (BD Biosciences, 309657) with a 27 gauge needle (BD Biosciences, 305109) and connected to the microfluidic device using tubing (Scientific Commodities, BB31695-PE/2). Barcoded beads (Fisher Scientific, NC0927472) were resuspended in lysis buffer consisting of 57% Opti-prep (Sigma-Aldrich, D1556-250ML), 2.4% Ficoll PM-400 (GE Healthcare, 17-0300-10), 0.2% Sarkosyl (Teknova, S3376), 20 mM EDTA pH 8.0, 200 mM Tris-HCl pH 7.4 (Sigma-Aldrich, T2663-1L) and 50 mM DTT (Sigma-Aldrich, 646563-10X.5ML) at a concentration of 300,000 beads per ml. Beads resuspended in lysis buffer were loaded into a 3 ml syringe with a magnetic mixing disc (V&P Scientific, 772DP-N42-5-2) and gently stirred during encapsulation using a magnetic mixer (V&P Scientific, 71OD2). A third syringe was loaded with oil for droplet generation (Bio-Rad, 186-4006). To perform Drop-seq experiments, pumps were run at 1,500 μ l h⁻¹ (cell mixture), 1,500 μ l h⁻¹ (barcoded beads) and 4,500 μ l h⁻¹ (oil) for approximately 15 min per sample. Droplets were collected, broken with 1H,1H,2H,2H-perfluoro-1-octanol (PFO) (Sigma-Aldrich, 370533), added at a ratio of 1:3 PFO:oil, washed with 10 ml 6× SSC (National Diagnostics, EC-873) and centrifuged for 1 min at 1,000g. Beads at the interface were removed, oil was eliminated and beads were washed 3 times with 6× SSC. Beads were then washed with Maxima H-minus 1× reverse transcriptase (RT) buffer (Thermo Fisher Scientific, EP0753) and were resuspended in 50 μ l Maxima H-minus 1× RT buffer. The following RT mixture was added to each tube of beads: 40 μ l 20% Ficoll PM-400, 30 μ l 5× Maxima H-minus RT buffer, 2 μ l 100 mM dNTPs (Life Technology, 4368813), 5 μ l 100 μ M template switching oligonucleotide primer (IDT), 5 μ l RNase inhibitor (Lucigen, 30281-2), 58 μ l nuclease-free water and 10 μ l Maxima H-minus RT (Thermo Fisher Scientific, EP0753). Beads suspended in RT mixture were incubated at room temperature for 30 min on an inverter, followed by 90 min at 42 °C on an inverter. Following reverse transcription, beads were washed once with 1 ml TE-SDS (10 mM Tris-HCl pH 8.0, 1 mM EDTA pH 8.0 and 0.5% SDS) and twice with TE-TW (10 mM Tris-HCl pH 8.0, 1 mM EDTA pH 8.0 and 0.01% Tween-20) and pelleted during each step by centrifuging at 1,000g for 1 min. Beads were washed once with 10 mM Tris-HCl pH 8.0 and resuspended in exonuclease mix consisting of 170 μ l nuclease-free water, 20 μ l 10× exonuclease I buffer and 10 μ l exonuclease I (Thermo Fisher Scientific, EN0582). Resuspended beads were incubated for 45 min at 37 °C with inversion. After treatment, beads were washed once with TE-SDS, twice with TE-TW and twice with nuclease-free water. Beads were counted and resuspended at a concentration of 80 beads per μ l in preparation for PCR. Beads were then added to a PCR tube at a concentration of 2,000 beads per tube. PCR mix (25 μ l HiFi HotStart ReadyMix (Kapa Biosystems, KK2602); 0.4 μ l 100 μ M SMART PCR primer (IDT)) was added to each tube and beads were manually mixed before PCR. PCR cycling conditions were as follows: 95 °C (3 min); 4 cycles of 98 °C (20 s), 65 °C (45 s) and 72 °C (3 min); 9 cycles of 98 °C (20 s), 67 °C (20 s) and 72 °C (3 min); 72 °C (5 min); and 4 °C hold. After PCR, cDNA samples were purified in a 96-well plate (Bio-Rad, HSP9611) on a magnetic stand (NEB, S151S) using Agencourt AMPure XP magnetic beads (Beckman Coulter, A63881) at a 0.6× ratio according to the standard protocol. The sample from each PCR tube was eluted in 10 μ l nuclease-free water, and technical replicates were pooled after elution. cDNA was run on a Bioanalyzer High Sensitivity DNA chip (Agilent Technologies, 5067-4626) on a 2100

Bioanalyzer (Agilent). For cDNA library fragmentation, 600 pg cDNA in 5 μ l was added to 10 μ l Nextera Tagment DNA buffer and 5 μ l Amplicon Tagment mix (Illumina, FC-131-1096). cDNA was fragmented at 55 °C for 5 min, followed by the addition of room-temperature-equilibrated 5 μ l Neutralize Tagment buffer (Illumina, FC-131-1096). Samples sat at room temperature for 5 min followed by the addition of 15 μ l Nextera PCR mix (Illumina, FC-131-1096), 8 μ l nuclease-free H₂O, 1 μ l 10 μ M New-P5-SMART PCR hybrid oligonucleotide (IDT) and 1 μ l of 10 μ M Nextera indexing oligonucleotide (Invitrogen). Samples underwent PCR using the following conditions: 95 °C (30 s); 12 cycles of 95 °C (10 s), 55 °C (30 s) and 72 °C (30 s); 72 °C (5 min); and 4 °C hold. Fragmented libraries were purified using Agencourt AMPure XP magnetic beads at a 0.6× ratio according to the manufacturer's protocol and eluted in 10 μ l nuclease-free H₂O. Samples were then run on a Bioanalyzer 2100 to assess library size. Libraries were quantified by qPCR using a Library Quantification kit (Kapa Biosystems, KK4824). Fragmented libraries were pooled at 5 nM concentration and sequenced using a NovaSeq S1 at the Broad Institute using a custom read 1 primer and 20 + 80 bp reads. Raw fastq files were processed as we previously described^{21,22,24,25,71} using the DropSeq Resources pipeline⁷² aligned against the mm10 mouse genome assembly. A digital count matrix was then generated for downstream processing. Thresholds for cells included in the analysis were 200–3,000 genes expressed per cell, at least 2 cells expressing a gene and <50% mitochondrial reads. Statistics per cell for those included in the final dataset were 447 genes, 772 unique molecular identifiers (UMIs) and 6.2% mitochondrial reads per cell. Data were normalized by read counts and highly variable genes were extracted. Data were then filtered and scaled, followed by principal component analysis. Trajectories were created using RNA velocity in scanpy⁷³. In brief, we drew a force-directed graph, determined spliced and unspliced transcripts, developed a pseudotime kernel and computed a transition matrix that was superimposed on the UMAP embedding. Differential expression analysis was performed by comparing each cluster to all others using scanpy.tl.rank_genes_groups, which were then used in downstream analyses such as Qiagen IPA by using the FC of the cluster of interest relative to all others.

Plasma collection

Blood was removed from the aorta with a 21 gauge needle (Becton Dickinson, 305165) and placed in a blood-collection tube containing the anti-coagulant heparin (Becton Dickinson, 365965) on ice. Blood was centrifuged at 4 °C for 10 min at 5,000g, and the upper, clear layer comprising the plasma was transferred to a 1.5-ml Eppendorf tube. Plasma was stored at –80 °C and used for downstream multiplexed Luminex assays.

Multiplexed Luminex assays

Multiplexing analysis was performed using a Luminex 200 system. For some samples, two markers were simultaneously measured in the samples using a Human Circadian/Stress Panel 2-Plex custom assay (MilliporeSigma, HNCSMAG-35K) according to the manufacturer's protocol. The 2-plex consisted of cortisol and melatonin. Assay sensitivity was >4.3 pg ml⁻¹. For a second set of samples, a mouse high-sensitivity 18-plex discovery assay (MilliporeSigma, FCYTMAG20KPKX19BK) was used according to the manufacturer's protocol. The 18-plex consisted of GM-CSF, IFN γ , IL-1 α , IL-1 β , IL-2, IL-4, IL-5, IL-6, IL-7, IL-10, IL-12(p70), IL-13, IL-17A, KC/CXCL1, LIX, MCP-1, MIP-2 and TNF. The assay sensitivity for each marker was >0.06 pg ml⁻¹.

Cloning of AAV vectors

Constructs were derived from the pAAV-FLEX-SaCas9-U6-sgRNA backbone (Addgene, 124844), a gift from L. Zweifel⁷⁴. The FLEX-containing portion was eliminated by PCR-based amplification of saCas9 using the forward primer 5'- AAAGTCGACGGCGGCCATGGC CCCAAAGAAGCGGAA-3' and the reverse primer 5'-TTTGAATTC

Article

TTAACGCGTAATCTGGAAACATCGT-3', followed by restriction digest using EcoRI-HF (NEB, R3101S) and Sall-HF (NEB, R0138S). Successfully cloned plasmids were sequenced by Plasmidsaurus. The plasmid was then digested with XbaI (NEB, R0145S) and Sall-HF (NEB, R0138S) in nuclease-free water (Thermo Fisher Scientific, AM9937) and CutSmart buffer. The linearized plasmid was run on a gel and purified (Qiagen, 28704). To substitute promoters, the *GfaABC1D* and *hSyn* promoters were amplified by PCR, PCR-purified (Qiagen, 28104) and digested with XbaI (NEB, R0145S), Sall-HF (NEB, R0138S) and DpnI (NEB, R0176S) in CutSmart buffer. The inserts were ligated into the plasmid with T4 DNA ligase (NEB, M0202S) in nuclease-free water (Thermo Fisher Scientific, AM9937) and T4 DNA ligase reaction buffer, and proper cloning was confirmed by whole-plasmid sequencing (Plasmidsaurus). For cloning CRISPR single-guide RNAs (sgRNAs), the sgRNA oligonucleotides were phosphorylated at 37 °C in PNK (NEB, M0201S) and ligase buffer. Subsequently, the phosphorylated oligonucleotides were placed in a heat block at 100 °C for 5 min and allowed to cool to room temperature for 1–2 h. The parent plasmids containing the promoters were digested with Bsal-HFv2 (NEB, R3733S) in CutSmart buffer and PCR-purified (Qiagen, 28104) into 50 µl EB buffer. Next, 4 µl PCR-purified plasmid was added to 10 µl annealed oligonucleotide mix with 1 µl T4 DNA ligase (NEB, M0202S) and incubated for 2 h at room temperature. Ligation products were transformed into NEB stable competent *Escherichia coli* (NEB, C3040H) and plated on LB agarose (Thermo Fisher Scientific, MP113002221) plates with ampicillin (Thermo Fisher Scientific, 11593027) at 37 °C overnight. Successful colonies were grown overnight in LB broth (Thermo Fisher Scientific, 50488764) supplemented with ampicillin (Thermo Fisher Scientific, 11593027). Cultures were purified (Qiaprep Spin Miniprep, 27104) and digested with HindIII-HF (NEB, R3104S) and BsaI-HFv2 (NEB, R3733S) in CutSmart buffer to confirm cloning of sgRNAs. Successful colonies were stored in 50% glycerol (Sigma Aldrich, G5516) at –80 °C. All sgRNA oligonucleotides were used at a concentration of 100 µM, desalting and scaled at 25 nmol (Thermo Fisher Scientific, custom standard DNA oligonucleotides). sgRNA sequences were designed for saCas9 cutting using CRISPICK: mouse GRCh38 reference genome. Sequences were chosen by focusing on those cutting >5% of the gene and targeting the most upstream exon position.

The following genes were targeted for KD using the pAAV-GfaABC1D-saCas9-U6-sgRNA delivery system: *Rosa26* forward, 5'-AAA CTCAGAGAGCCTCGGTAGGTA-3' and *Rosa26* reverse, 5'-CACCTACCT AGCCGAGGCTCTCTGAGTTT-3'; *Egfr* forward, 5'-CACCCATTGCCCTC AACACCGTGGGA-3' and *Egfr* reverse, 5'-AAACTCCACGGTGTGAGG GCAATG-3'; *Ptprs* forward, 5'-CACCCATGAATTGTGATTCGCCCA-3' and *Ptprs* reverse, 5'-AAACTGGCGAAATCACAATTATG-3'.

The following genes were targeted for KD using the pAAV-hSyn-saCas9-U6-sgRNA delivery system: *Rosa26* forward, 5'-AAACTCA GAGAGCCTCGGTAGGTA-3' and *Rosa26* reverse, 5'-CACCTACCTAGC CGAGGCTCTCTGAGTTT-3'; *Nr2f2* forward, 5'-CACCGCTGCTGCTGC TTGTCGCTGC-3' and *Nr2f2* reverse, 5'-AAACCGAGCAGCACAAGCAGC AGCAGC-3'; *Ets1* forward, 5'-CACCGAGGATCTTCAAAAGCGTTAA-3' and *Ets1* reverse, 5'-AAACTTAACGCTTTGAAGATCCTC-3'; *Cebpg* forward, 5'-CACCGTCGAGCCAGCCACTACTCC-3' and *Cebpg* reverse, 5'-AAACGGAGTAGTGCGCTGGCTGCGAC-3'; *Slitrk2* forward, 5'-CAC CAGCTGATAGTCGATACTGG-3' and *Slitrk2* reverse, 5'-AAACCCAGT ATCGCATCTATCAGCT-3'.

AAV production

To produce AAVs, previously described protocols were largely followed^{75,76}. In brief, pAAV2/5 (Addgene, 104964, a gift from M. Fan), pAdDeltaF6 (Addgene, 112867, a gift from J. M. Wilson), pAAV-GfaABC1D-saCas9-U6-sgRNA and pAAV-hSyn-saCas9-U6-sgRNA were maxi prepped (Qiagen, 12863). AAVpro 293T cells (Takara, 632273) were grown to confluence in DMEM (Life Technologies, 11965092) supplemented with 10% FBS (Life Technologies, 10438026) and

1% penicillin–streptomycin (Life Technologies, 15140122) in 150 mm tissue-culture plates (Corning, 353025). Medium was changed to DMEM (Life Technologies, 11965092) supplemented with 2% FBS (Life Technologies, 10438026) 2 h before transfection. For transfection, 11.4 µg pAAV2/5 (Addgene, 104964), 5.7 µg pAdDeltaF6 (Addgene, 112867) and 2.9 µg pAAV-GfaABC1D-saCas9-U6-sgRNA or pAAV-hSyn-saCas9-U6-sgRNA were pooled in 500 µl Opti-MEM I reduced-serum medium (Thermo Fisher Scientific, 31985070). Next, 80 µl of 1 mg ml⁻¹ PEI MAX (Polysciences, 49553-93-7) in nuclease-free water (Thermo Fisher Scientific, AM9937) was added to 500 µl Opti-MEM I reduced-serum medium (Thermo Fisher Scientific, 31985070) and incubated for 5 min at room temperature. The PEI and Opti-MEM solution was added to the Opti-MEM solution containing the plasmids, vortexed and incubated at room temperature for 20 min. The transfection solution was then added dropwise to the 293T cells (Takara, 632273), and the plate was gently swirled to mix the solution. After 24 h, the medium was removed and 20 ml DMEM (Life Technologies, 11965092) supplemented with 10% FBS (Life Technologies, 10438026) and 1% penicillin–streptomycin (Life Technologies 15140122) was added to the plate. The medium was collected in a 250 ml solution bottle 48 h after the medium change, stored at 4 °C and replaced with another 20 ml DMEM (Life Technologies, 11965092) supplemented with 10% FBS (Life Technologies, 10438026) and 1% penicillin–streptomycin (Life Technologies, 15140122). The medium was collected after another 48 h and pooled into the 250 ml solution bottle. Next, 2 ml of 1× PBS was added to the tissue-culture plate and cells were detached with a cell scraper (Westnet, 229311). The cells were pooled into the 250 ml solution bottle with the collected medium, and residual cells were removed with 10 ml of 1× PBS and collected into the 250 ml solution bottle. The medium and cells were centrifuged for 15 min at 2,000g at room temperature and supernatant was collected. Next, 400 g PEG8000 (Millipore Sigma, P5413) and 146.1 g NaCl (Millipore Sigma, SX0420-3) were dissolved in 1 litre ddH₂O. The viral supernatant was removed and incubated with 1:4 volume of 40% w/v PEG8000 and 2.5 M NaCl solution for 2 h on ice or overnight followed by centrifugation at 4,000g for 30 min at 4 °C. Next, 9.22 g NaCl (Millipore Sigma, SX0420-3), 4.85 g Tris base (MP Biomedicals, 819620) and 2.03 g MgCl₂·6H₂O (Macron Fine Chemicals, 5958-04) were dissolved in 1 litre of distilled water to make SAN buffer. SAN (700 U; Arcticzymes, 70910202) was added to 7 ml SAN buffer, and the supernatant pellet was resuspended in 1 ml of SAN + SAN buffer. The remaining viral pellet was resuspended with 5 ml of SAN + SAN buffer and both suspensions were incubated in a water bath for 1 h at 37 °C. The cell suspensions were centrifuged for 10 min at 2,000g at 4 °C. Supernatant was collected, and an equivalent volume of chloroform (Millipore Sigma, J67341) was added to each tube. The solution was vortexed for 3 min and spun down for 10 min at 4,000g at 4 °C. Ammonium sulfate (Millipore Sigma, A4418) was dissolved in distilled water to make 40% w/v ammonium sulfate solution. PEG8000 (Millipore Sigma, P5413) was dissolved in distilled water to make 40% PEG8000 solution. PEG8000 and ammonium sulfate solution were combined with virus to a final concentration of 10% and 13.2%, respectively. The solution was vortexed and incubated at room temperature for 20 min. After incubation, the solution was centrifuged for 15 min at 3,000g at 25 °C, and the clear, bottom layer containing AAV was removed with a syringe. The AAV was transferred to an Amicon ultra-15 centrifugal filter unit (EMD Millipore, UFC910024) and centrifuged for 15 min at 3,000 r.p.m. at 4 °C. Next, 10 ml of 1× PBS was added to the Amicon ultra-15 centrifugal filter unit (EMD Millipore, UFC910024) once the volume of AAV was at 1 ml, and the AAV was centrifuged for 15 min at 3,000 r.p.m. at 4 °C. This process was repeated for a total of 3 times with 1× PBS. The total volume was then brought to 200 µl, and the virus was stored at –80 °C. AAV was titrated with a qPCR AAV Titer kit (Applied Biological Materials, G931) according to the manufacturer's protocol. AAVs-CamKIIa-mCherry was a gift from K. Deisseroth (Addgene virus prep, 114469-AAV5).

Stereotaxic injections

Intracranial injections were used to deliver concentrated AAV to mice, similar to previous studies^{21–25,71}. Mice were anaesthetized with 1–3% isoflurane (Covetrus, 11695067772) in oxygen. Heads were shaved and cleaned with ethanol and betadine (Thermo Fisher, 19-027132) and a small incision was made in the skin with a scalpel (Exel International, 29550). Bilateral injections were made targeting the midpoint of the BLA with a 5 µl Hamilton syringe (Sigma-Aldrich, 20787) at ±3.3 mm (lateral), −1.6 mm (posterior) and −4.5 mm (ventral) relative to Bregma using a stereotaxic alignment system (Kopf, 1900) or an atlas-integrated robotic stereotaxic system (Neurostar). Virus was injected at a rate of 75 nl min^{−1} over 4 min. After injection, the needle remained at the injection site for 10 min before being withdrawn at a rate of 1 mm min^{−1}. Mice were sutured (Ethicon, 1667H) and allowed to recover in a clean cage on a heating pad for 1 h. Instruments were sterilized between each mouse using a glass bead sterilizer (CellPoint Scientific, GRM5-1450). Mice recovered for >2 weeks before experimental use. Stereotaxic targeting and KD were validated by immunostaining, genomic identification of marker genes and/or integration with previously published genomic samples. For analysis of BLA coverage by excitatory neurons, AAV targeting either *Nr2f2* or *Rosa26* was injected into the same mouse in opposing hemispheres, with a 1:10 dilution of AAV5-CaMKIIα::mCherry. In these experiments, mice underwent restraint stress, fear conditioning and fear extinction.

Forced-swim test

Mice were habituated to the testing room 30 min–1 h each day before the start of the forced-swim test. Mice were placed in a 2,000 ml glass beaker (Corning, 1,000 2 litres) filled with 1,300 ml water at 20–22 °C and recorded for 6 min. Following the end of the 6-min duration, mice were returned to their home cage on a heating pad and monitored for 30 min. To quantify behaviour during the forced-swim assay, we trained a model using DeepLabCut^{77,78} to systematically quantify swimming behaviour in this assay. In brief, 10 training videos of mice in the assay between 10 and 20 s were recorded, varying the lighting, angle, mouse coat colour and position of the testing apparatus. Approximately 200 frames were manually annotated to identify the forepaws, hind paws, nose, ears and base of the tail. A resnet_v1_50 model was then trained for 201,000 iterations, which was judged to be sufficient based on a plateau of the rate of error change. Testing accuracy was measured in DeepLabCut and found to be within an error range of 20 pixels from the trained dataset. Next, the last 4 min of experimental forced-swim videos were analysed in the Google Colab version of DeepLabCut, and the positions of each body part at each frame were recorded. The .csv files containing the body-position coordinates were analysed in RStudio (v.4.3.0) as previously described⁷⁹. In brief, data were preprocessed with imputeTS to interpolate values with likelihood values greater than 0.95 and body-position pixel coordinates were converted to centimetres. The area of the mice was calculated as a polygon using the coordinates of the left ear, right ear, nose and tail base. The immobility time calculated for the forced-swim test was calculated using the FSTAnalysis function pre-validated settings in the R package DLCAnalyzer. Mice were considered immobile if the rate of change of their body area was below a floating cut-off value of 0.03.

Immunostaining

Immunostaining was performed largely as previously described^{21–25,71}. Mice were intracardially perfused with ice-cold 1× PBS and the brain was embedded in OCT (Sakura, 4583) and flash-frozen using 2-methylbutane (Sigma-Aldrich, M32631). The brain was sectioned into 20 µm sections onto SuperFrost Plus slides (Fisher Scientific, 15-188-48), and sections were fixed in paraformaldehyde (PFA; Electron Microscopy Sciences, 15714-S) freshly diluted to 4% in 1× PBS for 10 min at room temperature. Sections were then washed with 1× PBS

and left to dry. A hydrophobic boundary was drawn around the tissue (Vector Laboratories, H-4000) and sections were washed 3 times for 5 min with 0.3% Triton X-100 (Thermo Fisher Scientific, NC9356391) in PBS (PBS-T) then blocked in 10% donkey serum or 5% goat serum for 30 min at room temperature. Sections were then incubated with primary antibodies diluted in 1× blocking buffer overnight at 4 °C. After primary antibody incubation, sections were washed 3 times with 0.3% PBS-T and incubated with secondary antibodies diluted in blocking solution for 2 h at room temperature. For synapse staining, the sections were permeabilized in 0.5% PBS-T for 15 min before blocking, washed using 0.1% PBS-T and secondary antibodies were incubated for 1 h at room temperature. After secondary antibody incubation, sections were washed 3 times with 0.3% PBS-T, dried and coverslips were mounted using Fluoromount-G with DAPI (SouthernBiotech, 0100-20). For immunocytochemistry, isolated cells were plated on a µ-plate 96-well square (iBidi, 89626) after poly-L-lysine (Sigma Aldrich, P4707) coating. After 24 h, the cells were fixed with 4% PFA for 15 min, followed by permeabilization with 0.3% PBS-T for 15 min. Subsequently, the cells were incubated with a blocking buffer (1% BSA, 10% FBS in PBS) for 1 h and then stained using the same protocol as tissue immunostaining with Hoechst 33342 (Invitrogen, 1:10,000, H3570). The following primary antibodies were used in this study: rabbit anti-mCherry (Abcam, 1:500, ab167453); chicken anti-GFAP (Abcam, 1:200, ab4674); mouse anti-GFAP (Millipore, 1:500, MAB360); rabbit anti-EGFR (D38B1) (Cell Signaling, 1:100, 4267); rabbit anti-GFP (Abcam, ab290, 1:400); chicken anti-GFP (Abcam, 1:200, ab13970); rabbit anti-HOMER1 (Synaptic systems, 1:500, 160002); guinea pig anti-VGLUT2 (Sigma, 1:1,000, AB2251-I); rabbit anti-cFOS (Cell Signaling, 1:100, 2250S); rabbit anti-PTPRS (Proteintech, 1:100, 13008-1-AP); rabbit anti-IL-1R1 (Abcam, 1:100, ab106278); mouse anti-S100β (Millipore Sigma, 1:200, S2532); rabbit anti-collagen IV (Bio-Rad, 1:100, 2150-1470); rabbit anti-IBA1 (Abcam, 1:100, ab178846); chicken anti-GFP (Abcam, 1:100, ab13970); and mouse anti-TUBB3 (BioLegend, 1:500, 801201). The following secondary antibodies were used in this study: donkey anti-rabbit IgG (H+L) highly cross-adsorbed Alexa Fluor 555 (Invitrogen, A31572); donkey anti-rabbit IgG (H+L) highly cross-adsorbed Alexa Fluor 488 (Invitrogen, A21206); donkey anti-mouse IgG (H+L) highly cross-adsorbed Alexa Fluor 488 (Invitrogen, A21202); donkey anti-chicken IgY (H+L) highly cross-adsorbed Alexa Fluor 488 (Invitrogen, A78948); Alexa Fluor 594 goat anti-guinea pig IgG (H+L) (Invitrogen, A11076); goat anti-rabbit IgG (H+L) highly cross-adsorbed Alexa Fluor 488 (Invitrogen, A11034); goat anti-rabbit IgG (H+L) highly cross-adsorbed Alexa Fluor 594 (Invitrogen, A11037); goat anti-mouse IgG (H+L) highly cross-adsorbed Alexa Fluor 594 (Invitrogen, A11032); and goat anti-chicken IgY (H+L) highly cross-adsorbed Alexa Fluor 488 (Invitrogen, A11039) all at 1:500 working dilution. Immunostaining of EGFP in Extended Data Fig. 3a was using AAV5 hSyn-eNpHR3.0-eYFP (Addgene, 26972, a gift from K. Deisseroth⁸⁰). Biotinylated IL-1β was labelled using Oregon Green 488 conjugate of NeutrAvidin biotin-binding protein (Invitrogen, 1:200, A6374). For quantification of mCherry coverage in excitatory neurons, images of the amygdala were captured using a ×63 objective lens with a z stack of 3 images at maximum intensity. Regions of interest (ROIs) were uniformly applied in Fiji (ImageJ, v.1.54k) using normalized intensity to discriminate dendritic patterns across all images, and coverage was quantified using the measurement tool in Fiji.

Confocal imaging and quantification

Sections were imaged using a Zeiss LSM710 confocal microscope with a ×5, ×10 (tile scans), ×20 or ×63 objective. For all analyses, the amygdala was identified on the basis of DAPI fluorescence. Imaging was performed using the LSM710 smart set-up parameters, with each channel acquired in sequence to minimize crosstalk between channels to essentially zero. Quantification of specific markers in brain sections was performed by first quantifying the number of positive cells for the given cell-type marker (for example, GFAP and IBA1) and

Article

then counting the absolute number of that type positive for a molecular marker with a visible cell body in the DAPI channel. For analysis of synapses, VGLUT2 and HOMER1 puncta colocalization was determined by generating a high-density signal mask for the VGLUT2 channel for each image in Fiji, followed by using automated thresholds to isolate only the puncta for both VGLUT2 and HOMER1 channels, largely as previously described⁸¹. These puncta were quantified and the number of overlapping puncta was normalized by the high-density area mask. For quantifying cFOS-positive cells, images of the amygdala were acquired using a 2 × 2 tile scan with a ×20 objective lens. The cFOS signals were detected by setting an automated threshold, and noise was minimized by filtering out puncta smaller than 10 pixels. The number of cFos-positive puncta was normalized to the total area of the imaged region. These parameters were consistently applied across all experimental groups. To measure the intensity of astrocytic PTPRS and IL-1RI, 5z stack images were acquired at 0.5 μm intervals. ROIs were then defined on the basis of S100β signals using Fiji, and maximal-intensity projections were used to quantify signal intensities for each marker in these ROIs. For immunocytochemistry, two ×20 images per mouse were captured and quantified using Fiji.

Isolation of astrocytes from adult mice

Astrocytes were isolated by magnetic-activated cell sorting (MACS) with a Miltenyi ACSA-2 Microbead kit (Miltenyi Biotec, 130-097-679) akin to previous protocols⁸². In brief, mice were perfused with 1× PBS, and using a stainless-steel mouse brain matrix (Kent Scientific, RBMS-205C) and a dissecting microscope, the amygdala was isolated into 500 μl Hibernate-A (Thermo Fisher Scientific, A12475-01) containing 7.5 μl papain suspension (Worthington, LS003126) and B-27 supplement (Thermo Fisher Scientific, 17504044). Tissue was shaken at 80 r.p.m. for 20 min at 37 °C, mechanically dissociated using a P1000 pipette and filtered through a 70 μm cell strainer (Millipore Sigma, BAH136800070). Cells were resuspended in 90 μl of 0.5% BSA, 2 mM EDTA pH 8.0 in 1× PBS and 10 μl FcR blocking reagent and incubated at 4 °C for 10 min. Next, 10 μl anti-ACSA-2 MicroBeads were added, and cells were incubated at 4 °C for an additional 15 min. Cells were washed with 1 ml of 0.5% BSA and 2 mM EDTA pH 8.0 in 1× PBS, centrifuged at 500g for 5 min and resuspended in 500 μl of 0.5% BSA and 2 mM EDTA pH 8.0 in 1× PBS. The cell suspension was applied onto a LS column (Miltenyi Biotec, 130-042-401) on a QuadroMACS Separator pre-rinsed with 3 ml of 0.5% BSA and 2 mM EDTA pH 8.0 in 1× PBS. The column was washed 3 times with 3 ml of 0.5% BSA and 2 mM EDTA pH 8.0 in 1× PBS, removed from the separator and placed in a 15 ml conical tube. Next, 5 ml of 0.5% BSA and 2 mM EDTA pH 8.0 in 1× PBS was added to the column, and astrocytes were removed with a plunger. Cells were centrifuged at 500g for 5 min, resuspended in 100 μl PicoPure extraction buffer (Thermo Fisher Scientific, KIT0204) and incubated in a heat block at 42 °C for 30 min. Samples were stored at –80 °C until further processing.

Isolation of neurons from adult mice

Neurons were isolated by MACS with a Miltenyi Adult Neuron Isolation kit (Miltenyi Biotec, 130-126-602) akin to previous protocols⁸². In brief, mice were perfused with 1× PBS, and using a stainless-steel mouse brain matrix (Kent Scientific, RBMS-205C) and a dissecting microscope, the amygdala was isolated into 500 μl Hibernate-A (Thermo Fisher Scientific, A12475-01) containing 7.5 μl papain suspension (Worthington, LS003126) and B-27 supplement (Thermo Fisher Scientific, 17504044). Tissue was shaken at 80 r.p.m. for 20 min at 37 °C, mechanically dissociated using a P1000 pipette and filtered through a 70 μm cell strainer (Millipore Sigma, BAH136800070). Cells were centrifuged at 500g for 5 min, resuspended in 90 μl of 0.5% BSA and 2 mM EDTA pH 8.0 in 1× PBS and 10 μl adult non-neuronal cell biotin-antibody cocktail and incubated for 5 min at 4 °C. Cells were washed with 1 ml of 0.5% BSA and 2 mM EDTA pH 8.0 in 1× PBS, centrifuged at 500g for 5 min and resuspended in 90 μl of 0.5% BSA and 2 mM EDTA pH 8.0 in 1× PBS and

10 μl of anti-biotin microbeads and incubated for 10 min at 4 °C. Next, 0.5% BSA and 2 mM EDTA pH 8.0 in 1× PBS was added to a total volume of 500 μl, and the cell suspension was applied to a LS column (Miltenyi Biotec, 130-042-401) pre-rinsed with 3 ml of 0.5% BSA and 2 mM EDTA pH 8.0 in 1× PBS. Neurons were collected into a 15 ml conical tube on ice, and the column was washed with 2 ml of 0.5% BSA and 2 mM EDTA pH 8.0 in 1× PBS to collect remaining cells. Cells were centrifuged at 500g for 5 min, resuspended in 100 μl PicoPure extraction buffer (Thermo Fisher Scientific, KIT0204) and incubated in a heat block at 42 °C for 30 min. Samples were stored at –80 °C until further processing.

Bulk RNA-seq

Bulk RNA isolated from sorted cells was processed using a PicoPure kit (Thermo Fisher, KIT0204) and used as input with the kit (NEB, E6420) according to the manufacturer's protocol. Reverse transcription was performed according to the Smart protocol using a template switching oligonucleotide. cDNA was amplified and cleaned using Ampure XP beads (Beckman-Coulter, A63881) and quantified using a Bioanalyzer DNA HS assay (Agilent, 50674626). Libraries were then fragmented, end-repaired and ligated to Illumina -compatible adaptors followed by sample barcoding using NEBNext Multiplex Oligos for Illumina (E7335S, E7500S, E7710S and E7730S). Samples were selected again using Ampure XP beads. Final libraries were quantified using a Bioanalyzer and a Kapa library quantification kit (Kapa Biosystems, KK4824). The libraries were then diluted and pooled at 4 nM in nuclease-free water (Thermo Fisher Scientific, AM9937) and run on an Illumina Next-Seq550 as 1× 75 bp reads with 6-bp index reads and de-multiplexed into fastq files. The fastq files of each RNA-seq data sample were aligned to the *Mus musculus* GRCm38 transcriptome using STAR (v.2.7.5c)⁸³. The raw sequencing reads were quality assessed using fastp (v.0.23.2)⁸⁴ and fastQC (v.0.11.9) and reported using multiqc (v.1.11)⁸⁵. Processed RNA-seq data were filtered, and genes with low read counts (average counts > 0.5) were removed. Feature counts were tabulated with featureCounts (v.2.0.1)⁸⁶. Differential expression analysis was done using EdgeR (v.3.42.4)⁸⁷. Enrichment plots for RNA-seq data were generated using GSEA⁸⁸ with molecular signatures from the following canonical pathways: KEGG/Reactome/Biocarta (c2.cp.all), Gene Ontology (c5.cp.all) and Hallmark (h.all) in astrocytes, neurons and monocytes individually. Pathway analysis was performed using IPA (Qiagen), ENRICHR^{89–91} and StringDB⁹². For all IPA analyses, 8,000 genes at the most were filtered on the basis of log FC values and uploaded for both upregulated and downregulated genes. For ENRICHR analyses, genes were selected on the basis of significance and a common FC direction. For StringDB analyses, significantly downregulated genes in sgNr2f2 compared with sgRosa26 samples associated with the GOBP Synaptic Signaling pathway (GO:0099536) were used as input, then PPI networks were clustered with k-means clustering using a resolution of 3 clusters. Cluster 2 is shown. Bulk RNA-seq data of amygdala neurons were obtained as fastq files from the Gene Expression Omnibus (GEO) with accession numbers GSE162417 (ref. 93), GSE66345 (ref. 94), GSE130268 (ref. 95), GSE138522 (ref. 96), GSE183092 (ref. 97) and GSE151798 (ref. 98) and processed according to the parameters described above.

Primary astrocyte cultures

Procedures were performed largely as previously described^{21–25,71}. Brains of mice aged P0–P3 were dissected into HBSS (Thermo Fisher Scientific, 14025-134) on ice. Tissue samples were mechanically dissociated, centrifuged at 500g for 10 min at 4 °C and resuspended in 0.25% trypsin-EDTA (Thermo Fisher Scientific, 25200-072) at 37 °C for 10 min. Trypsin was neutralized by adding DMEM/F12 + GlutaMAX (Thermo Fisher Scientific, 10565018) supplemented with 10% FBS (Thermo Fisher Scientific, 10438026) and 1% penicillin–streptomycin (Thermo Fisher Scientific, 15140148). Cells were passed through a 70 μm cell strainer. Cells were centrifuged at 500g for 5 min at 4 °C, resuspended in DMEM/F12 + GlutaMAX (Thermo Fisher Scientific, 10565018) supplemented

with 10% FBS (Thermo Fisher Scientific, 10438026) and 1% penicillin-streptomycin (Thermo Fisher Scientific, 15140148) and cultured in T-75 flasks (Falcon, 353136) pre-coated with poly-L-lysine (Sigma Aldrich, P4707) for 1 h at 37 °C and washed with 1× PBS. Cells were cultured at 37 °C in a humidified incubator with 5% CO₂ for 7–10 days until confluence was reached. Medium was replaced every 2–3 days. Microglia were removed by shaking the flask for 30 min at 180 r.p.m. and replacing the medium. To plate astrocytes, the flask was shaken for 2 h at 220 r.p.m., medium was removed and 5 ml trypsin was added at 37 °C for 3 min. Trypsin was neutralized with DMEM/F12 + GlutaMAX (Thermo Fisher Scientific, 10565018) supplemented with 10% FBS (Thermo Fisher Scientific, 10438026) and 1% penicillin-streptomycin (Thermo Fisher Scientific, 15140148). Cells were centrifuged at 500g for 5 min at 4 °C, resuspended in DMEM/F12 + GlutaMAX (Thermo Fisher Scientific, 10565018) supplemented with 10% FBS (Thermo Fisher Scientific, 10438026) and 1% penicillin-streptomycin (Thermo Fisher Scientific, 15140148) and cultured in a tissue-culture-treated plate pre-coated with poly-L-lysine (Sigma Aldrich, P4707). Astrocytes were plated for at least 5 days before in vitro treatments.

In vitro stimulation of mouse primary cells

For mouse astrocyte, neuron and astrocyte-neuron cultures, stimulations were performed for 24 h with compounds diluted in DMEM/F12 + GlutaMAX (Life Technologies, 10565042) supplemented with 10% FBS (Life Technologies, 10438026) and 1% penicillin-streptomycin (Life Technologies, 15140122). For peripheral CD11b⁺ cells from mice, stimulations were performed for 6 h with molecules diluted in DMEM/F12 + GlutaMAX (Life Technologies, 10565042) supplemented with 10% FBS (Life Technologies, 10438026), 1% penicillin-streptomycin (Life Technologies, 15140122), 1% sodium pyruvate (Life Technologies, 11360070), 1% HEPES (Life Technologies, 15630106) and 1% MEM non-essential amino acids (Life Technologies, 11140050). The following molecules were used to stimulate astrocytes, neurons and astrocyte-neuron cultures: 50 ng ml⁻¹ TNF (R&D Systems, 410-MT-010); 100 ng ml⁻¹ IL-1β (R&D Systems, 401-ML-005); 100 ng ml⁻¹ IL-12 (Pepro-Tech, 210-12); and 200 ng ml⁻¹ corticosterone. The corticosterone dose was chosen based on its serum concentration in chronically stressed mice⁹⁹ (Millipore Sigma, 27840). The following molecules were used to stimulate primary cells: 10 μM psilocybin (NIDA Drug Supply Program); 10 μM MDMA-HCl racemate (NIDA Drug Supply Program); 20 μM MDL 100907 (Tocris Biotechnique, 4173); 200 ng ml⁻¹ corticosterone (Millipore Sigma, 27840) and 10 ng ml⁻¹ LPS (InvivoGen, tlrl-3pelp).

RNA isolation from primary cells

Primary cells were lysed in buffer RLT (Qiagen), and RNA was isolated using a Qiagen RNeasy Mini kit (Qiagen, 74106). cDNA was transcribed using a High-Capacity cDNA Reverse Transcription kit (Life Technologies, 4368813). Gene expression was then measured by qPCR using Taqman Fast Universal PCR master mix (Life Technologies, 4367846). The following Taqman probes were used in this study: *Gapdh* (Mm99999915_g1), *Il1b* (Mm02620111_s1), *Ptprs* (Mm00465150_m1), *Cebpg* (Mm01266786_m1), *Ets1* (Mm01175819_m1), *Nr2f2* (Mm00772789_m1), *Cxcr3* (Mm99999054_s1), *Cxcr4* (Mm01996749_s1), *Cx3cr1* (Mm02620111_s1), *Htr2a* (Mm00555764_m1), *Htr2b* (Mm00434123_m1), *Htr2c* (Mm00434127_m1), *Ntrk2* (Mm00435422_m1), *Il1r1* (Mm00434237_m1) and *Actb* (Mm02619580_g1). qPCR data were analysed using the ΔΔCt method by normalizing the expression of each gene for each replicate to *Gapdh* and then to the control group.

Primary astrocyte-neuron co-cultures

Procedures were performed largely as previously described^{21–25,71} using a Worthington papain dissociation system (Worthington Biochemical, LK003150). Brains of mice aged P0–P3 were dissected into HBSS (Thermo Fisher Scientific, 14175103) supplemented with 1% sodium pyruvate (Invitrogen, H-4034), 0.1% w/v glucose (Sigma-Aldrich, G-6152)

in nuclease-free water (Thermo Fisher Scientific, AM9937) and 1% HEPES (Invitrogen, H-4034) in a Petri dish on ice. The meninges and brainstem were removed, and the remaining tissue was placed in a 15 ml conical tube with papain and DNase in 5.35 ml EBSS and incubated at 37 °C for 30 min. Brains were dissociated with a P1000 pipette, and cells were passed through a 70 μm filter into a 50 ml conical tube. Albumin ovomucoid inhibitor was reconstituted in 32 ml EBSS, and cells were resuspended in 2.7 ml EBSS supplemented with 0.3 ml reconstituted albumin ovomucoid inhibitor and 150 μl DNase I. The cell solution was layered on top of 5 ml ovomucoid inhibitor and centrifuged at 100g for 5 min at 22 °C. Cells were resuspended in MACS Neuro medium (Miltenyi Biotec, 130-093-570) supplemented with 2% MACS NeuroBrew-21 (Miltenyi Biotec, 130-093-566) and 1% penicillin-streptomycin (Thermo Fisher Scientific, 15140148). Cells were plated in tissue culture plates coated with laminin and poly-L-ornithine (Westnet, 354659). Medium was changed after 48 h then changed every 3 days. After 10–14 days of plating, co-cultures were transduced with AAV diluted in MACS Neuro medium (Miltenyi Biotec, 130-093-570) supplemented with 2% MACS NeuroBrew-21 (Miltenyi Biotec, 130-093-566) and 1% penicillin-streptomycin (Thermo Fisher Scientific, 15140148). Half of the total volume of medium was changed every 3 days following AAV transduction. The following molecules in MACS Neuro medium (Miltenyi Biotec, 130-093-570) supplemented with 2% MACS NeuroBrew-21 (Miltenyi Biotec, 130-093-566) and 1% penicillin-streptomycin (Thermo Fisher Scientific, 15140148) were used to stimulate co-cultures 7 days after transduction: 100 ng ml⁻¹ IL-1β (R&D Systems, 401-ML-005) and 200 ng ml⁻¹ corticosterone (Millipore Sigma, 27840). For qPCR analysis of co-cultures, astrocytes were isolated by MACS as described in the section 'Isolation of astrocytes from adult mice'. The remaining flow-through represented the isolated neuron population. Cells were lysed with RLT (Qiagen) 24 h after stimulation. Lysed cells were stored at -80 °C until processing.

ATAC-seq

Sequencing libraries were prepared largely as previously described^{22–24}. After isolation of nuclei, transposition was performed using a kit (Illumina, FC-121-1030) according to the original protocol¹⁰⁰. DNA was then amplified using NEBNext High Fidelity 2× PCR master mix (New England Biolabs, M0541S) for 5 cycles. DNA quantity was then measured using a ViiA 7 Real-Time PCR system (Thermo Fisher Scientific) and the number of cycles required to achieve 1/3 of maximal SYBR Green fluorescence was determined and libraries were amplified accordingly. TruSeq adaptors (universal: Ad1_noMX and barcoded: Ad2.1-Ad2.24) were used according to the standard protocol. Libraries were purified using a MiniElute PCR Purification kit (Qiagen, 28006) followed by double-sided Agencourt AMPure XP bead purification (Beckman Coulter, A63881) to remove primer dimers and large DNA fragments. Libraries were analysed on a 2100 Bioanalyzer (Agilent Technologies) and a High Sensitivity DNA kit (Agilent Technologies, 5067-4626). Libraries were sequenced on an Illumina NextSeq550 by 35 + 40 bp paired-end sequencing and de-multiplexed into fastq files. The fastq files of each ATAC-seq data sample were aligned to the *M. musculus* GRCh39/mm10 mouse genome assembly with BWA mem (v.0.7.17-r1188). Duplicate reads were removed using Picard MarkDuplicates (v.2.25.2). The raw sequencing reads were quality assessed using fastp (v.0.23.2)⁸⁴ and fastQC (v.0.11.9) and reported using multiqc (v.1.11)⁸⁵. Peak calling was performed using Macs2 (v.2.2.9.1). Peak differential analysis was done using DiffBind (v.3.10.0), and motif enrichment and annotation were performed using Homer (v.4.10).

Stereo-seq

Mouse brains were collected and immediately flash-frozen in Tissue-Tek OCT medium (Sakura Finetek, 4583) in 2-methylbutane and then stored at -80 °C until used for Stereo-seq. Cryosections were cut at the thickness of 10 μm and mounted on Stereo-seq permeabilization chips (STOmics, 210CP118) or transcriptomic chips (STOmics, 210CT114).

Article

Tissue fixation and the subsequent spatial transcriptomic procedure were performed according to the vendor's manual and previous publications^{101,102}. In brief, the tissue section on the Stereo-seq chip (0.5×0.5 cm) was incubated at 37°C for 5 min and subsequently fixed in pre-chilled methanol (Sigma, 34860, precooled for 30 mins at -20°C) at -20°C for 30 min. Once fixation was complete, the Stereo-seq chip was removed and the residual methanol was evaporated off in a chemical hood. The tissue section on the chip was then stained with nucleic acid reagent (Invitrogen, Q10212, 0.5% v/v) for 5 min and subsequently washed with $0.1\times$ SSC buffer (Ambion, AM9770; containing 0.05 U ml^{-1} RNase inhibitor). Images of nuclei were captured using a Zeiss Axio Scan Z1 microscope (at EGFP wavelength) and then the tissue section was incubated in permeabilization buffer (STOmics, 111KP118) for 12 min at 37°C . Stereo-seq transcriptomic-chip-captured RNA from the permeabilized tissue was then reverse-transcribed for 3 h at 42°C . The tissue was removed and the cDNA was released from the chip using a transcriptomics reagent kit (STOmics, 111KT114). The obtained cDNA was size-selected, amplified and purified, and the concentration was quantified using a Qubit dsDNA HS assay kit (Invitrogen, Q32854). Next, 20 ng cDNA from each sample was used for library construction with a library preparation kit (STOmics, 111KL114) and subsequently for DNA nano ball (DNB) generation. Finally, the DNBs were sequenced on a DNBSEQTM T7 sequencing platform (Complete Genomics) with 50 bp read 1 and 100 bp read 2 (Complete Genomics, 1000028455). The coordinate ID (CID; 25 bp in length) for each read was mapped to the designed coordinates of the *in situ* captured chip achieved from the first round of sequencing, allowing 1 base mismatch to correct for sequencing and PCR errors. Each read was also labelled with unique molecule ID (MID). Reads with MIDs containing either N bases or more than 2 bases with a quality score lower than 10 were filtered out. After CID mapping and MID assignment, retained reads were then aligned to the reference genome of the sample using STAR⁸³. Mapped reads with MAPQ > 10 were counted and annotated to their corresponding genes. UMIs with the same CIDs and the same gene locus were collapsed, allowing 1 mismatch to correct for sequencing and PCR errors. This information was then used to generate a CID-containing expression-profile matrix. For cell-segmentation analysis, nucleic-acid-stained images from the same section were projected to the Stereo-seq chips (image registration). The process started with summing up the total UMIs in each DNB spot, which have a specific spatial coordinate, to generate a spatial-density matrix, then the matrix was converted into an image in which each pixel corresponded to one DNB and the total UMI of a DNB spot corresponded to the greyscale of the pixel. The nucleic-acid-stained image was then aligned to the transcriptome image. After image alignment, cell-segmentation analysis was performed using Scikit-image (v.0.18.1)¹⁰³. In brief, the background of the stained image was removed with a global threshold approach, then the watershed algorithm was applied to obtain single-cell segmentations. The number of markers required for the watershed algorithm were obtained through Gaussian-weighted local threshold binarization with a block size of 41 and an offset value of 0.003. For each of the segmented cells, UMIs from all DNBs in the corresponding segmentation were aggregated per gene and then summed to generate a cell-by-gene matrix for downstream analysis. The centroid of each cell was determined using rearrr (<https://github.com/LudvigOlsen/rearr>). The analysis workflow with detailed documentation is publicly available from GitHub (<https://github.com/STOmics/SAW>). The SAW software version applied in this study was v.6.0.2. Data from cells segmented using the watershed algorithm from an entire coronal section taken from each biological replicate were aggregated together. Cells were included on the basis of 50–1,200 genes expressed and <5% mitochondrial reads. A gene was included only if at least five cells expressed it. Next, cell types were called using ingest¹⁰⁴ against a reference cell-type atlas of the amygdala³⁶. Thereafter, cells localized to the amygdala were extracted for each tissue section. The amygdala location was determined by haematoxylin and eosin staining,

the presence of excitatory neuron markers (*Slc17a7* and *Slc17a6*), inhibitory neuron markers (*Slc32a1*), BLA neuron markers^{105–113} (*Etv1*) and central amygdala markers¹¹⁴ (*Tac2*). In the selection of the amygdala, we also guided the ROI selection by two external references: (1) the Allen Reference Atlas, judged by the Allen Atlas coronal section that most closely matched the experimental histological section; (2) unsupervised low-resolution regional clustering of $100 \times 100\text{ }\mu\text{m}$ spots to approximate medial, central and basal-lateral amygdala regions. ROI selection of the amygdala was intended to be broad and therefore included the medial amygdala, the central amygdala, the basomedial amygdala, the cortical amygdala, the BLA and the lateral amygdala, as detected in a given section. From this analysis, most cell types were classified as inhibitory neurons, excitatory neurons, astrocytes, microglia and oligodendrocytes. We did detect four cells classified as vascular smooth muscle, endothelial cells, pericytes and perivascular macrophages, which were excluded from downstream analysis. The capture sensitivity of the Stereo-seq method, our thresholding parameters and the analysis of only a single brain slice per animal probably led to the underestimation of other cell types in the brain, including endothelial cells, and even classes of immune cells that are recruited to the left amygdala during chronic stress⁵. Amygdala cell-type objects were then subsetted and validated for the known marker genes *Gpc5* (astrocytes), *Slc17a7* (excitatory neurons), *Slc17a6* (excitatory neurons), *Slc32a1* (inhibitory neurons), *Cst3* (microglia) and *Plp1* (oligodendrocytes). To analyse astrocyte nearest neighbours to excitatory neuron cluster 2, the distance (d) between x - y coordinates of each cluster 2 excitatory neuron and astrocyte in a biological replicate from stressed mice was measured using $d = \sqrt{(x_2 - x_1)^2 + (y_2 - y_1)^2}$. The top 10% astrocytes with the shortest distance to the excitatory neuron were considered nearest neighbours. Trajectories were created using RNA velocity in scanpy⁷³. In brief, we drew a force-directed graph, determined spliced and unspliced transcripts, developed a pseudotime kernel and computed a transition matrix that was projected on the low-dimensional embedding. Differential expression analysis was performed by comparing each cluster to all others using scanpy.tl.rank_genes_groups, which were then used in downstream analyses such as Qiagen IPA by using the FC value of the cluster of interest relative to all others.

Isolation of meningeal cells

Animals were euthanized and blood was removed by cutting the right atrium. Following mouse perfusion, the head was severed and the skin was removed from the head. A cut was made around the cranium (from the foramen magnum to the frontal bone) to dissect the bones of the calvarium. The calvarium was then transferred to a dissection scope and the meninges were removed. Tissue was incubated for 30 min at 37°C in $500\text{ }\mu\text{l}$ RPMI-1640 (Life Technologies, 11875119) supplemented with 0.5 mg ml^{-1} collagenase P (Sigma-Aldrich, 11213865001), 0.5 mg ml^{-1} dispase (Worthington, LS02104) and 125 U ml^{-1} DNase I (Sigma-Aldrich, 10104159001). After incubation, samples were washed with 1 ml of 0.5% BSA and 2 mM EDTA in $1\times$ PBS. Cells were centrifuged at 500g for 10 min, resuspended in 1 ml ice-cold 0.5% BSA, 2 mM EDTA in $1\times$ PBS and gently dissociated using a wide-bore 1 ml pipette tip. Finally, the cell suspension was filtered through a $40\text{ }\mu\text{m}$ FlowMi filter (Sigma-Aldrich, BAH136800040-50EA) and prepared for downstream applications.

Isolation of mouse dCLN cells

dCLNs were isolated following mouse perfusion and mechanically dissociated. Cells were centrifuged at 1,500 r.p.m. for 5 min and prepared for downstream applications.

Isolation of mouse splenic cells

Spleens were isolated following mouse perfusion and mechanically dissociated. Red blood cells were lysed with ACK lysis buffer (Life Technology, A10492-01) for 5 min, washed with $1\times$ PBS and prepared for downstream applications.

FACS

Immune-cell populations were analysed largely as previously described^{21,23–25,115}. Splenic, dCLN and meningeal cell suspensions were stimulated with 50 ng ml⁻¹ phorbol 12-myristate 13-acetate (Sigma-Aldrich, P8139), 1 µM ionomycin (Sigma-Aldrich, I3909-1ML), GolgiStop (BD Biosciences, 554724, 1:500) and GolgiPlug (BD Biosciences, 555029, 1:500) diluted in complete RPMI (Life Technologies, 11875119) containing 10% FBS, 1% penicillin–streptomycin, 50 µM 2-mercaptoethanol (Sigma-Aldrich, M6250) and 1% non-essential amino acids (Life Technologies, 11140050). After 4 h, cell suspensions were washed with 0.5% BSA, 2 mM EDTA in 1× PBS and incubated with an FCyR-blocking antibody, surface antibodies and a live/dead fixable aqua stain (Thermo Fisher Scientific, L34966) on ice. After 30 min, cells were washed with 0.5% BSA, 2 mM EDTA in 1× PBS and fixed according to the manufacturer's protocol of an intracellular labelling kit (eBiosciences, 00-5523-00). The FCyR-blocking antibody used in this study was: CD16/CD32 (BD Biosciences, 553141, 1:200). The following surface antibodies were used in this study: BUV661 anti-mouse CD45 (BD Biosciences, 612975, 1:100); BV650 anti-mouse CD3 (BD Biosciences, 740530, 1:100); PE-Cy7 anti-mouse CD4 (BD Biosciences, 561099, 1:100); BV786 anti-mouse CD11b (BD Biosciences, 740861, 1:100); BV570 anti-mouse Ly6C (BioLegend, 128029, 1:100); BUV805 anti-mouse CD8a (BD Biosciences, 612898, 1:100); BUV563 anti-mouse Ly6G (BD Biosciences, 612921, 1:100); BUV737 anti-mouse CD11c (BD Biosciences, 612797, 1:100); BV750 anti-mouse NK1.1 (BD Biosciences, 746876, 1:100); and BV605 anti-mouse CD19 (BioLegend, 115539, 1:100). The following intracellular antibodies were used: Alexa Fluor 488 anti-GFP (BioLegend, 338007, 1:100); BV421 anti-mouse TNF (BD Biosciences, 563387, 1:100); and FITC anti-mouse CD192 (CCR2) (BioLegend, 150608, 1:100). Cells were counted at a 20× dilution on a LSRII Fortessa (BD Biosciences). FACS was performed on a Symphony A5 (BD Biosciences) with BD FACSDIVA software (v.8.0.1). Compensation was performed on single-stained beads and all samples were gated against unstained controls in experiments. Flow cytometry data were analysed using FlowJo software (FlowJo LLC, v.10.10.0). Cell populations were gated on SSC and FSC singlets followed by exclusion of dead cells, selection of CD45⁺ cells, then gated as follows: B cells were gated as CD45⁺CD3⁻CD19⁺; CD4⁺T cells were gated as CD45⁺CD3⁺CD4⁺; CD8⁺T cells were gated as CD45⁺CD3⁺CD8⁺; dendritic cells were gated as CD45⁺CD3⁻CD11c⁺; macrophages were gated as CD45⁺CD3⁻CD11c⁻Ly6C⁻Ly6G⁻; neutrophils were gated as CD45⁺CD3⁻CD11c⁻CD11b⁺Ly6C⁻Ly6G⁺; and pro-inflammatory monocytes were gated as CD45⁺CD3⁻CD11c⁻CD11b⁺Ly6C⁺.

In vivo photoconversion of *Cag*^{Kaede} mice

Photoconversion of the spleen was performed largely as previously described²⁵ following 18 days of restraint stress as mice were briefly anaesthetized. The surrounding tissue was covered with sterile aluminium foil and a small opening was made in the peritoneal cavity. The spleen was extended and exposed to 405 nm violet light using a 200 mW Electra Pro portable laser (Laserglow Technologies) for a total time of 90 s over the whole spleen surface with continuous application of PBS on the exposed spleen. After careful returning of the spleen to the peritoneal cavity, the peritoneum was closed with absorbable sutures (Ethicon, 1667H) and the skin was closed with surgical staples (Braintree Scientific, EZC-KIT). Mice were killed 36 h later for FACS analysis.

Adoptive transfer of monocytes

The skin and muscle of the legs were removed from mice following euthanasia. Bone marrow was isolated from C57Bl/6J mice by flushing PBS through the head of the femur and tibia with a 25-gauge needle (BD Biosciences, 305125). Red blood cells were lysed with ACK lysis buffer (Life Technologies, A10492-01) for 5 min, washed with 1× PBS, and centrifuged at 500g for 5 min at 4 °C. Monocytes were then isolated by MACS with a Miltenyi Monocyte Isolation kit (Miltenyi Biotec,

130-100-629). Cells were resuspended in 175 µl of 0.5% BSA, 2 mM EDTA pH 8.0 in 1× PBS with 25 µl FcR Blocking Reagent and 50 µl of Monocyte Biotin-Antibody Cocktail. Cells were incubated at 4 °C for 5 min and subsequently washed with 10 ml of 0.5% BSA, 2 mM EDTA pH 8.0 in 1× PBS. The samples were then centrifuged at 500g for 10 min, and cell pellet was resuspended in 400 µl of 0.5% BSA, 2 mM EDTA pH 8.0 in 1× PBS. Next, 100 µl anti-biotin microbeads were added to each sample, and cells were incubated at 4 °C for 10 min. The cell suspension was applied onto an LS column (Miltenyi Biotec, 130-042-401) on a QuadroMACS Separator pre-rinsed with 3 ml of 0.5% BSA, 2 mM EDTA pH 8.0 in 1× PBS and collected into a 15 ml conical tube. The column was washed 3 times with 3 ml of 0.5% BSA, 2 mM EDTA pH 8.0 in 1× PBS and flowthrough was collected. Cells were centrifuged at 500g for 5 min at 4 °C and resuspended in 1× sterile PBS. Mice were intravenously injected with 200 µl of PBS as a control or 10⁶ monocytes in 200 µl of PBS with an insulin syringe (BD Biosciences, 329410) 18 h before the first day of restraint. Subsequently, 1× PBS or monocytes were administered to the mice each day 2 h following the end of the 6 h restraint period for 7 consecutive days. Mice were subjected to behavioural testing following the 7 day restraint period.

Injections by i.c.m

Injections were carried out largely as previously described¹¹⁶. In brief, mice were anaesthetized with 1–3% isoflurane (Covetrus, 11695067772) in oxygen. Heads were shaved and cleaned with ethanol and betadine (Thermo Fisher, 19-027132) and a small opening was made in the skin at the back of the neck with surgical scissors. The head of the mouse was placed on a support box and angled down to expose the muscle around the cisterna magna. Muscle tissue blocking the cisterna magna was gently pulled away with fine-tip forceps. The tip of a 25-gauge Hamilton syringe needle was bent to a 45° angle and an injection of 6 µl of antibody was made into the cisterna magna with a 5 µl Hamilton syringe (Sigma-Aldrich, 20787) at a concentration of 4 µg µl. After injection, mice were sutured (Ethicon, 1667H) and allowed to recover in a clean cage on a heating pad for 1 h. Instruments were sterilized between each mouse using a glass bead sterilizer (CellPoint Scientific, GRMS-1450). Evans Blue (Thermo Scientific, A16774-09) was dissolved to 3% in DPBS and administrated to mice by i.c.m. injection. Following 18 days of restraint stress, 24 µg of isotype control (R&D Systems, MAB0061) or anti-CCR2 (R&D Systems, MAB55381) antibody were administered to mice by i.c.m. injection as previously described¹¹⁶; after fear acquisition mice underwent fear extinction 48 h later. Before injection of IL-1β, similar to previous studies¹¹⁷ mouse IL-1β (R&D Systems, 201-LB-025) was biotinylated by EZ-Link Sulfo-NHS-Biotin kit (Thermo Fisher, A39256) following the manufacturer's instructions and then purified using a Pierce C18 Spin Columns, 7K MWCO (Thermo Fisher, 89870). The biotinylated IL-1β was administered into the cisterna magna of anaesthetized 18-d stressed or control mice at a concentration of 250 ng ml⁻¹ in 5 µl 1× DPBS. Mice were killed 1 day after injection.

Isolation of monocytes from adult mice

To process the meninges, the head was severed, and the skin was removed from the head. A cut was made around the cranium (from the foramen magnum to the frontal bone) to dissect the bones of the calvarium. The calvarium was then transferred to a dissection scope and the meninges were removed. Tissue was incubated for 30 min at 37 °C in 500 µl RPMI-1640 (Life Technologies, 11875119) supplemented with 0.5 mg ml⁻¹ collagenase P (Sigma-Aldrich, 11213865001), 0.5 mg ml⁻¹ of dispase (Worthington, LS02104), and 125 U ml⁻¹ of DNase I (Sigma-Aldrich, 10104159001). After incubation, samples were washed with 1 ml of 0.5% BSA, 2 mM EDTA in 1× PBS. Cells were centrifuged at 500g for 10 min, resuspended in 1 ml ice-cold 0.5% BSA, 2 mM EDTA in 1× PBS, and gently dissociated using a wide-bore 1 ml pipette tip. Finally, the cell suspension was filtered through a 40 µm FlowMi filter (Sigma-Aldrich, BAH136800040-50EA). Monocytes

Article

were isolated by MACS with a Miltenyi Monocyte Isolation kit (Miltenyi Biotec, 130-100-629). Cells were centrifuged at 1,500 r.p.m. for 5 min and resuspended in 175 µl of 0.5% BSA, 2 mM EDTA pH 8.0 in 1× PBS with 25 µl of Fc Blocking Reagent and 50 µl of Monocyte Biotin-Antibody Cocktail. Cells were incubated at 4 °C for 5 min and subsequently washed with 10 ml of 0.5% BSA, 2 mM EDTA pH 8.0 in 1× PBS. The samples were then centrifuged at 500g for 10 min and cell pellet was resuspended in 400 µl of 0.5% BSA, 2 mM EDTA pH 8.0 in 1× PBS. 100 µl of anti-biotin microbeads were added to each sample, and cells were incubated at 4 °C for 10 min. The cell suspension was applied onto an LS column (Miltenyi Biotec, 130-042-401) on a QuadroMACS Separator pre-rinsed with 3 ml of 0.5% BSA, 2 mM EDTA pH 8.0 in 1× PBS and collected into a 15 ml conical tube. The column was washed 3 times with 3 ml of 0.5% BSA, 2 mM EDTA pH 8.0 in 1× PBS and flowthrough was collected. Monocytes were centrifuged at 500g for 5 min, resuspended in 100 µl of PicoPure extraction buffer (Thermo Fisher Scientific, KIT0204), and incubated in a heat block at 42 °C for 30 min. Samples were stored at -80 °C until processing.

Primary splenic CD11b⁺ cell culture

CD11b⁺ cells were isolated by MACS with Miltenyi CD11b microbeads (Miltenyi Biotec, 130-049-601). In brief, spleens were isolated following mouse perfusion and mechanically dissociated. Red blood cells were lysed with ACK lysing buffer (Life Technology, A10492-01) for 5 min and washed with 1× PBS. Cells were resuspended in 90 µl of 0.5% BSA, 2 mM EDTA pH 8.0 in 1× PBS and 10 µl of CD11b Microbeads and incubated at 4 °C for 10 min. Cells were washed with 1 ml of 0.5% BSA, 2 mM EDTA pH 8.0 in 1× PBS, centrifuged at 500g for 5 min, and resuspended in 500 µl of 0.5% BSA, 2 mM EDTA pH 8.0 in 1× PBS. The cell suspension was applied onto an LS column (Miltenyi Biotec, 130-042-401) on a QuadroMACS Separator pre-rinsed with 3 ml of 0.5% BSA, 2 mM EDTA pH 8.0 in 1× PBS. The column was washed 3 times with 3 ml of 0.5% BSA, 2 mM EDTA pH 8.0 in 1× PBS, removed from the separator and placed onto a 15 ml conical tube. 5 ml of 0.5% BSA, 2 mM EDTA pH 8.0 in 1× PBS was added to the column, and CD11b⁺ cells were removed with a plunger. Cells were centrifuged at 500g for 5 min and resuspended in DMEM/F12 + GlutaMAX (Life Technologies, 10565042) supplemented with 10% FBS (Life Technologies, 10438026), 1% penicillin-streptomycin (Life Technologies, 15140122), 1% sodium pyruvate (Life Technologies, 11360070), 1% HEPES (Life Technologies, 15630106) and 1% MEM non-essential amino acids (Life Technologies, 11140050). Cells were stimulated for 6 h after plating.

Administration of psychedelics

Similar to previous studies, 1 mg kg⁻¹ psilocybin⁴⁷ (NIDA Drug Supply Program) or 10 mg kg⁻¹ MDMA-HCl racemate^{50,51} (NIDA Drug Supply Program) were administered by intraperitoneal injection at a dose of 1 mg kg⁻¹ or 10 mg kg⁻¹, respectively in 1× PBS 24 h after the final day of restraint stress, or as otherwise indicated in figure legends (Extended Data Figs. 8g and 9e, f). Control mice were treated with equal volume of vehicle (1× PBS). Mice were monitored for 6 h following drug administration. We analysed psilocybin and MDMA because of their use in clinical trials^{48,49}, and because the effects of both are thought to be mediated by complementary activation of serotonin signalling¹¹⁸, either through binding of serotonin receptors, (primarily psilocybin¹¹⁹) or by limiting serotonin reuptake (MDMA⁴⁶). Of note, MDMA bioavailability at 10 mg kg⁻¹ peaks at about 2000 ng ml⁻¹ (ref. 120), a concentration in range of its affinity for 5-HT₁ and 5-HT₂ receptors^{121,122}, and it also is reported to bind 5-HT_{2B} receptors^{123,124}, hence in these studies it may also activate serotonin receptors. Although we did not directly examine other transporters or neurotransmitter systems, except for TrkB¹²⁵ expression, it is possible these mechanisms play a role as well^{123,125-127}. Please also note that the doses of psilocybin and MDMA we used in mice (1 mg kg⁻¹ and 10 mg kg⁻¹) roughly correspond to doses that have shown clinical benefit in trials for humans^{48,49} (that is, 25 mg psilocybin

corresponds to 0.32–0.42 mg kg⁻¹ and 180 mg MDMA corresponds to 2.25–3 mg kg⁻¹, in average weight human males and females, respectively). Finally, we note that although we sometimes use the term ‘psychedelic’ for semantic simplicity¹²⁸, psilocybin is considered a ‘classical’ psychedelic⁴⁵, whereas MDMA is considered a consciousness-altering drug¹²⁶ or empathogenic psychedelic⁵⁰.

Meningeal explants

Meningeal explants were performed largely as previously described¹¹⁶. In brief, animals were euthanized, and blood was removed by cutting the right atrium. Following mouse perfusion, the head was severed, and the skin was removed from the head. A cut was made around the cranium (from the foramen magnum to the frontal bone) to dissect the bones of the calvarium. The skull was placed in a 24-well plate with 1 ml of DMEM (Life Technologies, 11965092) and incubated at 32 °C for 30 min at 150 r.p.m. Medium was removed and stored in a 1.5 ml tube at -80 °C (IL-1β). The skull was subsequently incubated in 1 ml of 50 ng ml⁻¹ phorbol 12-myristate 13-acetate (Sigma-Aldrich, P8139) and 1 µM ionomycin (Sigma-Aldrich, I3909-1ML) diluted in complete RPMI (Life Technologies, 11875119) containing 10% FBS, 1% penicillin-streptomycin, 50 µM 2-mercaptoethanol (Sigma-Aldrich, M6250) and 1% non-essential amino acids (Life Technologies, 11140050) at 32 °C for 2 h at 150 r.p.m. Medium was removed and stored in a 1.5 ml tube at -80 °C until processing and analysis (TNF).

Administration of nifedipine

Nifedipine (Sigma-Aldrich, N7634) was prepared as a stock solution in DMSO (Sigma-Aldrich, 472301) at 50 mg ml⁻¹. This stock was diluted 20-fold in corn oil and sonicated for 30 min after vortexing. Working dilutions were administered by intraperitoneal injection at a dose of 30 mg kg⁻¹ in 300 µl corn oil (Sigma-Aldrich, C8267) 30 min before administration of psychedelics. A second dose of nifedipine (Sigma-Aldrich, N7634) was delivered 3 h after the initial psychedelic dosing. Control mice were treated with an equal volume of vehicle (300 µl corn oil for nifedipine or 100 µl of 1× PBS for psychedelics). Samples were processed for FACS 6 h after the initial nifedipine treatment.

Fluorescence imaging of vascularity

Mice were anaesthetized with isoflurane and heads shaved as described above to clearly visualize the skin on top of the head. Vascularity was measured by *in vivo* fluorescence imaging. IVISense Vascular 750 (Revity, NEV10011EX) was reconstituted in PBS according to the manufacturer’s protocol and 100 µl of suspension was intravenously administered by tail-vein injection 30 min before administration of psychedelics. Mice that underwent 18 days of restraint stress were then administered 1× PBS, 1 mg kg⁻¹ psilocybin or 10 mg kg⁻¹ MDMA following the tracer injection described above. Fluorescence was captured with an excitation of 750 nm and an emission of 790 nm at high sensitivity and 5 s of exposure time using an In-Vivo Xtreme Optical/X-ray imaging system (Bruker) 30 min and 6 h after injection. MISE software (v.7, Bruker) was used to quantify net fluorescence signal intensity in the area of the mouse skull by manually selecting a ROI comprising the signal in the head of the mouse and subtracting the median background intensity from the ROI.

Chemical sympathectomy

Sympathectomy was performed in a manner similar to previous studies¹²⁹. In brief, 6-hydroxydopamine hydrobromide (Tocris Bioscience, 2547) was dissolved in 0.1% sodium ascorbate (Sigma Aldrich, PHR1279) immediately before administration and protected from light. 6-Hydroxydopamine hydrobromide was administered by intraperitoneal injection at a dose of 100 mg kg⁻¹ for 3 consecutive days starting 24 h after the final day of tube restraint. Tissue samples were taken for processing 4 days after the final 6-hydroxydopamine hydrobromide treatment.

Whole-mount immunostaining of peripheral organs

These procedures were performed largely as we and others have done previously for peripheral neurons^{130,131}. In brief, organs were collected and post-fixed in PFA (Electron Microscopy Sciences, 15714-S) freshly diluted to 4% in 1× PBS for 2 days, then transferred to 1× PBS until processing. Organs were washed 3 times for 15 min with ice-cold 1× PBS at 4 °C. Organs were then incubated in blocking solution (5% donkey serum and 1% PBS-T) overnight in the cold. Organs were then incubated in primary antibodies diluted in blocking solution for 2 days overnight with rotation at 4 °C. Organs were then washed with 1% Triton X-100 (Thermo Fisher Scientific, NC9356391) in PBS (PBS-T) 3 times for 2 h at room temperature, then incubated with secondary antibodies diluted in blocking solution overnight at 4 °C. Organs were washed 3 times for 2 h at room temperature and serially dehydrated in methanol in PBS (50%, 80% and 100%). Organs were then cleared in a mixture of 2:1 BABB and imaged on a Leica DMI8 widefield fluorescence microscope at ×5 magnification. The primary antibody used in this analysis was rabbit anti-tyrosine hydroxylase (Millipore, AB152, 1:100). The secondary antibody used in this analysis was goat anti-rabbit Alexa Fluor 488 (Thermo Fisher, A-11008, 4 µg ml⁻¹).

ImmGen data browser analysis

Ultra-low-input mouse and human RNA-seq data were obtained from the ImmGen data browser¹³² and accessed from Skyline plots. Cell types from multiple tissues that were analysed in mouse ImmGen data are shown in the following order per gene plot: DC_4+_Sp, DC_8+_Sp, DC_pDC_Sp, GN_BM, GN_Sp, GN_Thio_PC, Mo_6C-II_-Bl, Mo_6C+II_-Bl, MF_102+480+_PC, MF_226+II+480lo_PC, MF_Alv_Lu, MF_AT, MF_Fem_PC, MF_microglia_CNS, MF_PC, MF_pIC_Alv_Lu, MF_RP_Sp, MMP2_150+48+_BM, MMP3_48+_BM, MMP4_135+_BM, LTHSC_34_-BM, LTHSC_34+_BM, MC_BM and STHSC_150_-BM. Cell types accessed from human data were all derived from the blood, and each cell class is listed in the legend associated with the plot. For mice, the minimum reported value of normalized expression in the data browser was 0.1, whereas in humans it was 1.

Primary human astrocyte cell culture

Human astrocytes (ScienCell, 1800) were cultured largely as previously described^{21–25,71}. Cells were centrifuged at 500g for 5 min at 4 °C, resuspended in DMEM/F12 + GlutaMAX (Thermo Fisher Scientific, 10565018) supplemented with 10% FBS (Thermo Fisher Scientific, 10438026) and 1% penicillin-streptomycin (Thermo Fisher Scientific, 15140148) and cultured in T-75 flasks (Falcon, 353136) pre-coated with poly-L-lysine (Sigma Aldrich, P4707) for 1 h at 37 °C and washed with 1× PBS. Cells were cultured at 37 °C in a humidified incubator with 5% CO₂ for 7–10 days until confluence was reached. Medium was replaced every 2–3 days. To plate astrocytes, the flask was shaken for 2 h at 220 r.p.m., the medium removed and 5 ml trypsin was added at 37 °C for 3 min. Trypsin was neutralized with DMEM/F12 + GlutaMAX (Thermo Fisher Scientific, 10565018) supplemented with 10% FBS (Thermo Fisher Scientific, 10438026) and 1% penicillin-streptomycin (Thermo Fisher Scientific, 15140148). Cells were centrifuged at 500g for 5 min at 4 °C, resuspended in DMEM/F12 + GlutaMAX (Thermo Fisher Scientific, 10565018) supplemented with 10% FBS (Thermo Fisher Scientific, 0438026) and 1% penicillin-streptomycin (Thermo Fisher Scientific, 15140148) and cultured in a tissue-culture-treated plate pre-coated with poly-L-lysine (Sigma Aldrich, P4707). Astrocytes were plated for 5 days before in vitro treatments. The following molecules in DMEM/F12 + GlutaMAX (Thermo Fisher Scientific, 10565018) supplemented with 10% FBS (Thermo Fisher Scientific, 10438026) and 1% penicillin-streptomycin (Thermo Fisher Scientific, 15140148) were used to stimulate human astrocytes for 6 h: 50 ng ml⁻¹IL-1β (Sigma Aldrich, H6291); 50 ng ml⁻¹IL-6 (Sigma Aldrich, H7416); 50 ng ml⁻¹TNF (Sigma Aldrich, SRP3177); and 200 ng ml⁻¹cortisol (Sigma Aldrich, C-106) or 1 pg ml⁻¹

IL-1β (for *EGFR*). Following stimulation, astrocytes were treated with buffer RLT (Qiagen) and stored at –80 °C. Taqman probes used in this study were *GAPDH* (Hs02786624_g1), *PTPRS* (Hs01548375_m1) and *EGFR* (Hs01076090_m1).

Primary human monocyte cell culture

Primary human monocytes (iQ Biosciences, IQB-Hu1-M10) were cultured largely as previously described¹³³. Cells were centrifuged and resuspended in 10 ml RPMI-1640 (Life Technologies, 11875119) supplemented with 10% FBS (Life Technologies, 10438026) and 1% penicillin-streptomycin (Life Technologies, 15140122). Cells were stimulated 24 h after plating. Stimulations were performed for 6 h with the following molecules in RPMI (Life Technologies, 11875119) containing 10% FBS and 1% penicillin-streptomycin: 10 µM psilocybin (NIDA Drug Supply Program); 10 µM MDMA-HCl racemate (NIDA Drug Supply Program); 200 ng ml⁻¹cortisol (Sigma Aldrich, C-106); and 100 ng ml⁻¹LPS (InvivoGen, tRL-3pelp).

10x Genomics snRNA-seq

Flash-frozen amygdala samples from patients (matched for sex, age and race) were obtained from the NIH NeuroBioBank. Patient recruitment at the NIH NeuroBioBank is approved programmatically through the Institutional Review Board (IRB) of each institution providing patient samples. Specifically, “Donations are obtained from individuals who register before death, and/or from next-of-kin who authorize a post-mortem donation. Eligibility for postmortem donation of brain and other tissues is determined by trained staff at the individual BTR. BTR staff notification of a request for postmortem donation may come from surviving family members, treating physicians, hospital systems, donor services, organ and tissue banks, disease advocacy groups, specialized residential facilities, and/or collaborating medical examiners. Although the specific procedures for enrollment and consent may vary between the BTR sites, the policies and procedures of each bank have been reviewed and approved by their respective Institutional Review Board (IRB) and any additional appropriate oversight committees of the BTR site’s home institution. Trained individuals request and document consent for brain tissue donation from the deceased’s next-of-kin or legally authorized representative. Individual requests for release of medical records, questionnaires, and/or interviews with individuals knowledgeable of the deceased are obtained according to IRB approved policies and procedures.” The tissue samples were processed using a 10× Chromium Nuclei Isolation kit (10x Genomics, PN-1000494). In brief, 25 mg flash-frozen amygdala was placed in a 1.5 ml DNA LoBind tube (Eppendorf, 022431021) with 200 µl lysis reagent supplemented with 0.2 µl reducing agent B and 2.0 µl surfactant A. Tissue was dissociated with a plastic pestle and 300 µl lysis reagent supplemented with 0.3 µl reducing agent B, and 3.0 µl surfactant A was added once tissue was homogenized. Homogenized tissue was incubated on ice for 10 min. Dissociated tissue was transferred to a pre-chilled nuclei isolation column and centrifuged at 4 °C for 20 s at 16,000g. The column was discarded and nuclei were centrifuged at 4 °C for an additional 3 min at 500g. The pellet was resuspended in 500 µl debris-removal reagent supplemented with 0.5 µl reducing agent B and centrifuged at 4 °C for 10 min at 700g. Supernatant was discarded, and nuclei were resuspended in 875 µl of 1× PBS supplemented with 100 µl of 10% BSA and 25 µl RNase inhibitor. Nuclei were centrifuged at 4 °C for 5 min at 500g, resuspended again in 875 µl of 1× PBS supplemented with 100 µl of 10% BSA and 25 µl RNase Inhibitor, and centrifuged at 4 °C for 5 min at 500g. The nuclei were resuspended in 100 µl resuspension buffer and counted with a Nexcelom cell counter. Equal numbers of nuclei were pooled for samples from healthy individuals and from patients with MDD, centrifuged at 4 °C for 5 min at 500g and resuspended in diluted nuclei buffer containing 20× nuclei buffer, DTT, RNase inhibitor and nuclease-free water. Nuclei were then encapsulated using a 10x Genomics kit (10x Genomics, PN-1000283) with Chip J (10x Genomics,

Article

1000234) and a Chromium X controller according to the manufacturer's protocol to produce gel beads-in-emulsion (GEMs). GEMs were incubated following formation to produce reverse-transcribed cDNA and quenched at the end of the incubation period. GEMs were then broken with recovery agent. Reverse-transcribed cDNA was purified with Dynabeads and SPRIselect beads (Beckman Coulter, B23317). The purified cDNA was then amplified and used for library construction. Samples were indexed with Dual Index Plate TT set A (10x Genomics, PN-1000215). Final libraries were quantified using a Bioanalyzer DNA HS assay kit (Agilent, 50674626) and by qPCR with a Kapa library quantification kit (Kapa Biosystems, KK4824). The libraries were then diluted and pooled to 4 nM in nuclease-free water (Thermo Fisher Scientific, AM9937), run on an Illumina NextSeq550 and de-multiplexed into fastq files. The following read lengths were used for the run: read 1 = 28 bp, i7 index = 10 bp, i5 index = 10 bp, read 2 = 44 bp. Raw fastq files for each of the lanes for the MDD and control samples were uploaded and processed on the 10x Genomics Cloud CLI using the 3' Gene Expression pipeline using standard settings and cellranger (v.7.1.0). In brief, intron mode was used to align samples against GRCh38-2020-A, and the top 10,000 barcodes were selected for downstream analysis based on the input number of nuclei per experiment. Each sample was then merged using Cell Ranger Aggr (v.7.1.0), and the Loupe Browser file was output. Overall, and before filtering, per cell, we detected 31,787 reads, 1,345 median UMIs and 883 median genes. Using 10x Genomics Loupe Browser, only cells expressing 500–20,000 UMIs and <15% mitochondrial reads were included. Using k-means clustering parameters of eight clusters, we could distinguish major amygdala cell types. One cluster of approximately 110 cells did not express clear marker genes of a known cell population so it was excluded from downstream analyses, as well as any duplicate barcodes between the MDD and control samples. From there, we focused on the seven remaining cell-type clusters, which were identified using known marker genes for each cell type as follows: oligodendrocytes (*MOG*), astrocytes (*AQP4*), oligodendrocyte precursor cells (*PDGFRA*), excitatory neurons (*SLC17A7*), inhibitory neurons (*GAD1*) and microglia (*P2RY12*). On the basis of these markers, specific cell-type populations were subclustered, such as astrocytes or excitatory neurons. During astrocyte subclustering, we detected a cluster that expressed high levels of the endothelial-cell marker gene *CLDN5*, hence all cells in this cluster were removed from the analysis of subclustered astrocytes, and astrocytes were reclustered. To develop the EGFR signalling score for astrocytes, we compiled a list of common genes known to be increased by EGFR signalling from the pathways Gene Ontology 0007173, KEGG N00279 and KEGG N00284. The following genes were included in the list: *CBLC*, *SHC1*, *SPRY1*, *EPGN*, *TGFBI*, *NUP62*, *SOCS4*, *PIK3C2A*, *GRB2*, *DUSP3*, *RNF126*, *MTOR*, *HBEGF*, *ITGA1*, *SLC30A10*, *EGFR*, *CEACAM1*, *STAM2*, *RAB7A*, *MAP2K1*, *BRAF*, *BCAR3*, *DAB2IP*, *VIL1*, *ERRFI1*, *SPRY2*, *RNF115*, *ABL1*, *NEU3*, *PTPN12*, *GAREM1*, *RAF1*, *CHMP6*, *EPS15L1*, *CNOT9*, *FER*, *ZGPAT*, *CBL*, *RPS6KB1*, *ZFYVE28*, *PLAUR*, *IQGAP1*, *CCDC88A*, *CBLB*, *ARHGEF7*, *NCK2*, *HIP1*, *HAPI*, *ADAM17*, *VPS25*, *GAB1*, *PTPRJ*, *DGKD*, *SHKBP1*, *SH3KBP1*, *GPER1* and *CDH13*. These features were combined and the 'Feature Avg' was taken per cluster in the subclustered astrocytes with endothelial cells removed. Statistics were determined for the EGFR pathway signature score by performing pre-ranked GSEA on the log₂(FC) in cluster 2 astrocytes relative to all other astrocyte clusters. For excitatory neurons, the 'Feature Sum' of *NR2F2* and *SLTRK2* was taken in the subclustered excitatory neurons. For Qiagen IPA analyses, the log₂(FC) of genes of a cell-type subcluster relative to all other cell type subclusters was used as input.

Immunostaining of human tissue

Patient recruitment at the NIH NeuroBioBank is approved programmatically through the IRB of each institution providing patient samples and consent is given as described above. For staining of human amygdala tissue, flash-frozen samples obtained from the NIH NeuroBioBank were fixed in 4% PFA at 4 °C overnight and subsequently incubated in

30% sucrose for 24 h. Tissues were washed 3 times for 5 min each in DPBS then embedded in OCT. Brain sections (20 µm) were obtained using a cryostat and placed onto SuperFrost Plus slides (Fisher Scientific, 15-188-48). Sections were incubated in blocking solution (5% goat serum in 0.3% PBS-T) for 2 h at room temperature. Primary antibodies, diluted in the same blocking solution, were applied in a hydrophobic boundary drawn around the tissue and incubated at 4 °C overnight. The following day, sections were washed 3 times in 0.3% PBS-T at room temperature, then incubated with secondary antibodies diluted in blocking solution for 2 h at room temperature. After five final washes in DPBS, sections were mounted using Fluoromount-G with DAPI (SouthernBiotech, 0100-20). Confocal images were captured with a Zeiss LSM880 using a ×63 objective, with an 8-plane z stack at 1 µm intervals. Maximal intensity of GFAP-positive cells was quantified using Fiji. The primary antibodies used were mouse anti-EGFR antibody (Abcam, 1:100, ab30) and rabbit anti-GFAP (Abcam, 1:200, ab68428), with the following corresponding secondary antibodies: goat anti-rabbit IgG (H+L) highly cross-adsorbed Alexa Fluor 594 (Invitrogen, A11037) and goat anti-mouse IgG (H+L) highly cross-adsorbed Alexa Fluor 488 (Invitrogen, A11029).

Statistics

Statistical analyses were performed using GraphPad Prism 10. For analyses of gene expression represented by volcano plots, the control group is listed second (Figs. 1j,q, 2f and 5c and Extended Data Fig. 8j). Hence, gene expression is shown as the experimental group relative to the control group. For t-tests, all tests were two-tailed unless explicitly specified otherwise. For the EPM data, unpaired two-tailed t-tests were used (Fig. 4d,h and Extended Data Figs. 1d, 2d and, 7g,l). For fear conditioning and extinction data (Figs. 1b,i, 2e and 4e,i and Extended Data Figs. 1b,c, 3f,g and 8f,g), two-way repeated-measures ANOVA was used; Extended Data Fig. 1b was analysed using the interaction statistic, whereas other panels were analysed using the group statistic. Independent experiments were grouped together. Analyses of mouse plasma were performed by two-way ANOVA to determine differences as a function of condition followed by unpaired two-tailed t-tests to determine significance by group (Fig. 1c). Plasma analyses of all other cytokines were analysed by two-way ANOVA by condition (Extended Data Figs. 1e and 2c). The presented representative confocal images were replicated at least three times (Fig. 1m and Extended Data Figs. 3a,j, 4a, 6a,b, 7k,o,p,q and 9h), except for Figs. 2k and 4k and Extended Data Fig. 2b,f, which were replicated twice. All figures were replicated at least three times, excluding Fig. 1c and Extended Data Figs. 2b, 7d,e and 10i, which were repeated twice. For mouse tdTomato⁺ scRNA-seq data (Fig. 1e), the cluster FCs in response to stress relative to control are as follows: 0.48 (cluster 0); 1.96 (cluster 1); 2.39 (cluster 2); 1.05 (cluster 3); 1.32 (cluster 4); 1.04 (cluster 5); 0.98 (cluster 6); 106.41 (cluster 7); and 1.44 (cluster 8). For human astrocyte snRNA-seq data (Fig. 5g), the cluster FCs in MDD relative to control are as follows: 0.12 (cluster 1); 7.55 (cluster 2); 0.40 (cluster 3); 1.72 (cluster 4); 0.01 (cluster 5); and 4.60 (cluster 6). For human excitatory neuron snRNA-seq data (Fig. 5j), the cluster FCs in MDD relative to control are as follows: 0.92 (cluster 1); 5.27 (cluster 2); 0.48 (cluster 3); 47.83 (cluster 4); 3.09 (cluster 5); 1.07 (cluster 6); 0.14 (cluster 7); 0.24 (cluster 8); and not detected in MDD (cluster 9). Significance levels if not explicitly indicated in figures are as follows: *P < 0.05, **P < 0.01, ***P < 0.001 and NS (P > 0.05).

Reporting summary

Further information on research design is available in the Nature Portfolio Reporting Summary linked to this article.

Data availability

Data in this study have been deposited into the GEO under the super series accession number GSE262989. Bulk RNA-seq datasets of

amygdala neurons were obtained from the GEO with accession numbers GSE162417 (ref. 93), GSE66345 (ref. 94), GSE130268 (ref. 95), GSE138522 (ref. 96), GSE183092 (ref. 97) and GSE151798 (ref. 98). A mouse atlas of brain structures²⁷ was accessed at <https://cells.ucsc.edu/?ds=mouse-nervous-system>, and .loom files for each brain region included were downloaded with annotations from a previous study²⁷. An atlas of amygdala cell types³⁶ was accessed from FigShare (<https://doi.org/10.6084/m9.figshare.20412573>)³⁴. Gene-expression data of purified human immune cell populations were accessed using the ImmGen Skyline RNA-seq data browser¹³² (<https://www.immgen.org/Databrowser19/DatabrowserPage.html>). Source data are provided with this paper.

Code availability

No new code was developed for this study.

61. Shultz, L. D. et al. Human lymphoid and myeloid cell development in NOD/LtSz-scid IL2R γ null mice engrafted with mobilized human hemopoietic stem cells. *J. Immunol.* **174**, 6477–6489 (2005).
62. Coughlan, A. M. et al. Myeloid engraftment in humanized mice: impact of granulocyte-colony stimulating factor treatment and transgenic mouse strain. *Stem Cells Dev.* **25**, 530–541 (2016).
63. Srinivasan, R. et al. New transgenic mouse lines for selectively targeting astrocytes and studying calcium signals in astrocyte processes *in situ* and *in vivo*. *Neuron* **92**, 1181–1195 (2016).
64. Madisen, L. et al. A robust and high-throughput Cre reporting and characterization system for the whole mouse brain. *Nat. Neurosci.* **13**, 133–140 (2010).
65. Buch, T. et al. A Cre-inducible diphtheria toxin receptor mediates cell lineage ablation after toxin administration. *Nat. Methods* **2**, 419–426 (2005).
66. Xu, Z. et al. Efficient strategies for microglia replacement in the central nervous system. *Cell Rep.* **32**, 108041 (2020).
67. Tomura, M. et al. Monitoring cellular movement *in vivo* with photoconvertible fluorescence protein “Kaeche” transgenic mice. *Proc. Natl Acad. Sci. USA* **105**, 10871–10876 (2008).
68. Chu, C. et al. The microbiota regulate neuronal function and fear extinction learning. *Nature* **574**, 543–548 (2019).
69. Shen, Y. et al. CCR5 closes the temporal window for memory linking. *Nature* **606**, 146–152 (2022).
70. Woodburn, S. C., Levitt, C. M., Koester, A. M. & Kwan, A. C. Psilocybin facilitates fear extinction: importance of dose, context, and serotonin receptors. *ACS Chem. Neurosci.* **15**, 3034–3043 (2024).
71. Clark, I. C. et al. Barcoded viral tracing of single-cell interactions in central nervous system inflammation. *Science* **372**, eabf1230 (2021).
72. Macosko, E. Z. et al. Highly parallel genome-wide expression profiling of individual cells using nanoliter droplets. *Cell* **161**, 1202–1214 (2015).
73. Bergen, V., Lange, M., Peidli, S., Wolf, F. A. & Theis, F. J. Generalizing RNA velocity to transient cell states through dynamical modeling. *Nat. Biotechnol.* **38**, 1408–1414 (2020).
74. Hunker, A. C. et al. Conditional single vector CRISPR/SaCas9 viruses for efficient mutagenesis in the adult mouse nervous system. *Cell Rep.* **30**, 4303–4316 (2020).
75. Lee, J.-H. et al. Astrocytes phagocytose adult hippocampal synapses for circuit homeostasis. *Nature* **590**, 612–617 (2020).
76. Challis, R. C. et al. Systemic AAV vectors for widespread and targeted gene delivery in rodents. *Nat. Protoc.* **14**, 379–414 (2019).
77. Mathis, A. et al. DeepLabCut: markerless pose estimation of user-defined body parts with deep learning. *Nat. Neurosci.* **21**, 1281–1289 (2018).
78. Nath, T. et al. Using DeepLabCut for 3D markerless pose estimation across species and behaviors. *Nat. Protoc.* **14**, 2152–2176 (2019).
79. Sturman, O. et al. Deep learning-based behavioral analysis reaches human accuracy and is capable of outperforming commercial solutions. *Neuropsychopharmacology* **45**, 1942–1952 (2020).
80. Grdinariu, V. et al. Molecular and cellular approaches for diversifying and extending optogenetics. *Cell* **141**, 154–165 (2010).
81. He, D. et al. Disruption of the IL-33-ST2-AKT signaling axis impairs neurodevelopment by inhibiting microglial metabolic adaptation and phagocytic function. *Immunity* **55**, 159–173 (2022).
82. Leites, E. P. & Morais, V. A. Protocol for the isolation and culture of microglia, astrocytes, and neurons from the same mouse brain. *STAR Protoc.* **5**, 102804 (2024).
83. Dobin, A. et al. STAR: ultrafast universal RNA-seq aligner. *Bioinformatics* **29**, 15–21 (2012).
84. Chen, S., Zhou, Y., Chen, Y. & Gu, J. fastp: an ultra-fast all-in-one FASTQ preprocessor. *Bioinformatics* **34**, i884–i890 (2018).
85. Ewels, P., Magnusson, M., Lundin, S. & Käller, M. MultiQC: summarize analysis results for multiple tools and samples in a single report. *Bioinformatics* **32**, 3047–3048 (2016).
86. Liao, Y., Smyth, G. K. & Shi, W. featureCounts: an efficient general purpose program for assigning sequence reads to genomic features. *Bioinformatics* **30**, 923–930 (2014).
87. Robinson, M. D., McCarthy, D. J. & Smyth, G. K. edgeR: a Bioconductor package for differential expression analysis of digital gene expression data. *Bioinformatics* **26**, 139–140 (2010).
88. Subramanian, A. et al. Gene set enrichment analysis: a knowledge-based approach for interpreting genome-wide expression profiles. *Proc. Natl Acad. Sci. USA* **102**, 15545–15550 (2005).
89. Chen, E. Y. et al. Enrichr: interactive and collaborative HTML5 gene list enrichment analysis tool. *BMC Bioinformatics* **14**, 128 (2013).
90. Kuleshov, M. V. et al. Enrichr: a comprehensive gene set enrichment analysis web server 2016 update. *Nucleic Acids Res.* **44**, W90–W97 (2016).
91. Xie, Z. et al. Gene set knowledge discovery with Enrichr. *Curr. Protoc.* **1**, e90 (2021).
92. Szklarczyk, D. et al. The STRING database in 2023: protein–protein association networks and functional enrichment analyses for any sequenced genome of interest. *Nucleic Acids Res.* **51**, D638–D646 (2023).
93. Laricchia, D. et al. Optogenetic stimulation of prelimbic pyramidal neurons maintains fear memories and modulates amygdala pyramidal neuron transcriptome. *Int. J. Mol. Sci.* **22**, 810 (2021).
94. Namburi, P. et al. A circuit mechanism for differentiating positive and negative associations. *Nature* **520**, 675–678 (2015).
95. Samineni, V. K. et al. Cellular, circuit and transcriptional framework for modulation of itch in the central amygdala. *eLife* **10**, e68130 (2021).
96. Levitan, D. et al. Deletion of *Stk11* and *Fos* in mouse BLA projection neurons alters intrinsic excitability and impairs formation of long-term aversive memory. *eLife* **9**, e61036 (2020).
97. Knodel, J. R. et al. A functional cellular framework for sex and estrous cycle-dependent gene expression and behavior. *Cell* **185**, 654–671 (2022).
98. Yamaguchi, T. et al. Posterior amygdala regulates sexual and aggressive behaviors in male mice. *Nat. Neurosci.* **23**, 1111–1124 (2020).
99. Golden, S. A. et al. Basal forebrain projections to the lateral habenula modulate aggression reward. *Nature* **534**, 688–692 (2016).
100. Buenrostro, J. D., Wu, B., Chang, H. Y. & Greenleaf, W. J. ATAC-seq: a method for assaying chromatin accessibility genome-wide. *Curr. Protoc. Mol. Biol.* **109**, 21.29.1–21.29.9 (2015).
101. Chen, A. et al. Spatiotemporal transcriptomic atlas of mouse organogenesis using DNA nanoball-patterned arrays. *Cell* **185**, 1777–1792 (2022).
102. Chen, A. et al. Single-cell spatial transcriptome reveals cell-type organization in the macaque cortex. *Cell* **186**, 3726–3743 (2023).
103. van der Walt, S. et al. scikit-image: image processing in Python. *PeerJ* **2**, e453 (2014).
104. Wolf, F. A., Angerer, P. & Theis, F. J. SCANPY: large-scale single-cell gene expression data analysis. *Genome Biol.* **19**, 15 (2018).
105. Waclaw, R. R., Ehrman, L. A., Pierani, A. & Campbell, K. Developmental origin of the neuronal subtypes that comprise the amygdala fear circuit in the mouse. *J. Neurosci.* **30**, 6944–6953 (2010).
106. Kuerbitz, J. et al. Loss of intercalated cells (ITCs) in the mouse amygdala of *Tshz1* mutants correlates with fear, depression, and social interaction phenotypes. *J. Neurosci.* **38**, 1160–1177 (2018).
107. Garcia-Calero, E., Martínez-de-la-Torre, M. & Puelles, L. A radial histogenetic model of the mouse pallial amygdala. *Brain Struct. Funct.* **225**, 1921–1956 (2020).
108. Glendinning, K. A., Fisher, L. C. & Jasoni, C. L. Maternal high fat diet alters offspring epigenetic regulators, amygdala glutamatergic profile and anxiety. *Psychoneuroendocrinology* **96**, 132–141 (2018).
109. Nery, S., Fishell, G. & Corbin, J. G. The caudal ganglionic eminence is a source of distinct cortical and subcortical cell populations. *Nat. Neurosci.* **5**, 1279–1287 (2002).
110. Huang, W.-C., Chen, Y. & Page, D. T. Hyperconnectivity of prefrontal cortex to amygdala projections in a mouse model of macrocephaly/autism syndrome. *Nat. Commun.* **7**, 13421 (2016).
111. Stenman, J., Yu, R. T., Evans, R. M. & Campbell, K. *Tlx* and *Pax6* co-operate genetically to establish the pallio-subpallial boundary in the embryonic mouse telencephalon. *Development* **130**, 1113–1122 (2003).
112. Tosches, M. A. et al. Evolution of pallium, hippocampus, and cortical cell types revealed by single-cell transcriptomics in reptiles. *Science* **360**, 881–888 (2018).
113. Boyle, M. P. et al. Cell-type-specific consequences of Reelin deficiency in the mouse neocortex, hippocampus, and amygdala. *J. Comp. Neurol.* **519**, 2061–2089 (2011).
114. Ressler, K. J. et al. Post-traumatic stress disorder: clinical and translational neuroscience from cells to circuits. *Nat. Rev. Neuro.* **18**, 273–288 (2022).
115. Rothhammer, V. et al. Type I interferons and microbial metabolites of tryptophan modulate astrocyte activity and central nervous system inflammation via the aryl hydrocarbon receptor. *Nat. Med.* **22**, 586–597 (2016).
116. Pinho-Ribeiro, F. A. et al. Bacteria hijack a meningeal neuroimmune axis to facilitate brain invasion. *Nature* **615**, 472–481 (2023).
117. Wilk, C. M. et al. Circulating senescent myeloid cells infiltrate the brain and cause neurodegeneration in histiocytic disorders. *Immunity* **56**, 2790–2802 (2023).
118. Barnes, N. M. et al. International Union of Basic and Clinical Pharmacology. CX. Classification of receptors for 5-hydroxytryptamine; pharmacology and function. *Pharmacol. Rev.* **73**, 310–520 (2021).
119. Gumpfer, R. H. & Roth, B. L. SnapShot: psychedelics and serotonin receptor signaling. *Cell* **186**, 232–232 (2023).
120. Baumann, M. H. et al. Effects of dose and route of administration on pharmacokinetics of (+)-3,4-methylenedioxymethamphetamine in the rat. *Drug Metab. Dispos.* **37**, 2163–2170 (2009).
121. Lyon, R. A., Glennon, R. A. & Titeler, M. 3,4-Methylenedioxymethamphetamine (MDMA): stereoselective interactions at brain 5-HT₁ and 5-HT₂ receptors. *Psychopharmacology* **88**, 525–526 (1986).
122. Nash, J., Roth, B., Brodkin, J., Nichols, D. & Gudelsky, G. Effect of the R(–) and S(+) isomers of MDA and MDMA on phosphotidyl inositol turnover in cultured cells expressing 5-HT_{2A} or 5-HT_{2C} receptors. *Neurosci. Lett.* **177**, 111–115 (1994).
123. Setola, V. et al. 3,4-methylenedioxymethamphetamine (MDMA, “Ecstasy”) induces fenfluramine-like proliferative actions on human cardiac valvular interstitial cells *in vitro*. *Mol. Pharmacol.* **63**, 1223–1229 (2003).
124. Doly, S. et al. Serotonin 5-HT_{2B} receptors are required for 3,4-methylenedioxymethamphetamine-induced hyperlocomotion and 5-HT release *in vivo* and *in vitro*. *J. Neurosci.* **28**, 2933–2940 (2008).
125. Moliner, R. et al. Psychedelics promote plasticity by directly binding to BDNF receptor TrkB. *Nat. Neurosci.* <https://doi.org/10.1038/s41593-023-01316-5> (2023).

Article

126. McClure-Begley, T. D. & Roth, B. L. The promises and perils of psychedelic pharmacology for psychiatry. *Nat. Rev. Drug Discov.* **21**, 463–473 (2022).
127. Cameron, L. P. et al. Beyond the 5-HT_{2A} receptor: classic and nonclassic targets in psychedelic drug action. *J. Neurosci.* **43**, 7472–7482 (2023).
128. Nichols, D. E., Nichols, C. D. & Hendricks, P. S. Proposed consensus statement on defining psychedelic drugs. *Psychedelic Med.* **1**, 12–13 (2023).
129. Schneider, K. M. et al. The enteric nervous system relays psychological stress to intestinal inflammation. *Cell* **186**, 2823–2838 (2023).
130. Wheeler, M. A. et al. TNF- α /TNFR1 signaling is required for the development and function of primary nociceptors. *Neuron* **82**, 587–602 (2014).
131. Glebova, N. O. & Ginty, D. D. Heterogeneous requirement of NGF for sympathetic target innervation in vivo. *J. Neurosci.* **24**, 743–751 (2004).
132. Heng, T. S. P., Painter, M. W. & Immunological Genome Project Consortium. The Immunological Genome Project: networks of gene expression in immune cells. *Nat. Immunol.* **9**, 1091–1094 (2008).
133. Sanmarco, L. M. et al. Lactate limits CNS autoimmunity by stabilizing HIF-1 α in dendritic cells. *Nature* **620**, 881–889 (2023).
134. Zeisel, A. Amy_FC_allcells_with_metadata_31-Jul-2022.txt. Figshare <https://doi.org/10.6084/m9.figshare.20412573> (2022).

Acknowledgements M.A.W. acknowledges support from the NIMH, NIDA and NINDS (R01MH130458, R01MH132632, R01DA061199 and R00NS114111), the Boston Claude D. Pepper Older Americans Independence Center and the Brigham Research Institute. F.J.Q. acknowledges support from grants NS102807, ES02530, ES029136 and AI126880 from the NIH; RG4111A1 and JF2161-A-5 from the NMSS; RSG-14-198-01-LIB from the American Cancer Society; and PA-1604-08459 from the International Progressive MS Alliance. V.K.K. acknowledges support from NIH grants R01AG080992 and R01AI139536. I.M.C. acknowledges support from grants R01AI168005 and R01DK127257 from the NIH; the Chan-Zuckerberg Initiative; the Jackson-Wijaya Fund; and the Burroughs Wellcome Fund. E.N.C. acknowledges a Research Supplement to Promote Diversity in Health-Related Research from the NINDS (R00NS114111-S1) and the Brigham Research Institute. C.M.P. was supported by the National Multiple Sclerosis Society (FG-2307-42209) and the Mayer Foundation. M.K. was supported by a Leopoldina Research Fellow Grant of the German Academy of Sciences. S.S.D. was supported by a Banting Postdoctoral Fellowship from the Canadian Institutes for Health Research. J.-H.L. was supported

by the Basic Science Research Program funded by the NRF of Korea/Ministry of Education (2022R1A6A3A03071157) and by a long-term postdoctoral fellowship funded by the Human Frontier Science Program (LT0015/2023-L). H.-G.L. was supported by the Basic Science Research Program through the NRF funded by the Ministry of Education (2021R1A6A3A14039088) and The Gene Lay Institute of Immunology and Inflammation of Brigham and Women's Hospital, Massachusetts General Hospital and Harvard Medical School (FP-0034491). D.F. was supported by the Gemeinnützige Hertie-Stiftung foundation. Illustrations in Figs. 1a,d,h, 2c,d and 4b,g,k,n and Extended Data Figs. 1a,f, 2g and 7d,f were created using BioRender (<https://www.biorender.com>). We thank L. Ding and staff at the Neurotechnology Studio at Brigham and Women's Hospital for equipment access; F. Pinho-Ribeiro for discussions on meningeal immune cells; M. Lee and staff at the Gene Lay Institute Genomics Platform for equipment access; Z. Houston, R. Gessner and K. Quick for discussions related to IVIS imaging; R. Krishnan for assistance with flow cytometry; L. Gaffney for assistance with figure illustrations; C. Jennings for feedback on the manuscript text; staff at STOMics, Eve Technologies, Watershed Bioinformatics and Via Foundry; staff at the NIH NeuroBioBank for providing human amygdala samples from healthy individuals and from patients with MDD; staff at the NIDA Drug Supply Program and the Research Triangle Institute for providing psilocybin and MDMA; and the patients and their families for agreeing to participate in this study.

Author contributions E.N.C., J.L., C.M.P., J.C., C.F.A., M.K., W.M.W., G.G., M.Y., T.H.H., S.S.D., L.Y., C.R.G.L.d., J.-H.L., L.D., D.F., A.M.S., H.-G.L., O.A. and M.A.W. performed experiments, analysed data and/or interpreted data. S.G. aided with interpretation of data involving psychedelics. S.G., S.M.S., I.M.C., V.K.K. and F.J.Q. contributed specific reagents or methods, interpreted data and provided input on the experiments. E.N.C., J.L. and M.A.W. wrote the manuscript with input from all co-authors. M.A.W. directed and supervised the study.

Competing interests The authors declare no competing interests.

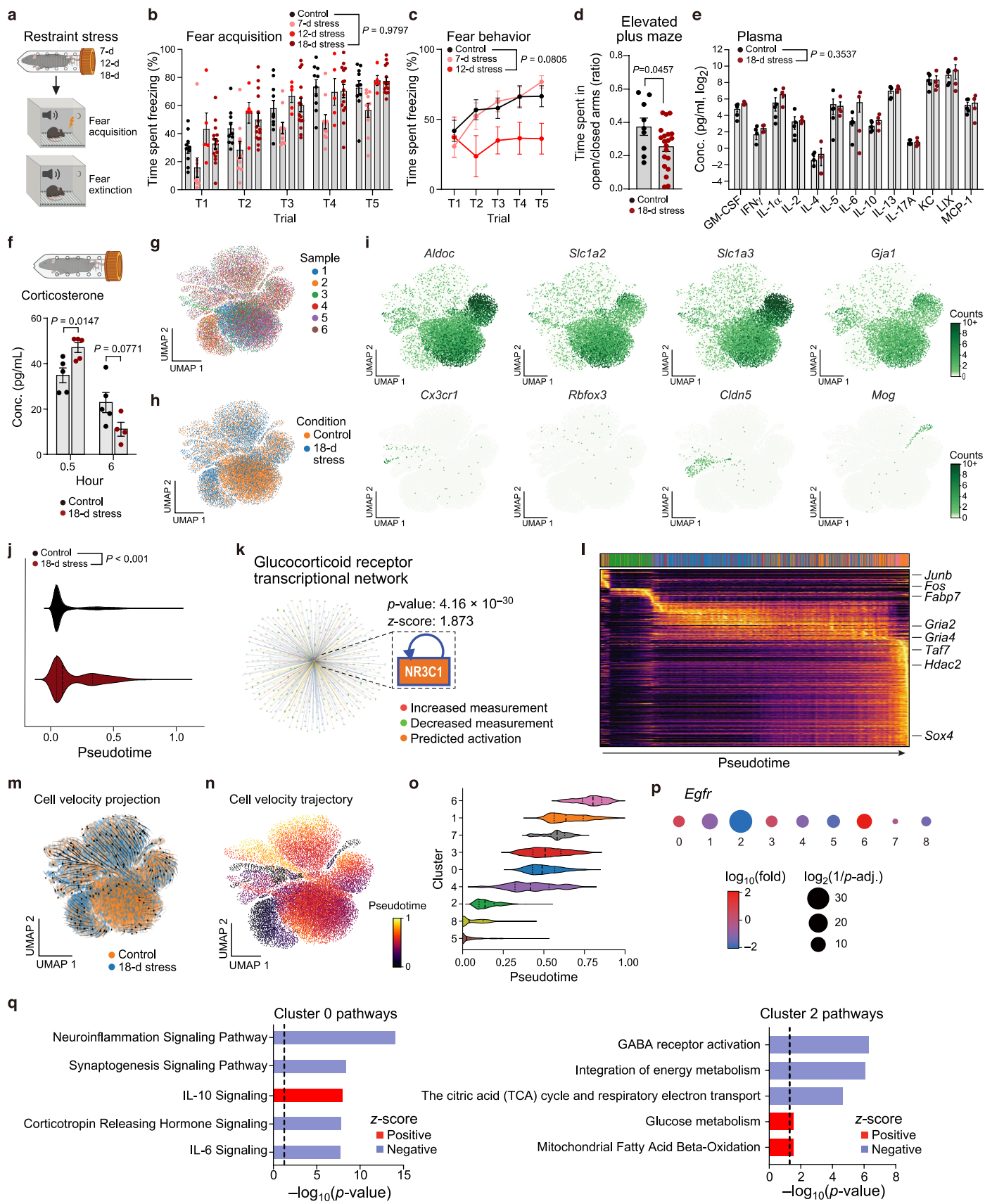
Additional information

Supplementary information The online version contains supplementary material available at <https://doi.org/10.1038/s41586-025-08880-9>.

Correspondence and requests for materials should be addressed to Michael A. Wheeler.

Peer review information *Nature* thanks Scott Russo, Marco Colonna and the other, anonymous, reviewer(s) for their contribution to the peer review of this work.

Reprints and permissions information is available at <http://www.nature.com/reprints>.



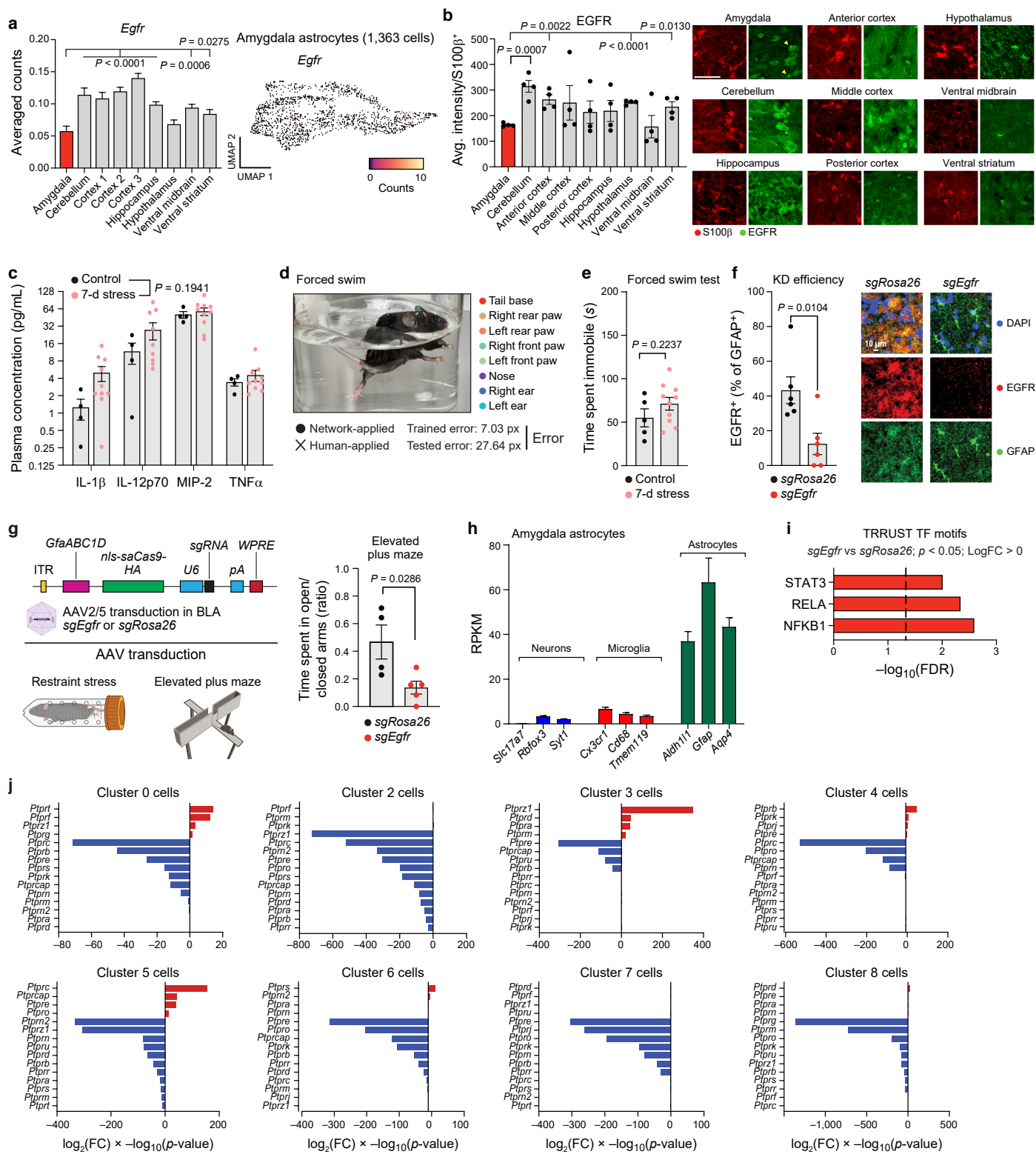
Extended Data Fig. 1 | See next page for caption.

Article

Extended Data Fig. 1 | Molecular and behavioral changes after 18-days restraint stress.

a, Schematic of behavioral paradigm. Tube restraint for 7, 12, or 18 days, followed by cued fear acquisition, with fear retrieval conducted the next day in a novel context with only cue presentation. **b**, Acquisition of fear behavior in mice exposed to 7-days ($n = 10$), 12-days ($n = 5$), or 18-days ($n = 15$) of stress or controls ($n = 14$). Two-way repeated measures ANOVA. **c**, Time spent freezing in conditioned fear behavior across trials. $n = 10$ mice per group. Two-way repeated measures ANOVA. **d**, Time in open/closed arm of elevated plus maze (EPM) in mice exposed to 18-days of stress ($n = 20$) or controls ($n = 9$). Unpaired t-test. **e**, Cytokines detected by ELISA in the plasma of mice exposed to 18-days of restraint stress ($n = 4$) or controls ($n = 5$). Two-way ANOVA. **f**, Changes in corticosterone levels in 18-day stressed mice or control mice, measured at

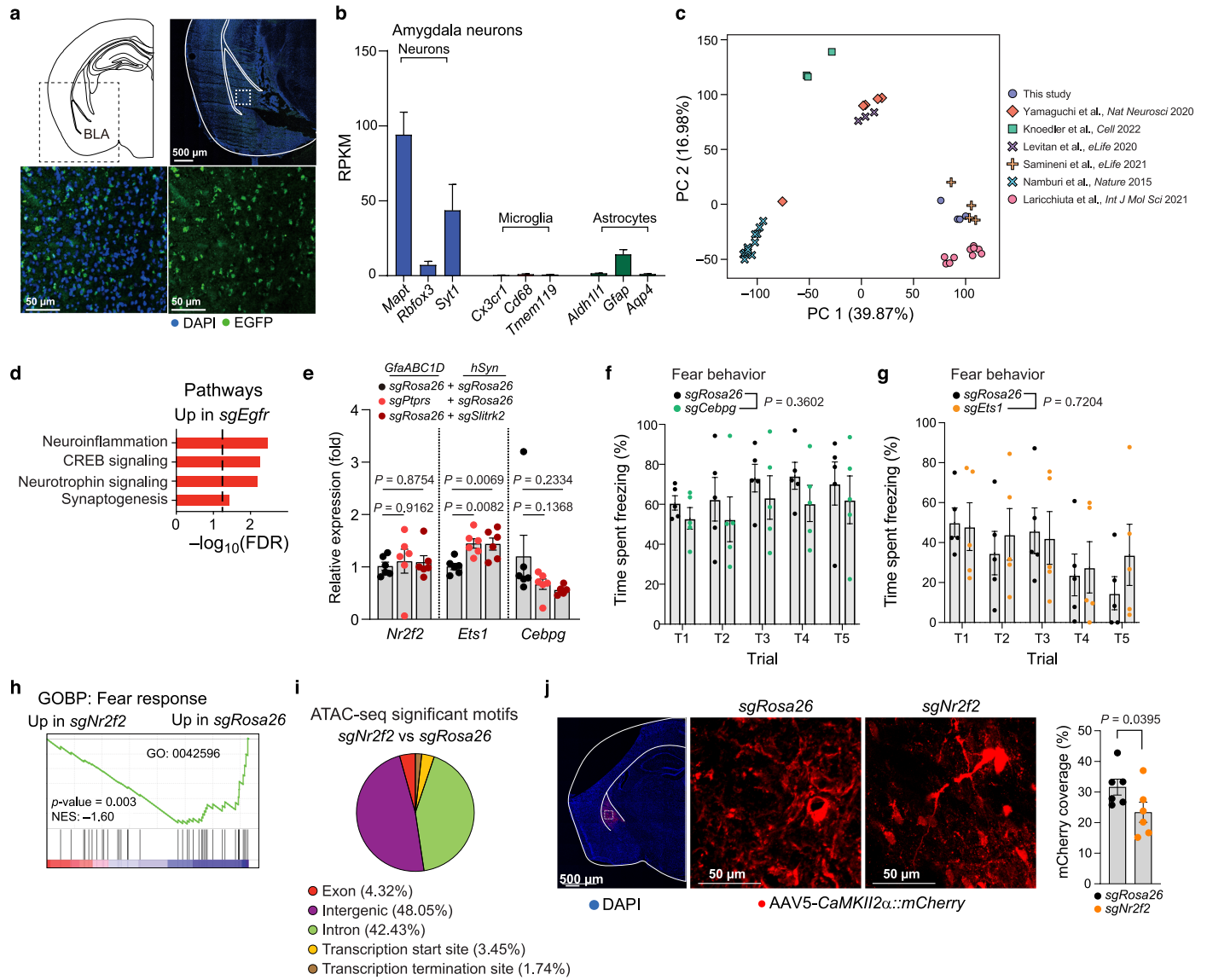
30-min ($n = 5$ per group) and 6-h (control, $n = 5$; 18d-stress, $n = 4$) after final session of restraint stress concluded. Unpaired t-test. **g**, UMAP plot of *Aldh1l1^{tdTomato/+}* cells from control ($n = 3$) and 18-day stress ($n = 3$) mice. **h**, UMAP plot of *Aldh1l1^{tdTomato/+}* cells from individual mice. **i**, Scatterplots of astrocyte (top row) or control (bottom row) markers. **j**, Pseudotime violin plot of captured *Aldh1l1^{tdTomato/+}* cells. Unpaired t-test. **k**, Prediction by Qiagen IPA of glucocorticoid receptor as a transcriptional regulator of cluster 1 *Aldh1l1^{tdTomato/+}* cells. **l-o**, Heatmap (**l**), UMAP (**m,n**), and violin plot (**o**) of RNA velocity data associating *Aldh1l1^{tdTomato/+}* cell clusters to stages of the pseudotime trajectory. **p**, Dot plot of *Egrf* expression in each cluster. **q**, Plots of pathways in cluster 0 (left) and cluster 2 (right) cells. Schematics (**a,f**) were created using BioRender (<https://biorender.com>). Data shown as mean \pm SEM.



Extended Data Fig. 2 | Amygdala astrocytes regulate chronic stress responses. **a**, Analysis of astrocyte *Egfr* expression across brain regions using a previously annotated mouse brain single-cell atlas²⁷. One-way ANOVA, Fisher post-test. **b**, Quantification and confocal images of EGFR expression in astrocytes across multiple brain regions. $n = 4$ per group. Yellow arrows indicate EGFR⁺S100 β ⁺ cells. Unpaired t-test. **c**, Analysis by ELISA of cytokines from control ($n = 4$) or 7-day stressed ($n = 10$) mice. Two-way ANOVA. **d,e**, Validation of DeepLabCut forced swim model (**d**) and quantification (**e**) of time spent immobile in forced swim. $n = 5$ per control group, $n = 10$ for 7-day restraint. Unpaired t-test. **f**, Quantification (left) and staining (right) validating EGFR KD. $n = 6$ images from $n = 3$ mice per group. Unpaired t-test. **g**, Schematic

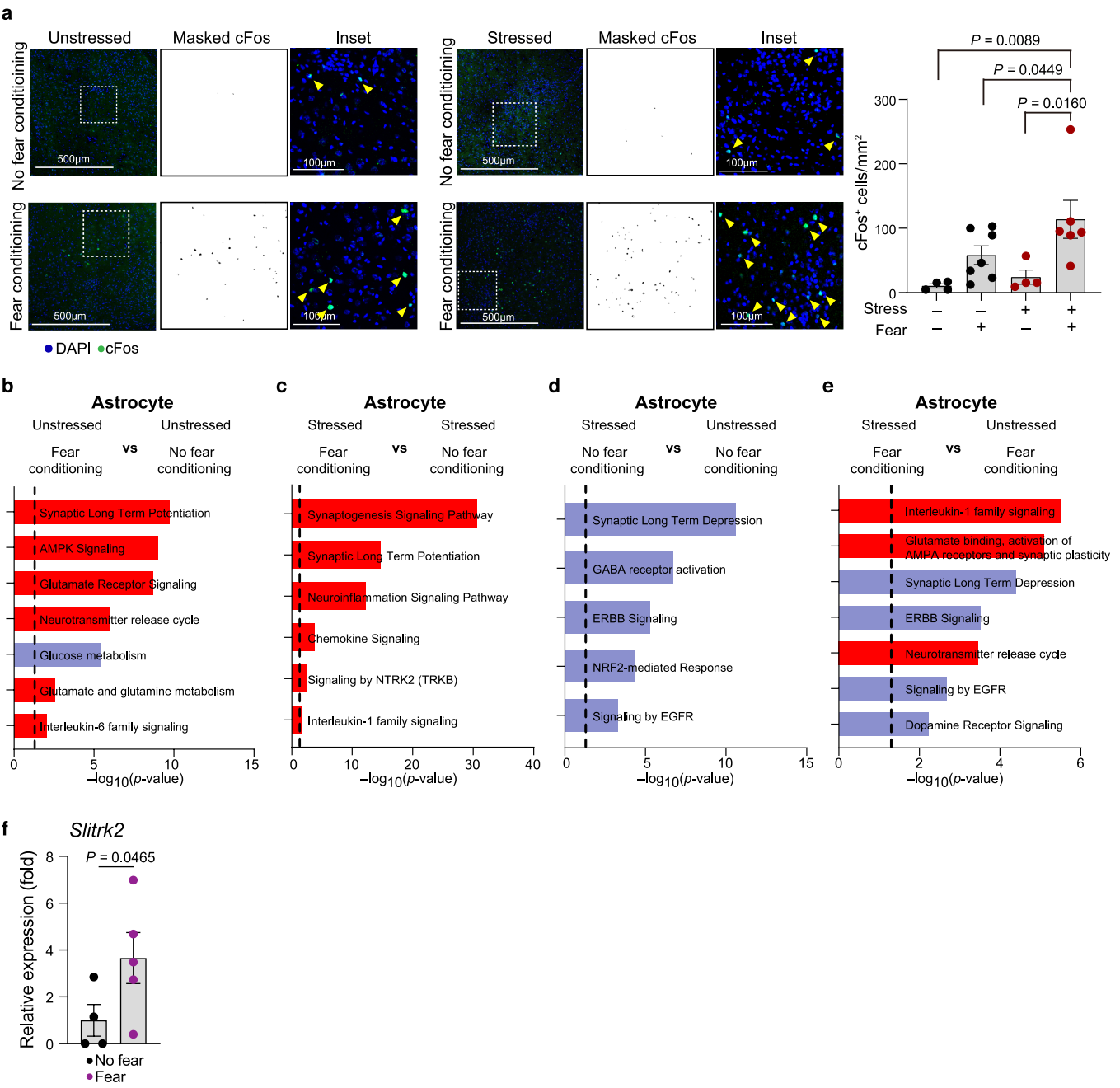
and bar graph of elevated plus maze (EPM) analysis in mice with astrocytic *Egfr* knockdown via AAV vector delivery to the basolateral amygdala. Mice were subjected to 7-days restraint stress prior to testing in the EPM (*sgRosa26*, $n = 4$; *sgEgfr*, $n = 5$). Unpaired t-test. **h**, Validation of astrocyte cell type markers detected by bulk RNA-seq of amygdala astrocytes. $n = 7$ mice. **i**, Analysis of transcription factor motifs detected in *sgEgfr* ($n = 3$) versus *sgRosa26* ($n = 4$) astrocytes. **j**, Plots of PTPR family member expression in cells of each cluster from *Aldh1l1*^{tdTomato/+} cells analyzed by scRNA-seq. saCas9, *S. aureus* Cas9; NS, not significant. FDR, false discovery rate. RPKM, Reads Per Kilobase of transcript per Million mapped reads. Schematic (**g**) was created using BioRender (<https://biorender.com>). Data shown as mean \pm SEM.

Article



Extended Data Fig. 3 | Screening neuron transcription factors involved in fear behavior. **a**, Validation of stereotaxic targeting of BLA neurons by immunostaining, using an AAV5 delivering *hSyn*-driven EGFP. **b**, Cell type markers for neurons versus other amygdala cell types in samples analyzed in these studies. $n = 7$ mice. **c**, Principal component analysis of control amygdala neuron samples collected in this study versus previously published studies. $n = 4$ mice. **d**, Pathways upregulated in bulk RNA-seq data of amygdala neurons from astrocyte-targeted *sgEgfr* ($n = 3$) relative to controls ($n = 3$). **e**, qPCR analysis of the indicated genes in neuron-astrocyte co-cultures following viral transduction with either *sgPtprs* under the *GfaABC1D* promoter, *sgSlitrk2* under the *hSyn* promoter, or *sgRosa26* controls. $n = 5$ per group. One-way

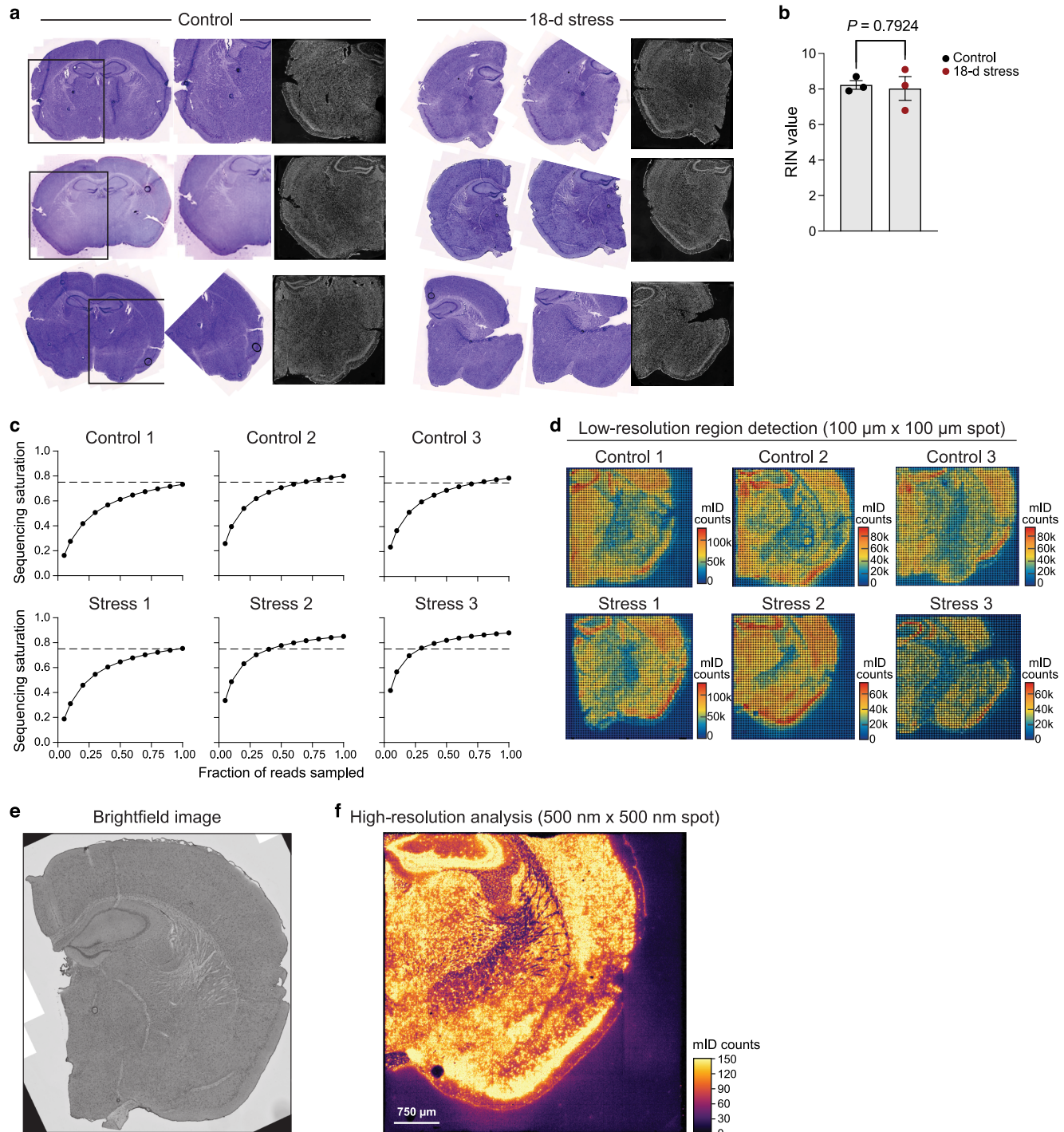
ANOVA, Dunnett post-test. **f,g**, Freezing behavior of mice exposed to 7-days of restraint stress following injection of AAV delivering *saCas9* under the *hSyn* promoter and targeting *sgRosa26*, *sgCebpg*, or *sgEts1*. $n = 5$ mice per group. Two-way repeated measures ANOVA. **h**, GSEA plot comparing bulk RNA-seq data of amygdala neurons targeting *sgNr2f2* ($n = 3$) or *sgRosa26* ($n = 4$) in neurons. **i**, Pie chart showing distribution of detected ATAC-seq motifs in neurons isolated from neuron-targeting *sgNr2f2* ($n = 4$) or *sgRosa26* ($n = 4$) mice. **j**, Quantification of BLA coverage by excitatory neurites as a function of *Nr2f2* KD. Cortical notching was used to differentiate between hemispheres. $n = 6$ images per group. One-tailed unpaired t-test. RPKM, Reads Per Kilobase of transcript per Million mapped reads. NS, not significant. Data shown as mean \pm SEM.



Extended Data Fig. 4 | Chronic stress and fear conditioning combinatorially regulate neural activity and astrocyte transcriptional signatures. **a**, Representative images and bar graph of cFos signals in the BLA of unstressed and stressed mice exposed to 18-days restraint stress, and/or fear conditioning, and/or a control context (control, n = 4; fear conditioning, n = 7; 18-day stress, n = 4; 18-day stress with fear conditioning, n = 6). Yellow arrows

indicate masked cFos signals. One-way ANOVA, Holm-Sidak post-test. **b-e**, Bar plots of bulk RNA-seq data comparing pathways detected in amygdala astrocytes in stressed versus unstressed conditions, with and without fear conditioning. n = 5 mice per group. **f**, Expression levels of *Slitrk2* in neurons of control (n = 4 mice) or fear conditioning (n = 5 mice). One-tailed unpaired t-test. Data shown as mean \pm SEM.

Article



Extended Data Fig. 5 | Analysis of the chronically stressed brain by Stereo-seq. **a**, H&E and nuclei staining of coronal brain sections used in Stereo-seq.

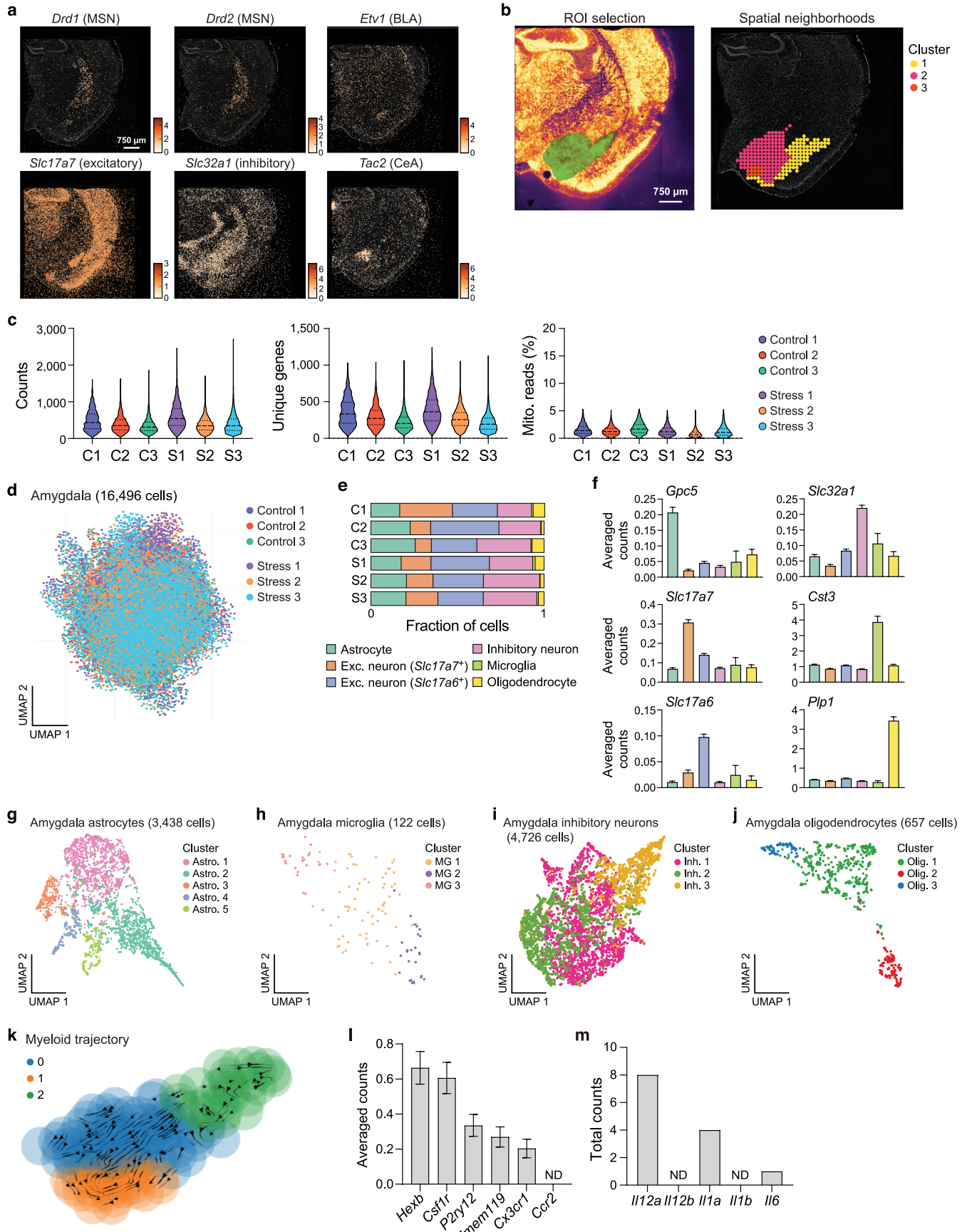
b, RIN number of samples used in Stereo-seq analyses. $n = 3$ per group. Unpaired t-test. **c**, Rarefaction curve of sequencing depth for each sample used.

d, Abundance of RNA molecules detected per spot at a resolution of bin200,

meaning a $100 \mu\text{m}^2$ spot. Please note that Stereo-seq transcriptomic data were analyzed using cellbin analysis, which maintains a resolution of 500-nm.

e, Representative tissue architecture for sections used.

f, Representative mID counts in an 18-day stressed mouse at cellbin resolution (500-nm). RIN, RNA integrity number. Data shown as mean \pm SEM.



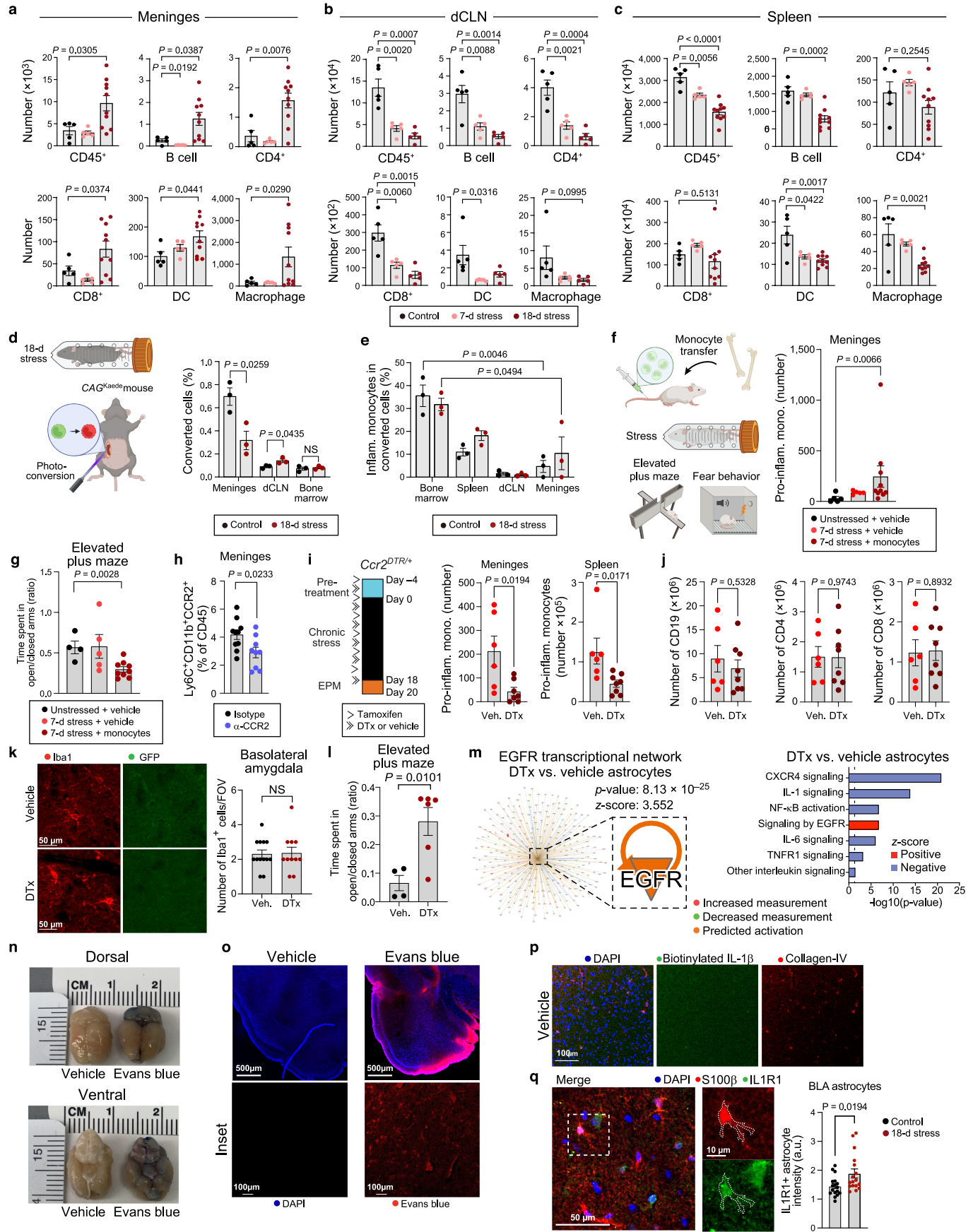
Extended Data Fig. 6 | See next page for caption.

Article

Extended Data Fig. 6 | Determination of amygdala cell types and states by Stereo-seq.

a, Marker genes used in differentiating the amygdala from other brain areas. **b**, Representative ROI used (green) to select the amygdala (left) and StereoMap neighborhood-based spatial clustering analysis at bin200 resolution (right). **c**, Quality control data per cell of mID counts (left), unique genes expressed (middle), and percent of mitochondrial reads (right) within the selected amygdalae. **d,e**, Projection of sample distribution by cluster (**d**)

and fraction of cell type within each sample (**e**). n = 16,496 cells. **f**, Marker genes of cell types detected in the amygdala. **g-j**, Subclustered cell types detected in the amygdala **k**, RNA velocity analysis of myeloid cell clusters. **l**, Plot of microglial or monocyte marker genes in microglial cells detected by Stereo-seq. **m**, Total counts of selected cytokine genes in analyzed amygdala samples. MSN, medium spiny neurons. CeA, central amygdala. BLA, basolateral amygdala. ROI, region of interest. ND, not detected. Data shown as mean ± SEM.

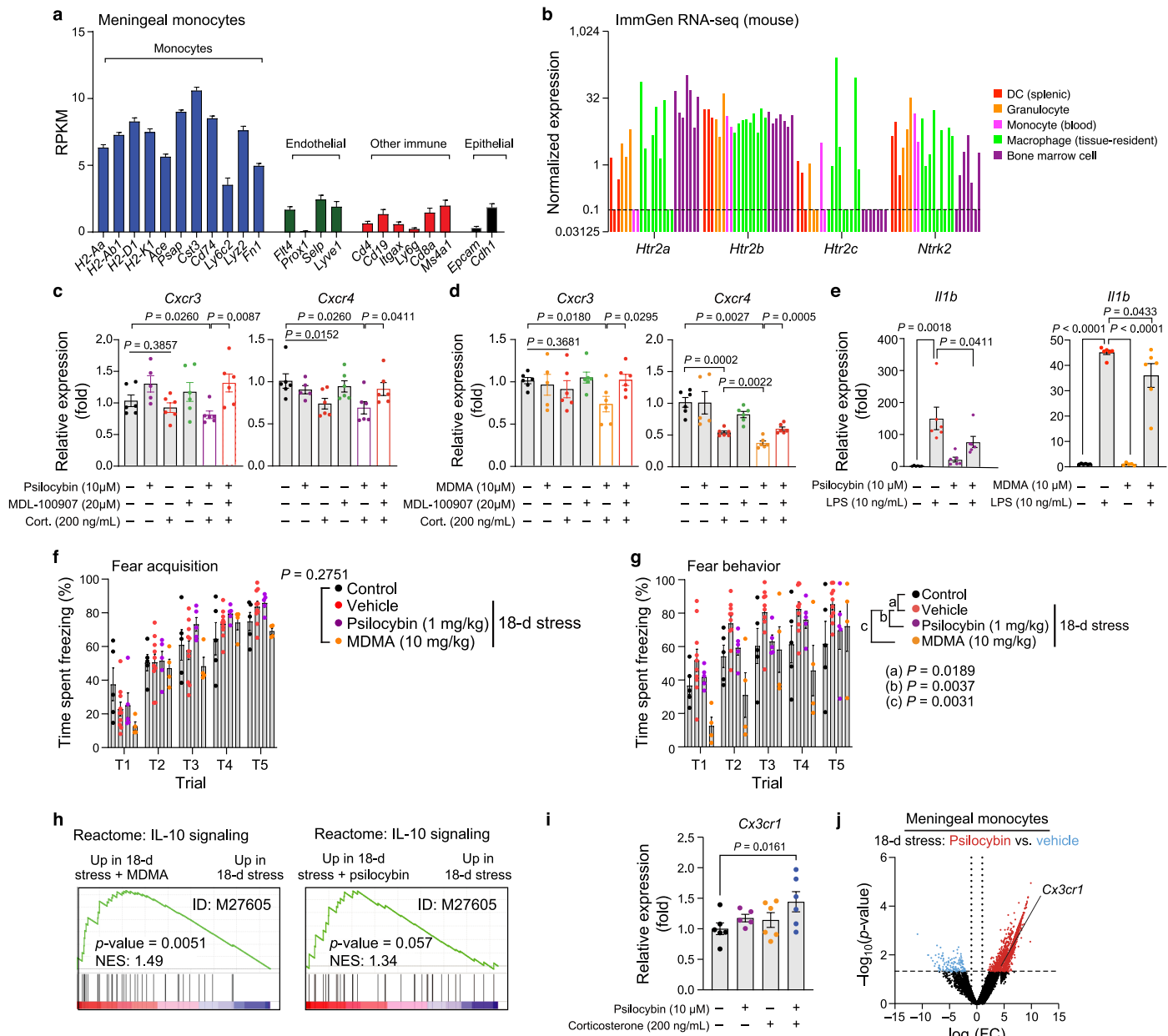


Extended Data Fig. 7 | See next page for caption.

Article

Extended Data Fig. 7 | Mobilization of immune cells in response to chronic stress. **a-c**, FACS analysis of immune cell types in meninges (**a**), dCLN (**b**), and spleen (**c**) in mice exposed to 0-, 7-, or 18-days of restraint stress. n = 10 per group for meninges and spleen 18-day stress, n = 5 otherwise. Unpaired t-test. **d,e**, Schematic of photoconversion in the spleen of Kaede mice (left) and number of photoconverted cells (right) (**d**); percentage of photoconverted monocytes in the meninges, dCLN, bone marrow, and spleen of stressed and unstressed mice (**e**). n = 3 mice per group. Unpaired t-test. **f**, Schematic and FACS analysis of monocyte adoptive transfer via i.v. injection in stressed and control NSG mice. (Unstressed mice (vehicle, n = 5); 7-day stressed mice (vehicle, n = 5; monocyte, n = 10). Kruskal-Wallis test, with Dunn post-test. **g**, Time spent in open arms versus closed arms in EPM. (Unstressed mice (vehicle, n = 4); 7-day stressed mice (vehicle, n = 5; monocyte, n = 9). Unpaired t-test. **h**, FACS analysis of CCR2⁺ pro-inflammatory meningeal monocytes following i.c.m. injection of α-CCR2 or isotype control. n = 5 per group. Unpaired t-test. **i**, Experimental schematic and FACS validation of meningeal and splenic monocyte depletion in *Ccr2*^{DTR/+} mice. Unpaired t-test. **j**, Bar graph of immune cell numbers in mice

administered DTx (n = 8) or vehicle (n = 6). Unpaired t-test. **k**, Immunostaining of Iba1⁺ microglia in *Ccr2*^{DTR/+} mice treated with DTx (n = 11 images from 3 mice) or vehicle (n = 12 images from 4 mice). Note absence of EGFP (driven by *Ccr2* promoter) in microglia. Unpaired t-test. **l**, Time spent in open arms versus closed arms in EPM in *Ccr2*^{DTR/+} mice treated with DTx (n = 6) or vehicle (n = 4). Unpaired t-test. **m**, EGFR transcriptional network (left) and pathway analysis from bulk RNA-seq of amygdala astrocytes (right) from *Ccr2*^{DTR/+} mice with or without monocyte depletion after 18-days of restraint stress. Fisher's exact test. **n**, Dorsal and ventral images of a mouse brain 2-h after i.c.m. injection of 3% Evans blue dye or 1X PBS. **o**, Confocal images of coronal brain sections showing Evans blue dye signal in the amygdala. **p**, Secondary-only negative control of biotinylation signal using mice injected i.c.m. with 1X PBS. **q**, Expression of IL-1R1 in S100 β ⁺ astrocytes in 18-day stress and control groups. n = 17 cells per group. Unpaired t-test. FOV, field of view. NS, not significant. Schematics (**d,f**) were created using BioRender (<https://biorender.com>). Data shown as mean ± SEM.

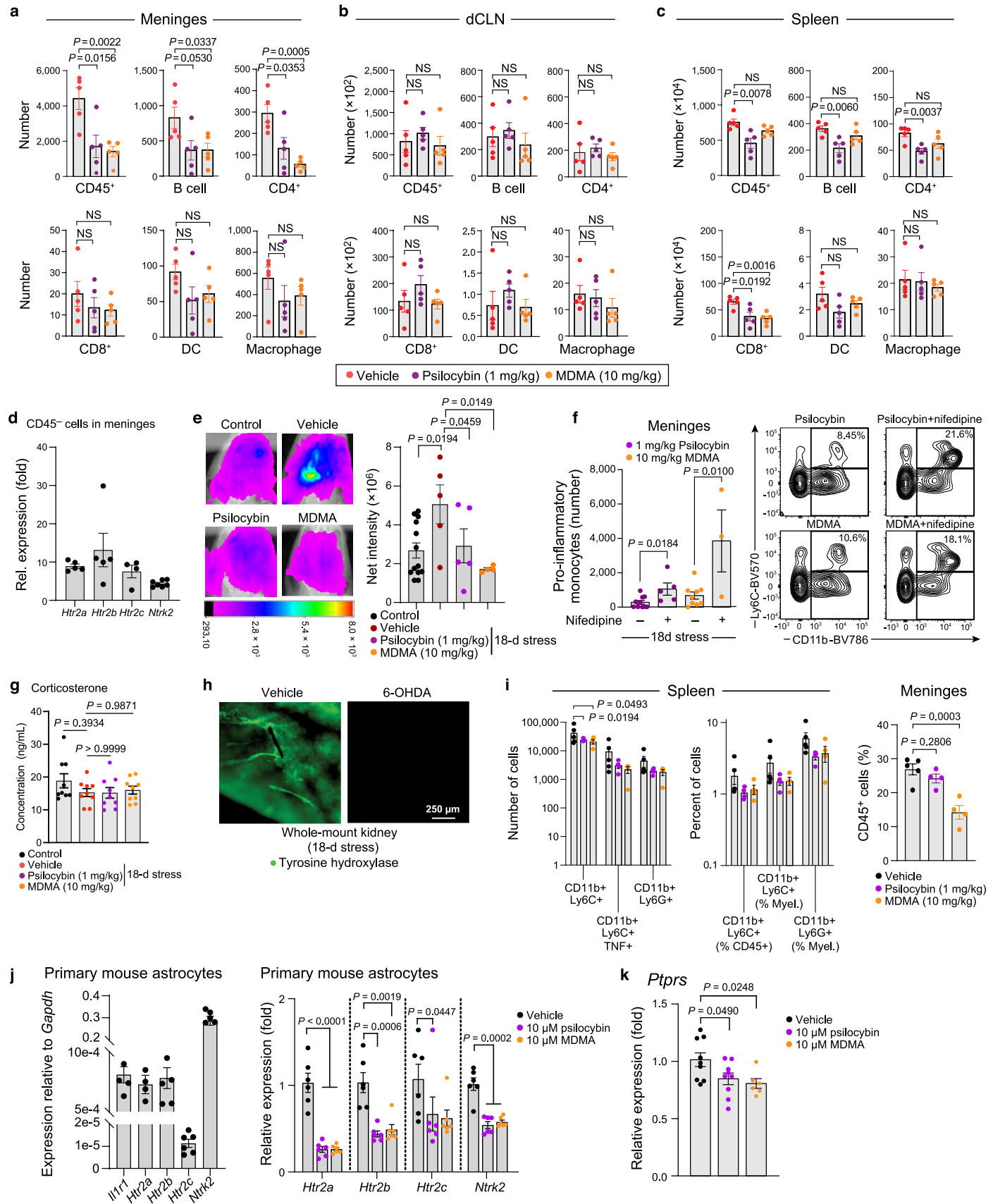


Extended Data Fig. 8 | Regulation of the immune response by psychedelics.

a, Expression of marker genes in meningeal monocytes. $n = 6$ mice per group. **b**, Normalized gene expression data obtained from ImmGen ultra-low-input bulk RNA-seq across several progenitor, circulating, and tissue-resident myeloid cell types in mice collated in the database. **c,d**, qPCR analysis of primary splenic CD11b⁺ cells treated with the given compounds for 6-h. $n = 6$ per group, except for the compound-only group ($n = 5$). Mann-Whitney t-test. **e**, qPCR analysis of gene expression in primary CD11b⁺ splenic cells treated with or without 10 μ M psilocybin (left; $n = 6$ per group) 10 μ M MDMA racemate (right; $n = 6$ per group, except for the MDMA-only group ($n = 5$)) or 10 ng/mL LPS for 6-h. One-way ANOVA, Mann-Whitney t-test. **f,g** Fear acquisition (f) and freezing behavior (g) from mice exposed to 18-days restraint stress or controls. All mice were untreated during fear acquisition and are grouped according to future

treatment during fear extinction. Two hours before fear extinction mice were treated with the given compounds. $n = 5$ (control), $n = 10$ (vehicle), $n = 5$ (psilocybin), and $n = 4$ (MDMA). Two-way repeated measures ANOVA. **h**, GSEA plots from bulk RNA-seq data of meningeal monocytes exposed to 18-days of restraint stress and treated with 1 mg/kg psilocybin or 10 mg/kg MDMA racemate. $n = 3$ mice per group. **i**, qPCR analysis of primary CD11b⁺ splenic cells treated with indicated compounds for 6-h. $n = 6$ per group, except for the psilocybin-only group ($n = 5$). One-way ANOVA, Dunnett post-test. **j**, Volcano plot of differentially expressed genes from bulk RNA-seq of meningeal monocytes after 18-days of restraint stress and treatment with 1 mg/kg psilocybin or vehicle. $n = 3$ per group. RPKM, Reads Per Kilobase of transcript per Million mapped reads. Data shown as mean \pm SEM.

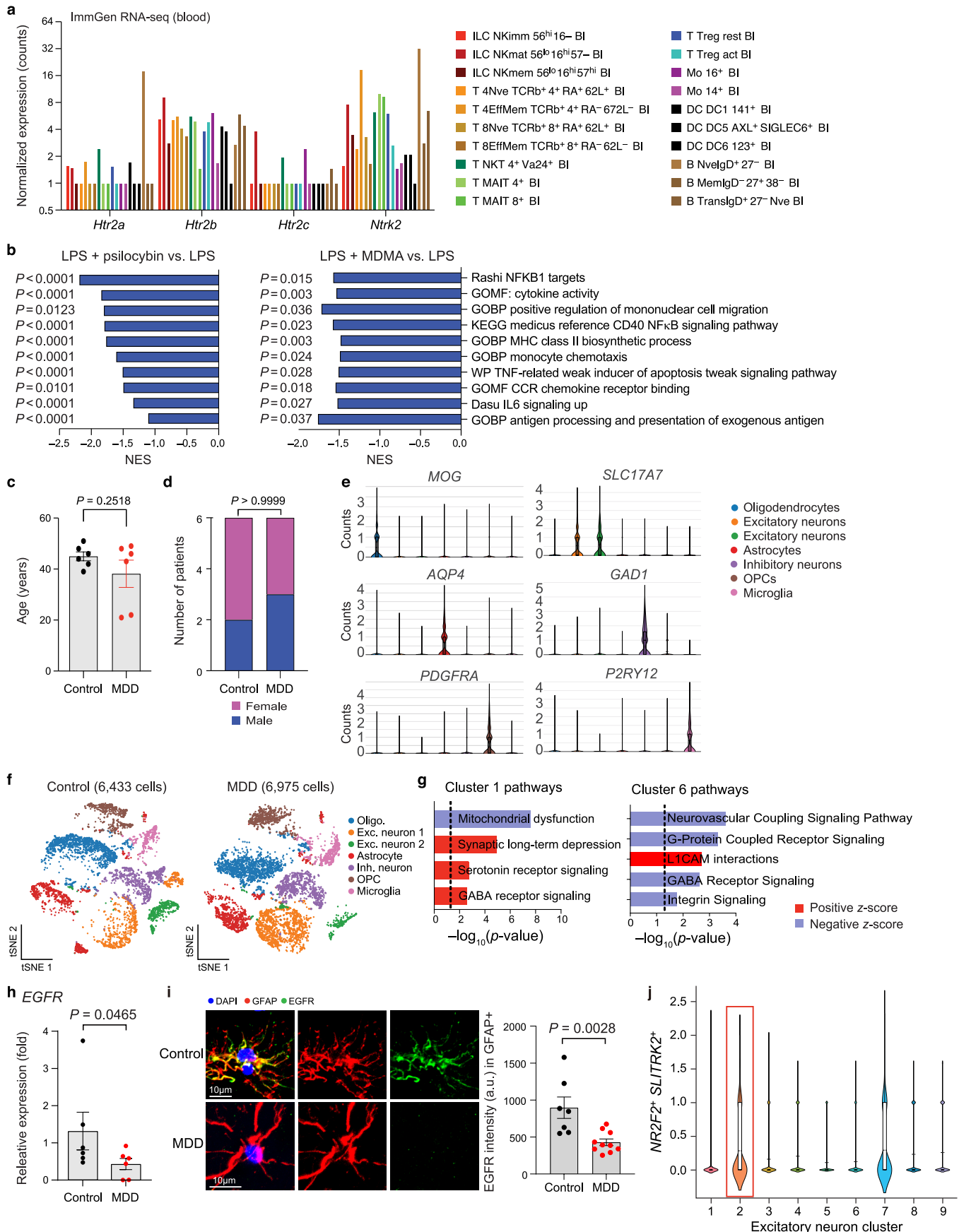
Article



Extended Data Fig. 9 | See next page for caption.

Extended Data Fig. 9 | Psychedelic control of the immune response across tissues. **a–c**, FACS analysis of major cell types in the meninges (**a**), dCLN (**b**), and spleen (**c**) in mice exposed to 18 days of restraint stress and treated with vehicle ($n = 5$), 1 mg/kg psilocybin ($n = 5$), or 10 mg/kg MDMA racemate ($n = 5$). Unpaired t-test. **d**, Expression levels of serotonergic receptors in CD45⁺ cells within the meninges (*Htr2a*, $n = 5$; *Htr2b*, $n = 5$; *Htr2c*, $n = 4$; *Ntrk2*, $n = 7$). **e**, Representative images and quantification of vascular fluorescent signals following tail vein injection in unstressed ($n = 13$) and stressed mice treated with vehicle ($n = 5$), 1 mg/kg psilocybin ($n = 5$), or 10 mg/kg MDMA ($n = 4$). One-way ANOVA, Holm-Sidak post-test. **f**, Bar graph and FACS plots showing the number of monocytes in the meninges of mice treated for 6 h with 30 mg/kg nifedipine and psilocybin ($n = 10$ or $n = 5$ for vehicle or nifedipine groups, respectively) or MDMA ($n = 9$ or $n = 3$ for vehicle or nifedipine groups, respectively). Unpaired t-test. **g**, Quantification of plasma corticosterone in controls or mice exposed to 18-days of restraint stress and treated with vehicle, 1 mg/kg psilocybin, or 10 mg/kg MDMA racemate. $n = 9$ mice per group. One-way ANOVA, Tukey post-test. **h**, Representative images showing validation of chemical sympathectomy by whole mount TH immunostaining of the mouse kidney. **i**, FACS analysis of splenic (left) and meningeal (right) cells in mice that underwent 18-days of restraint stress followed by chemical sympathectomy, followed by treatment with the given compounds (vehicle, $n = 5$; psilocybin, $n = 4$; MDMA, $n = 4$). Two-way ANOVA, Dunnett post-test (left) or unpaired t-test (right). **j**, qPCR analysis in primary astrocytes at baseline (left: *Il1rl*, $n = 4$; *Htr2a*, $n = 4$; *Htr2b*, $n = 5$, *Htr2c*, $n = 6$; *Ntrk2*, $n = 6$) or after a 6-h treatment with 10 μ M psilocybin, 10 μ M MDMA, or vehicle (right, $n = 6$ per group). One-way ANOVA per gene. **k**, *Ptprs* expression level by qPCR in primary astrocytes treated with indicated compounds for 6-h (vehicle, $n = 9$; psilocybin, $n = 9$; MDMA, $n = 6$). Unpaired t-test. Data shown as mean \pm SEM.

Article



Extended Data Fig. 10 | See next page for caption.

Extended Data Fig. 10 | Control analyses of human samples. **a**, Normalized expression of genes detected by ultra-low-input bulk RNA-seq from human immune cell populations in the blood from the ImmGen human immune system cell atlas. **b**, Pathways detected by GSEA in primary human monocytes treated for 6-h with 100 ng/mL LPS with or without 10 μ M psilocybin or 10 μ M MDMA racemate. $n = 3$ per group. **c,d**, Demographics of patient samples used for snRNA-seq. $n = 6$ per group. Unpaired t-test (**c**) or Fisher's exact test (**d**). **e**, Violin plots of cell type markers for cells detected in the amygdala by snRNA-seq. **f**, Separation by disease status of samples used in snRNA-seq. **g**, Pathway plots of cluster 1 and 6 astrocytes from snRNA-seq. **h**, qPCR analysis of EGFR expression in human amygdala. $n = 6$ per group. One-tailed unpaired t-test. **i**, Representative confocal images and bar graphs showing EGFR expression in control and MDD patient amygdala astrocytes. $n = 7\text{--}10$ images and $n = 3$ patients per group. Unpaired t-test. **j**, Violin plot of NR2F2 and SL/TRK2 expression in excitatory neurons. In violin plots, Solid horizontal line: median; white box: interquartile range (25th–75th percentile); whiskers: min and max values; dashed line: mean. Data shown as mean \pm SEM.

Reporting Summary

Nature Portfolio wishes to improve the reproducibility of the work that we publish. This form provides structure for consistency and transparency in reporting. For further information on Nature Portfolio policies, see our [Editorial Policies](#) and the [Editorial Policy Checklist](#).

Statistics

For all statistical analyses, confirm that the following items are present in the figure legend, table legend, main text, or Methods section.

n/a Confirmed

- The exact sample size (n) for each experimental group/condition, given as a discrete number and unit of measurement
- A statement on whether measurements were taken from distinct samples or whether the same sample was measured repeatedly
- The statistical test(s) used AND whether they are one- or two-sided
Only common tests should be described solely by name; describe more complex techniques in the Methods section.
- A description of all covariates tested
- A description of any assumptions or corrections, such as tests of normality and adjustment for multiple comparisons
- A full description of the statistical parameters including central tendency (e.g. means) or other basic estimates (e.g. regression coefficient) AND variation (e.g. standard deviation) or associated estimates of uncertainty (e.g. confidence intervals)
- For null hypothesis testing, the test statistic (e.g. F , t , r) with confidence intervals, effect sizes, degrees of freedom and P value noted
Give P values as exact values whenever suitable.
- For Bayesian analysis, information on the choice of priors and Markov chain Monte Carlo settings
- For hierarchical and complex designs, identification of the appropriate level for tests and full reporting of outcomes
- Estimates of effect sizes (e.g. Cohen's d , Pearson's r), indicating how they were calculated

Our web collection on [statistics for biologists](#) contains articles on many of the points above.

Software and code

Policy information about [availability of computer code](#)

Data collection	BD FACSDIVA (v.8.0.1)
Data analysis	R (v4.1.2); Python (v3.0); Seurat (v. 3.0); Monocle (v 2.9.0); GSEA (v 6.3); IPA (Qiagen); MSigDB (v 6.2); STAR (v2.7.3a); fastp (version 0.23.2); fastQC (version 0.11.9); multiqc (version 1.11); featureCounts (version 2.0.1); EdgeR (version 3.42.4); BWA mem (v0.7.8); Picard MarkDuplicates (version 2.25.2); SAMtools (v1.3); Loupe Brower (v7.0.1); MACS2 callpeak (v2.2.9.1); DiffBind (version 3.10.0); Homer (version 4.10); Cutadapt (v1.14); Trim Galore (version 0.6.0); IDR (v2.0.2); MAST (5.0.5); Scikit-image package (v0.18.1); rearr (v0.3.3); SAW (v6.0.2); scanpy (v0.3.2); Cell Ranger Aggr (v7.1.0); Prism v10.0; ENRICHR; PantherDB(19.0); Adobe Illustrator 2024; FIJI(ImageJ, v1.54k); FlowJo (FlowJo LLC, version 10.10.0); StringDB; Noldus Ethovision System (Noldus Information Technology, version 17.0).

For manuscripts utilizing custom algorithms or software that are central to the research but not yet described in published literature, software must be made available to editors and reviewers. We strongly encourage code deposition in a community repository (e.g. GitHub). See the Nature Portfolio [guidelines for submitting code & software](#) for further information.

Data

Policy information about [availability of data](#)

All manuscripts must include a [data availability statement](#). This statement should provide the following information, where applicable:

- Accession codes, unique identifiers, or web links for publicly available datasets
- A description of any restrictions on data availability
- For clinical datasets or third party data, please ensure that the statement adheres to our [policy](#)

Data in this study have been deposited into GEO under the SuperSeries accession number GSE262989. Bulk RNA-seq datasets of amygdala cell types were obtained under the GEO accession numbers GSE162417; GSE66345; GSE130268; GSE138522; GSE183092; and GSE151798. A mouse atlas of brain structures was accessed

at: <https://cells.ucsc.edu/?ds=mouse-nervous-system> and .loom files for each brain region included were downloaded. An atlas of amygdala cell types was accessed at FigShare under the URL: <https://doi.org/10.6084/m9.figshare.20412573>. Gene expression data of purified human immune cell populations was accessed using the ImmGen Skyline RNA-seq data browser under the URL: <https://www.immgen.org/Databrowser19/DatabrowserPage.html>. All data supporting the study are included in the manuscript. Correspondence and request for materials should be addressed to M.A.W.

Field-specific reporting

Please select the one below that is the best fit for your research. If you are not sure, read the appropriate sections before making your selection.

- Life sciences Behavioural & social sciences Ecological, evolutionary & environmental sciences

For a reference copy of the document with all sections, see nature.com/documents/nr-reporting-summary-flat.pdf

Life sciences study design

All studies must disclose on these points even when the disclosure is negative.

Sample size	No statistical methods were used to predetermine sample sizes. Sample sizes are similar to those used in the field, as previously reported: Sanmarco and Wheeler et al. <i>Nature</i> 2021; Wheeler et al. <i>Nature</i> 2020; Wheeler et al. <i>Cell</i> 2019; Wheeler et al., <i>Science</i> 2023; Clark and Gutierrez and Wheeler et al. <i>Science</i> 2021; Clark and Wheeler et al., <i>Nature</i> 2023.
Data exclusions	Exclusion criteria via formal outlier testing (Prism, v.9.2.0) were pre-established. This is similar to recent publications: (Vujkovic-Cvijin et al., <i>Nature</i> 2020; Ballesta et al., <i>Nature</i> 2020; Lukonin et al., <i>Nature</i> 2020; Badimon et al., <i>Nature</i> 2020; Wheeler et al., <i>Nature</i> 2020; Wheeler et al., <i>Cell</i> 2019; Hur et al., <i>Nature</i> 2020; Sahin et al., <i>Nature</i> 2020; Lee et al., <i>Nature</i> 2024; Cathomas et al. <i>Nature</i> 2024).
Replication	To ensure replication, all deep sequencing data were across multiple independent samples per group per timepoint. For most in vitro and in vivo experiments, experiments were repeated independently at least twice. All attempts at replication were successful.
Randomization	All samples were randomly allocated into treatment groups.
Blinding	Experimenters were blinded to genotype during chronic stress and fear conditioning. Otherwise, blinding was not performed, such as during in vitro experiments, where experimenters were required to know the conditions of each well. Automated analyses such as machine vision and automated image quantification were used where possible to ensure unbiased analyses.

Reporting for specific materials, systems and methods

We require information from authors about some types of materials, experimental systems and methods used in many studies. Here, indicate whether each material, system or method listed is relevant to your study. If you are not sure if a list item applies to your research, read the appropriate section before selecting a response.

Materials & experimental systems

- | | |
|-------------------------------------|---|
| n/a | Involved in the study |
| <input type="checkbox"/> | <input checked="" type="checkbox"/> Antibodies |
| <input type="checkbox"/> | <input checked="" type="checkbox"/> Eukaryotic cell lines |
| <input checked="" type="checkbox"/> | <input type="checkbox"/> Palaeontology and archaeology |
| <input type="checkbox"/> | <input checked="" type="checkbox"/> Animals and other organisms |
| <input type="checkbox"/> | <input checked="" type="checkbox"/> Human research participants |
| <input checked="" type="checkbox"/> | <input type="checkbox"/> Clinical data |
| <input checked="" type="checkbox"/> | <input type="checkbox"/> Dual use research of concern |

Methods

- | | |
|-------------------------------------|--|
| n/a | Involved in the study |
| <input checked="" type="checkbox"/> | <input type="checkbox"/> ChIP-seq |
| <input type="checkbox"/> | <input checked="" type="checkbox"/> Flow cytometry |
| <input checked="" type="checkbox"/> | <input type="checkbox"/> MRI-based neuroimaging |

Antibodies

Antibodies used

For FACS staining: CD16/CD32 (BD Biosciences, #553141), BUV661 anti-mouse CD45 (BD Biosciences, #612975), BV650 anti-mouse CD3 (BD Biosciences, #740530), PE-Cy7 anti-mouse CD4 (BD Biosciences, #561099), BV786 anti-mouse CD11B (BD Biosciences, #740861), BV570 anti-mouse Ly6C (BioLegend, #128029), BUV805 anti-mouse CD8a (BD Biosciences, #612898), BUV563 anti-mouse Ly6G (BD Biosciences, #612921), BUV737 anti-mouse CD11c (BD Biosciences, #612797), BV750 anti-mouse NK1.1 (BD Biosciences, #746876), FITC anti-mouse CD192 (CCR2) Antibody (BioLegend, #150608), BV605 anti-mouse CD19 (BioLegend, #115539), Alexa Fluor 488 anti-GFP (BioLegend, #338007) and BV421 anti-mouse TNF (BD Biosciences, #563387).

For Cell or tissue immunostaining: rabbit anti-tyrosine hydroxylase (Millipore, #AB152), goat anti-rabbit Alexa Fluor 488 (Thermofisher, #A-11008), rabbit anti-mCherry (Abcam, ab167453), chicken anti-GFAP (Abcam, #ab4674), mouse anti-GFAP(GA5) (Millipore, #MAB360), rabbit anti-EGFR (D38B1) (Cell Signaling, #4267), rabbit anti-Homer1 (Synaptic systems, #160 002), chicken anti-GFP (Abcam, ab13970), rabbit anti-cFos (Cell Signaling, #2250S), rabbit anti-Ptprs (Proteintech, 13008-1-AP), rabbit anti-IL1r1 (Abcam, ab106278), mouse anti-S100beta (Millipore Sigma, S2532), rabbit anti-Collagen IV (BioRad, #2150-1470), rabbit anti-Iba1 (Abcam, ab178846), guinea pig anti-Vglut2 (Sigma, #AB2251-I), and Mouse anti-TUBB3 (BioLegend, #801201). Secondary antibodies used in this study were: donkey anti-goat IgG Alexa Fluor 488 (Jackson Immunoresearch, #705-545-003), donkey anti-rabbit IgG (H+L)

Highly Cross-Adsorbed, Alexa Fluor 568 (Life Technologies, #A10042), Alexa Fluor 647 donkey anti-mouse (Abcam, #ab150107), Goat anti-Chicken IgY (H+L) Alexa Fluor 488 (Life Technologies, #A11039), Alexa Fluor 594 Goat anti-Guinea pig IgG (H+L) (Invitrogen, #A11076), goat anti-rabbit IgG (H+L) Highly Cross-Adsorbed Alexa Fluor 488 (Invitrogen, #A11034), goat anti-rabbit IgG (H+L) Highly Cross-Adsorbed Alexa Fluor 594 (Invitrogen, #A11037), goat anti-mouse IgG (H+L) Highly Cross-Adsorbed Alexa Fluor 594 (Invitrogen, #A11032), and goat anti-chicken IgY (H+L) Highly Cross-Adsorbed Alexa Fluor 488 (Invitrogen, #A11039), Oregon Green 488 conjugate of NeutrAvidin biotin-binding protein (Invitrogen, A6374), IgG (R&D Systems, #MAB0061), and CCR2 (R&D Systems, #MAB55381)

Validation

All antibodies were commercial in origin and validated for FACS and tissue immunostaining by the company. Specifically, BioLegend (<https://www.biologend.com/en-us/quality/quality-control>), Abcam (<https://www.abcam.com/primary-antibodies/how-we-validate-our-antibodies>), BD Biosciences, Miltenyi (<https://www.miltenyibiotec.com/US-en/resources/macsc-academy/live-webinars/antibody-validation-for-reproducible-flow-cytometry-analysis.html#gref>), Thermo Fisher (<https://www.thermofisher.com/us/en/home/life-science/antibodies/invitrogen-antibody-validation.html>), R&D Systems (<https://www.rndsystems.com/quality/antibodies-built-for-reproducibility#:~:text=R%26D%20Systems%C2%AE%20takes%20rigorous%20steps%20towards%20antibody%20validation%20and%20reproducibility.&text=By%20developing%20and%20testing%20our,100%25%20guarantee%20for%20our%20products.>), and Millipore (<https://www.emdmillipore.com/US/en/life-science-research/antibodies-assays/antibodies-overview/Antibody-Development-and-Validation/cFOb.qB.8McAAFOb64qQvSS,nav>), purify antibodies from cell line supernatant using affinity chromatography followed by validation using proper negative and positive controls in functional assays, relevant for all antibodies used for flow cytometry and immunostaining.

Eukaryotic cell lines

Policy information about [cell lines](#)

Cell line source(s)

HEK 293T Cells for AAV production were obtained from Takara Bio (#632273). Human monocyte samples were obtained from iQ Biosciences (#IQB-Hu1-M10). Human astrocyte samples were obtained from ScienCell (#1800).

Authentication

HEK293T cells were obtained from commercial vendors and authenticated by the vendor through STR profiling. Monocytes are validated by magnetic bead purification. Human astrocytes are validated by immunostaining.

Mycoplasma contamination

Cell lines were obtained from commercial vendors, and therefore not tested for mycoplasma contamination.

Commonly misidentified lines (See [ICLAC](#) register)

No commonly misidentified cell lines were used.

Animals and other organisms

Policy information about [studies involving animals; ARRIVE guidelines](#) recommended for reporting animal research

Laboratory animals

Mice were group-housed under a standard light cycle (12h light/dark) (lights on from 7am to 7pm) at 20-23C and humidity (~50%) with ad libitum access to water and food. Laboratory mice used in these studies were: Adult male mice 8-10 weeks old and P0-P3 pups were used on a C57Bl/6J background (The Jackson Laboratory, #000664); C57Bl/6-Gt(ROSA)26Sortm1(HBEGF)Awai/J (The Jackson Laboratory, #007900) females were bred to C57Bl/6-Ccr2em1(icre/ERT2)Peng/J males (The Jackson Laboratory, #035229) to generate heterozygous Ccr2DTR/+ F1 mice; Aldh1l1Cre-ERT2/+ mice (The Jackson Laboratory, #031008) were bred to B6.Cg-Gt(ROSA)26Sortm9(CAG-tdTomato)Hze/J (Jackson #007909) mice to produce F1 Aldh1l1 reporter mice. Male NOD.Cg-Prkdcidil2rgtm1Wjl/Szj (NSG mice, The Jackson Laboratory, #005557) were used for adoptive transfer studies. Male Tg(CAG-Kaede)15Kgwa mice were used on a C57Bl/6J background. All behavioral studies were initiated at 8-10 weeks of age.

Wild animals

The study did not involve wild animals

Field-collected samples

The study did not involve samples collected from the field.

Ethics oversight

Brigham and Women's Hospital IACUC.

Note that full information on the approval of the study protocol must also be provided in the manuscript.

Human research participants

Policy information about [studies involving human research participants](#)

Population characteristics

Human amygdala samples were analyzed from n=6 MDD patients and n=6 controls (snRNA-seq) or n=3 patients per group (immunostaining). To minimize the influence of technical variables, we included a balanced distribution of age and sex. Other patient information is contained in Supplementary Table 18.

Human monocyte samples were obtained from a commercial vendor that harvests cells from peripheral blood samples.

Recruitment

Patient recruitment at the NIH NeuroBioBank is approved programmatically through the IRB of each institution providing patient samples. Specifically: "Donations are obtained from individuals who register before death, and/or from next-of-kin who authorize a postmortem donation. Eligibility for postmortem donation of brain and other tissues is determined by trained staff at the individual BTR. BTR staff notification of a request for postmortem donation may come from surviving family members, treating physicians, hospital systems, donor services, organ and tissue banks, disease advocacy groups, specialized residential facilities, and/or collaborating medical examiners."

"Although the specific procedures for enrollment and consent may vary between the BTR sites, the policies and procedures

of each bank have been reviewed and approved by their respective Institutional Review Boards (IRB) and any additional appropriate oversight committees of the BTR site's home institution. Trained individuals request and document consent for brain tissue donation from the deceased's next-of-kin or legally authorized representative. Individual requests for release of medical records, questionnaires, and/or interviews with individuals knowledgeable of the deceased are obtained according to IRB approved policies and procedures."

Monocyte samples from iQ Biosciences are "...lawfully obtained in accordance with Local, State, and Federal U.S. requirements, and the collection of cells complies with ethical requirements. Our cells are obtained from normal or disease patient volunteers participating in a donor program that is approved by an Institutional Review Board (IRB) or Human Subject Committee."

Ethics oversight

Ethical oversight is determined programmatically via the NIH NeuroBioBank. The specific details are found on their web site here: <https://neurobiobank.nih.gov/about-best-practices/>

Ethical considerations for iQ Biosciences is stated on their web site: "iQ Biosciences' human primary cell products are lawfully obtained in accordance with Local, State, and Federal U.S. requirements, and the collection of cells complies with ethical requirements. Our cells are obtained from normal or disease patient volunteers participating in a donor program that is approved by an Institutional Review Board (IRB) or Human Subject Committee. A signed and witnessed consent form is obtained from donor volunteers prior to starting the collection protocol. Strict controls on personal identifiers of volunteers are in place in order to protect their privacy."

Note that full information on the approval of the study protocol must also be provided in the manuscript.

Flow Cytometry

Plots

Confirm that:

- The axis labels state the marker and fluorochrome used (e.g. CD4-FITC).
- The axis scales are clearly visible. Include numbers along axes only for bottom left plot of group (a 'group' is an analysis of identical markers).
- All plots are contour plots with outliers or pseudocolor plots.
- A numerical value for number of cells or percentage (with statistics) is provided.

Methodology

Sample preparation

Meninges: Animals were euthanized and blood was removed by cutting the right atrium. Following mouse perfusion, the head was severed, and the skin was removed from the head. A cut was made around the cranium (from the foramen magnum to the frontal bone) to dissect the bones of the calvarium. The calvarium was then transferred to a dissection scope and the meninges were removed. Tissue was incubated for 30 minutes at 37C in 500- μ L RPMI-1640 (Life Technologies, #11875119) supplemented with 0.5 mg/mL collagenase P (Sigma-Aldrich, #11213865001), 0.5 mg/mL of dispase (Worthington, #LS02104), and 125 U/mL of DNase I (Sigma-Aldrich, #10104159001). After incubation, samples were washed with 1-mL of 0.5% BSA, 2mM EDTA in 1X PBS. Cells were centrifuged at 500g for 10 minutes, resuspended in 1-mL ice-cold 0.5% BSA, 2mM EDTA in 1X PBS, and gently dissociated using a wide-bore 1 mL pipette tip. Finally, the cell suspension was filtered through a 40 μ m FlowMi filter (Sigma-Aldrich, #BAH136800040-50EA) and prepared for downstream applications.

Spleen: Spleens were isolated following mouse perfusion and mechanically dissociated. Red blood cells were lysed with ACK lysing buffer (Life Technology, #A10492-01) for 5 min, washed with 1X PBS and prepared for downstream applications.

Lymph nodes: Deep cervical lymph nodes were isolated following mouse perfusion and mechanically dissociated. Cells were centrifuged at 1500rpm for 5 minutes and prepared for downstream applications.

Bone marrow : Bone marrow was isolated from C57BL/6J mice by flushing PBS through the head of the femur and tibia with a 25-gauge needle (BD Biosciences, #305125).

Splenic, deep cervical lymph node, and meningeal cell suspensions were stimulated with 50 ng/mL phorbol 12-myristate 13-acetate (PMA, Sigma-Aldrich, #P8139), 1 μ M ionomycin (Sigma-Aldrich, #I3909-1ML), GolgiStop (BD Biosciences, #554724, 1:500) and GolgiPlug (BD Biosciences, #555029, 1:500) diluted in complete RPMI (Life Technologies, #11875119) containing 10% FBS, 1% penicillin/streptomycin, 50 μ M 2-mercaptoethanol (Sigma-Aldrich, #M6250), and 1% non-essential amino acids (Life Technologies, #11140050). After 4 hours, cell suspensions were washed with 0.5% BSA, 2 mM EDTA in 1X PBS and incubated with an FCyR-blocking antibody, surface antibodies and a live/dead fixable aqua stain (Thermo Fisher Scientific, #134966) on ice. After 30 min, cells were washed with 0.5% BSA, 2mM EDTA in 1X PBS and fixed according to the manufacturer's protocol of an intracellular labeling kit (eBiosciences, #00-5523-00).

For tdTomato+ cells, mice were perfused with 1X PBS and the CNS was isolated into 10 mL of enzyme digestion solution consisting of 75 μ L Papain suspension (Worthington, #LS003126) diluted in enzyme stock solution (ESS) and equilibrated to 37C. ESS consisted of 10 mL 10X EBSS (Sigma-Aldrich, #E7510), 2.4 mL 30% D(+)-Glucose (Sigma-Aldrich, #G8769), 5.2 mL 1M NaHCO3 (VWR, #AAJ62495-AP), 200 μ L 500 mM EDTA (Thermo Fisher Scientific, #15575020), and 168.2 mL ddH2O, filter-sterilized through a 0.22 μ m filter. Samples were shaken at 80rpm for 30-40 minutes at 37C. Enzymatic digestion was stopped with 1 mL of 10X hi ovomucoid inhibitor solution and 20 μ L 0.4% DNase (Worthington, #LS002007) diluted in 10 mL inhibitor stock solution (ISS). 10X hi ovomucoid inhibitor stock solution contained 300 mg BSA (Sigma-Aldrich, #A8806), 300 mg ovomucoid trypsin inhibitor (Worthington, #LS003086) diluted in 10 mL 1X PBS and filter sterilized using at 0.22 μ m filter. ISS contained 50 mL 10X EBSS (Sigma-Aldrich, #E7510), 6 mL 30% D(+)-Glucose (Sigma-Aldrich, #G8769), 13 mL 1M NaHCO3

(VWR, #AAJ62495-AP) diluted in 170.4 mL ddH₂O and filter-sterilized through a 0.22 µm filter. Tissue was mechanically dissociated using a 5 mL serological pipette and filtered through at 70 µm cell strainer (Fisher Scientific, #22363548) into a fresh 50 mL conical. Tissue was centrifuged at 500g for 5 minutes and resuspended in 10 mL of 30% Percoll solution (9 mL Percoll (GE Healthcare Biosciences, #17-5445-01), 3 mL 10X PBS, 18 mL ddH₂O). Percoll suspension was centrifuged at 500g for 25 minutes with no brakes. Supernatant was discarded and the cell pellet was washed 1X with 1X PBS, centrifuged at 500g for 5 minutes and prepared for downstream applications. Cells were sorted on a FACS Aria IIu (BD Biosciences). For gating of TdTomato+ cells, cells were sorted according to TdTomato fluorescence judged against a WT control animal using a yellow-green laser on a FACS Aria IIu.

Instrument

BD FACSAria IIu or BD FACSAria SORP. For meninges, lymph nodes, and spleen, cells were counted on a LSRFortessa (BD Biosciences). FACS was performed on a Symphony A5 (BD Biosciences). Confocal imaging were conducted on a Zeiss LSM710 confocal

Software

BD FACSDIVA and FlowJo software (FlowJo LLC, version 10.10.0).

Cell population abundance

Abundance is reported in figures where relevant. FACS sorting was performed with "Purity" settings, thus purity is >95%. MACS purification of astrocytes and neurons was validated by staining at ~92-97.5%.

Gating strategy

Gating strategies are shown for each flow cytometry experiment (Supp. Data 1-5)

Tick this box to confirm that a figure exemplifying the gating strategy is provided in the Supplementary Information.